PURDUE UNIVERSITY
Purdue Research Foundation
Lafayette, Indiana

School of Mechanical Engineering
Heat Transfer Laboratory

Improved Fluid Dynamics Similarity, Analysis and Verification

Final Report - Part III

TWO-PHASE FLOW IN VIBRATING DISCHARGE LINES

by

R. W. Griebe, E. R. F. Winter,
R. J. Schoenhals

Improved Fluid Dynamics Similarity, Analysis and Verification

Final Report - Part III

TWO-PHASE FLOW IN VIBRATING DISCHARGE LINES

Submitted by

Heat Transfer Laboratory
School of Mechanical Engineering
Purdue University
Lafayette, Indiana

to

NATIONAL AERONAUTICS AND SPACE ADMINISTRATION
George C. Marshall Space Flight Center
Applied Mechanical Research Branch
Propulsion Division
Propulsion and Vehicle Engineering Laboratory
Huntsville, Alabama

Period Covered: June 29, 1965 - June 28, 1968

Principal Investigators: E. R. F. Winter and R. J. Schoenhals

Contracting Officer's Representatives: Hugh M. Campbell
William E. Dickson
Carl G. Fritz

Contract Number: NAS 8-20222
Control Number: DCN 1-5-52-01195-01 (1F) & S1 (1F)

Authors: R. W. Griebe
E. R. F. Winter
R. J. Schoenhals

July 1968

ABSTRACT

An analytical and experimental investigation of two phase flow in a discharge line with a sharp edged entrance is presented for both vibratory and non-vibratory conditions.

Initial efforts were devoted to single phase liquid flow in the discharge line. Classical one-dimensional fluid flow relations yielded analytical predictions which were closely matched by experimental data. While no attempt was made to develop predictions in the vibratory cases, an extensive experimental investigation showed that vibration of the test section generally caused an increase in pressure losses.

A modified cavitation number was developed based on a free streamline analysis which considered the flow into the sharp-edged entrance as flow from an orifice. Good agreement with experimental data was shown to exist for several different geometric configurations. Furthermore, a time dependent cavitation number was developed for the cases where vibration was present. An analytical model describing choked two-phase flow was developed using the free streamline theory. Excellent agreement between theory and experimental data was achieved. No effect of vibration on choked flow was detected experimentally. Expressions associated with the normal shock separating the two-phase fluid (liquid-vapor) and single

phase fluid (liquid) were derived. In particular, equations defining the minimum pressure drop for choked flow and equations predicting the shock position as a function of the stagnation pressure loss are given. Good agreement between the analytical predictions and experimental data was obtained in both cases.

TABLE OF CONTENTS

LIST OF TABLES

LIST OF FIGURES

Figure Page

Figure Page

NOMENCLATURE

A	arbitrary cross-sectional area
A_d	cross-sectional area of discharge line
A_{jet}	asymptotic cross-sectional area of jet
A_n	cross-sectional area at reference n, n=0,1,2,..
a	geometric constant in the free streamline solution
B	bulk modulus
B	width of two-dimensional discharge tank
b	width of two-dimensional slot in bottom of two-dimensional discharge tank
C	acoustic velocity
C_a	influence coefficient of area change on pressure gradient
C_c	contraction coefficient defined as the asymptotic area of the jet divided by the orifice
C_f	influence coefficient of friction on pressure gradient
C_g	influence coefficient of gravity on pressure gradient
C_L	acoustic velocity in a pure liquid

C_X	influence coefficient of phase change on pressure gradient
D	diameter of simulated discharge tank
D_o	diameter of flow line at reference position o
d	diameter of discharge line
E	Young's Modulus
E	geometric constant in free streamline solution
E'	geometric constant in free streamline solution
e	geometric constant in free streamline solution
F	frequency of forced vibration (cycles per second)
F_r	Froude number
f	friction factor for single phase liquid flow
f_{TP}	friction factor for two-phase liquid-vapor flow
$\overline{G}$	acceleration level of forced vibration
G	total mass flux
G_f	mass flux of liquid phase
G_g	mass flux of vapor phase
G_n	mass flux at reference n, n=0,1,2,...
g	gravitational acceleration
H	geometric constant in free streamline solution
h	geometric constant in free streamline solution
J	volumetric flux
J_f	volumetric flux of liquid phase
J_{fn}	volumetric flux of liquid phase at reference position n, n=1,2,3,...
J_g	volumetric flux of vapor phase

$\Delta P_{friction}$ stagnation pressure loss due to friction in the single-phase liquid

$\Delta P_{friction, TP}$ stagnation pressure loss due to friction in the two-phase liquid-vapor flow

ΔP_s magnitude of oscillating stagnation pressure component

p' static pressure along free streamline

p_n static pressure at reference n, n=0,1,2,...

Δp_1 magnitude of oscillating component of static pressure at reference position 1

Q volumetric flow rate of liquid as measured by the turbine flow meters

q heat flux

r radial coordinate in axisymmetric coordinates

S wall thickness of simulated discharge tank

V' velocity along the free streamline

V_f velocity of the liquid phase

V_f^* apparent liquid velocity in the discharge line; defined as the volumetric liquid flow rate measured by the turbine meters divided by the cross sectional area of the discharge line

V_{fn} liquid velocity at reference position n, n=0,1,2,...

V_g velocity of the vapor phase

V_{gn} velocity of the vapor phase at reference position n, n=0,1,2,...

J_{gn}	volumetric flux of vapor phase at reference position n, n=1,2,3,...
J_n	volumetric flux at reference position n, n=1, 2,3,...
L	length of discharge line
ℓ	characteristic height of simulated discharge tank
M	Mach number
$P_{dynamic}$	dynamic pressure of liquid due to velocity
P_e	exit stagnation pressure of discharge line
P_n	stagnation pressure at reference position n, n=0,1,2,...
P_s	stagnation pressure at entrance to discharge line
P_v	vapor pressure of liquid at bulk temperature
PD	phase angle relationship between the flash of the strobe lamp and the position of the shaker table
ΔP	stagnation pressure loss across the discharge line
$\Delta P_{entrance}$	stagnation pressure loss due to vena-contracta effects
$\Delta P_{entrance, TP}$	stagnation pressure loss at entrance in the flashing two phase flow
$\Delta P_{expansion}$	stagnation pressure loss due to unrestricted expansion of flow out of discharge line

V_m	velocity of the two-phase liquid-vapor homogeneous mixture
V_n	fluid velocity at reference position n, n=0,1,2,...
W	mass flow rate
y	vertical (longitudinal) coordinate in the simulated propellent tank
z	longitudinal coordinate within the discharge line
α	void fraction; defined as volume of vapor per volume of mixture
β	asymptotic jet width for two-dimensional free streamline solution
γ	surface tension of liquid
δ	asymptotic jet diameter for axisymmetric free streamline solution
ε	roughness of wall used in defining friction factor
ξ	position coordinate of two-phase single-phase normal shock
η	position coordinate of transformation from jet flow to homogeneous flow
Θ	angular position coordinate in cylindrical coordinate system
μ_f	viscosity of liquid phase
ρ_f	density of single phase liquid

ρ_g	density of single phase vapor
ρ_m	density of two phase homogeneous mixture
σ	classical cavitation number
$\bar{\sigma}^*$	modified cavitation number
$\sigma^*(t)$	time dependent modified cavitation number
τ	angular orientation of discharge line with respect to vertical direction
Ω	non-dimensional frequency based on geometric parameters of simulated propellent tank and vibrational frequency
ω	frequency of vibration

CHAPTER 1

INTRODUCTION

High speed transfer of liquids is required for many modern engineering applications. Numerous examples can be cited in rocket propulsion, automatic food processing manufacturing, rapid emergency shut-down of nuclear reactor power plants, and in several other areas of technology. In the development of equipment required for these applications, three major fluid flow problems have been encountered. First, rapid liquid transfer has often been accompanied by unacceptably large frictional losses, as would be expected. Second, local regions of very high velocity have induced liquid cavitation resulting in adverse operating characteristics, and even causing ultimate damage to the system in some instances. Third, totally two-phase flows have appeared in situations where they were not expected, usually producing very detrimental effects which severely limit system performance. The last two problems have been particularly important for cryogenic liquids where heat transfer typically contributes to significantly increasing the amounts of vapor formation. In some cases vibration of equipment due to external sources (such as combustion instabilities in rocket motors or improperly balanced rotating machinery) has affected fluid flow

rates significantly, but in ways which previously have not been well understood.

The research described in this thesis was concerned with fluid flow in tubes with a view toward a study of flow conditions occurring in propellant tank discharge lines of liquid fuel rockets. The overall investigation comprised three major topics:

1. Single phase liquid flow
2. Cavitation inception (onset of two-phase flow)
3. Totally two-phase flow accompanied by liquid flashing, choking, and normal shock phenomena

Each of these flow regimes was studied both in the absence and in the presence of longitudinal vibration of the system.

For accomplishing the goals of the research in each of the three areas listed above, an experimental facility was designed and constructed. Major initial efforts were devoted to a study of its operating characteristics and the functioning of its associated instrumentation. The experimental portion of Topic 1 (single phase liquid flow) was then begun. The classical predictions for single phase liquid pipe flow, flow through an orifice, and flow through a restriction were used as the established information against which the experimental data were compared. The details of this initial single phase flow research are described in Chapter 6.

The second major portion of the investigation was concerned with the generation of two-phase flow as the result of cavitation. The classical cavitation parameter was used

as a basis from which a more comprehensive relation was developed for correlating cavitation inception. A modified cavitation number was also formulated to account for cavitation in the presence of time dependent pressure oscillations resulting from vibration of the system. The analytical results of the cavitation study are contained in Chapter 7 along with the appropriate experimental verifications.

The third and final major portion of the investigation was associated with the experimental observation of flashing flow phenomena and the corresponding analytical predictions. Two unique correlations were developed which were used to predict the occurrence of choked flow as well as the inception and position of a normal shock. These items are discussed in Chapter 8.

To summarize the various topics outlined above, a diagram illustrating the organizational arrangement of the entire investigation is given in Figure 1. While the results of this research (Chapters 6-8) are pertinent to many flow applications, the initial interest was prompted by the problems associated with liquid fuel rocket systems. For this reason, Chapter 2 contains a general description of several two-phase flow phenomena, and Chapter 3 contains a description of the background of some typical fluid flow problems associated with liquid propellant rocket technology. These chapters are followed by a literature survey in Chapter 4 and a description of the experimental facility in Chapter 5 prior to the presentation of the three major topics of the present research.

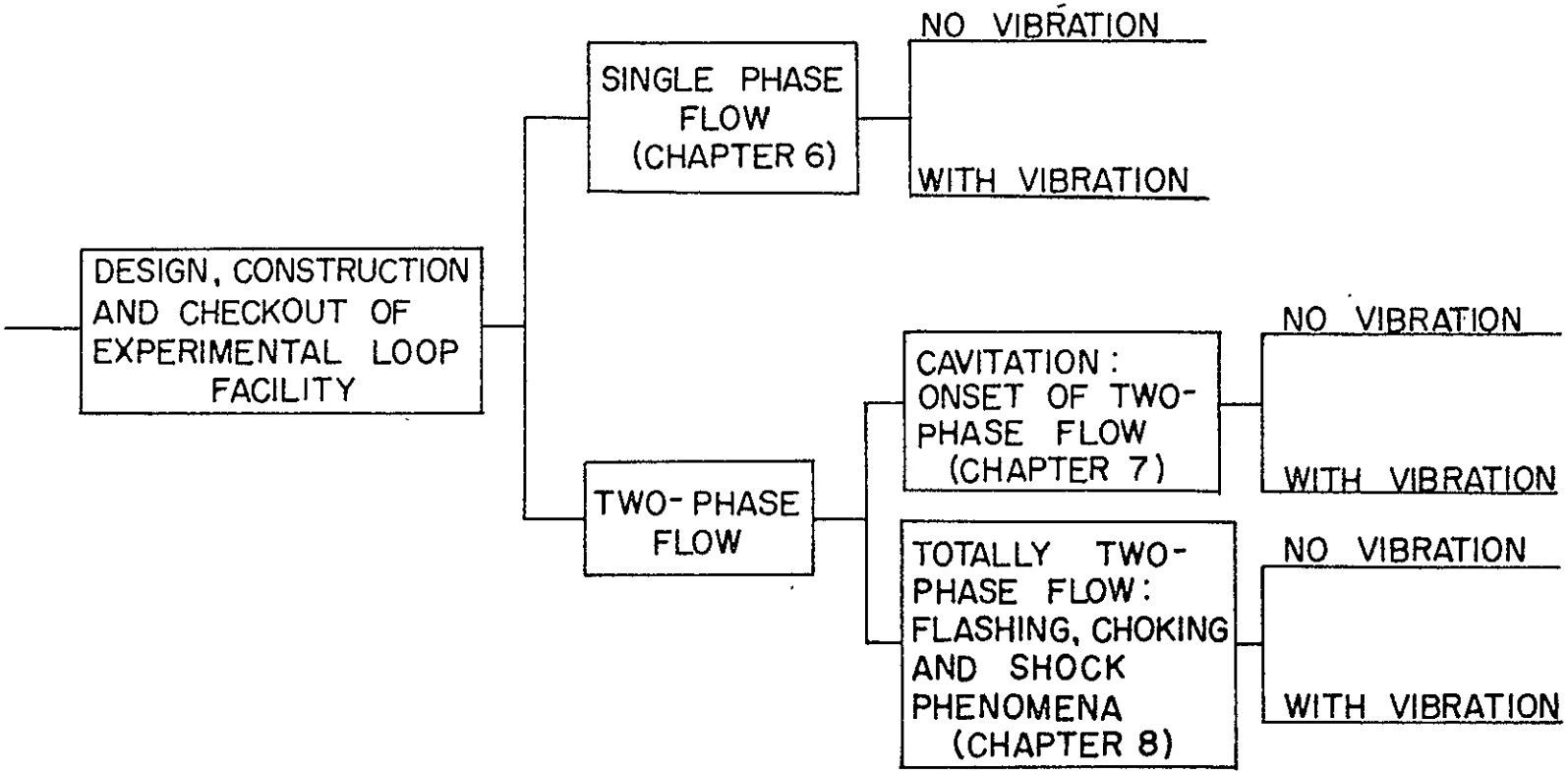

Figure 1. Organizational Arrangement of Overall Investigation.

CHAPTER 2
GENERAL DESCRIPTION OF LIQUID FLOW AND LIQUID-GAS FLOW PHENOMENA

In this chapter liquid flow and liquid-gas flow are described, and some of the useful analytical methods for treating them are briefly discussed. Consider a liquid flowing through a constriction in a line or past a sharp edged boundary. A localized region of high velocity and low pressure is present in either situation because of the necessary forces acting on the liquid to produce its rapid acceleration in such a region. If the pressure becomes low enough, the liquid may vaporize causing the onset of two-phase flow. Once two-phase flow occurs in these low pressure regions, the resulting bulk flow rate of the fluid can be changed very drastically in some instances.

A similarity analysis of adiabatic cavitation, which involves vapor generation in the absence of heat transfer, has led to the formulation of the cavitation number, σ. This parameter can be used to predict the onset of two-phase conditions in a given system; however, its effectiveness in such an application is limited by the condition of the liquid. Dissolved gases and entrained gas bubbles, as well as solid particles suspended within the liquid, tend to affect the

inception of cavitation. Consequently, these factors lessen the usefulness of the cavitation number in accurately predicting the onset of two-phase flow.

In high speed liquid flows, cavitation and other forms of two-phase generation can severely limit the validity of a single phase liquid flow analysis. The major difficulty lies in determining the limits of application of a predetermined liquid flow solution. Whether analytical solutions for the flow patterns are obtained from the use of Bernoulli's equation for incompressible flow, conformal transformation techniques, or very lengthy numerical solutions to the Navier-Stokes equations, they necessarily become invalid at the onset of a two-phase flow.

Since a high speed liquid flow can generate a two-phase flow situation, it also becomes desirable to obtain analytical descriptions of these more complex two-phase flow phenomena. However, the analysis of two-phase flow has been found to be quite difficult in general. Only recently has a concentrated effort been directed towards obtaining solutions to basic relations for two-phase flow. Many models have been postulated to describe the different flow regimes that characterize two-phase systems and to compare them with equivalent single phase systems. A few of the generally accepted flow patterns are classified as homogeneous, bubbly, stratified, annular, wavy, slug, plug, and spray. These patterns exist separately or in various combinations (such as spray-annular

or .-homogeneous bubbly flow), and the patterns may exist in different forms for vertical and horizontal flow situations. Generally speaking, the interactions between the two phases are not completely understood. Therefore, the relations for two-phase flow are not considered to be as well substantiated as those for single phase flow.

Choking of two-phase flows can occur just as in the case of single phase flow, but the resulting maximum two-phase flow rate is in general much lower than the maximum flow rate for the corresponding single phase flow. This phenomenon occurs when the fluid velocity equals its acoustic velocity at some location in the flow path. For an ideal incompressible liquid, the acoustic velocity is theoretically infinite. However, any real liquid that is typically assumed incompressible in reality does have some compressibility, and therefore possesses a correspondingly large, but finite value of the acoustic velocity. When a gas or vapor is present in a nearly incompressible liquid, the resulting two-phase fluid mixture displays some of the physical behavior of a highly compressible fluid. The available analytical expressions which predict choking conditions for such a two-phase fluid yield different results depending upon the type of flow pattern that is assumed. The homogeneous flow model is the most direct to use in deriving an acoustic velocity relation. This model is based on the concept of a pseudo fluid having homogeneous properties and a single,

definable two-phase acoustic velocity. In this formulation the two phases are combined, and the mixture is treated as a single, compressible fluid. The other models usually consider the acoustic velocities in the two phases as being different from each other. For the homogeneous mixture model, the predicted acoustic velocity exhibits a functional dependency on the void fraction and can be shown to have a minimum value at a void fraction of one-half.

When a saturated liquid flows into a region where the pressure is lower than the vapor pressure of the liquid, some of the liquid can "flash" into vapor resulting in a two-phase mixture. This phenomenon occurs due to very rapid property changes of the fluid which are brought about by bulk nucleation within the liquid. The validity of the homogeneous model for predicting the acoustic velocity and the resulting choking conditions becomes questionable when the homogeneous mixture results from flashing. The assumption that the vapor phase obeys the relations which describe compressible fluids is questionable because of the non-equilibrium effects of the flashing process.

The lack of a proper definition for the acoustic velocity in a flashing flow severely limits the usefulness of the acoustic velocity criterion for predicting the corresponding choking conditions analytically. A general definition for choking to be used in the remainder of this thesis,

and which can be applied to any type of flow, is the following:

> A flow system is choked when the mass flow rate reaches a maximum value for given upstream stagnation conditions which is not exceeded regardless of the downstream conditions. This implies that there is a critical exit pressure at which the maximum flow rate is attained, and a decrease in exit pressure below this critical value causes no further increase in the flow rate for the given, fixed, upstream stagnation conditions.

Obviously this definition can be applied to a gas, liquid, or a two-phase fluid, including one that is flashing, even though the non-equilibrium conditions in a flashing flow are not fully understood.

While the flow phenomena such as cavitation, flashing, and choking can be described on an individual basis to a limited degree of accuracy, the application of this knowledge should be extended to situations where interdependencies between them exist within a single flow system. The threshold conditions accompanying the onset of a two-phase mixture in an otherwise pure liquid flow should be investigated and specified for use in those areas of technology where these situations develop. That is, the limiting conditions of single phase liquid flow should be determined, and the initial conditions within the two-phase mixture should be specified to provide the necessary correlation between the two types of flow. Also, for any given flow system, the relationship between the two-phase phenomena and their overall effect on the flow and the overall system

performance should be described. That is, the pressure losses, flow rates, and velocities should be related to the many different flow conditions that can exist within a flow line. Only in this manner can effective engineering design of these systems be accomplished.

The following chapter describes the relationships between an application area of considerable interest (liquid fuel rocket technology), high speed liquid flow phenomena, and the research described in this investigation.

CHAPTER 3

RELATION OF RESEARCH TO LIQUID FUEL ROCKET TECHNOLOGY

The effects associated with high velocity liquid flows are ever present in liquid fuel rocket technology. This is due to the low temperatures of the cryogenic liquids used and the resulting high heat transfer rates that typically occur. In the case of the onset of two-phase flow, vaporization is brought about when the liquid reaches its saturation temperature corresponding to the local pressure. Thus, the presence of heat transfer enhances the occurrence of this condition. As a result of heat transfer, vaporization of liquid can occur in propellant tanks by boiling, and cavitation can be induced in the lines, both having possible detrimental effects on the total propellant discharge system performance.

Large flow rates are a necessity in some of the advanced rocket designs. For example, the first stage of the Saturn V rocket consumes approximately fifteen tons of propellants during each second of operation. The propulsion systems of liquid fuel rockets, including fuel tanks, discharge lines, pumps, valves, and associated hardware items, are designed to handle the propellants in their liquid phase. When

two-phase flow occurs due to vaporization of the liquid, serious effects on the performance of the total system can result.

Two-phase conditions which develop in propellant supply systems are believed to contribute to the existence of combustion instabilities in the rocket motors. These instabilities can cause severe vibration of the entire structure of a rocket. The dynamic effects are sometimes directly responsible for sizeable pressure fluctuations within the liquid propellants. The exact manner in which the structural vibrational characteristics of discharge lines affect liquid flow, as well as the inception of two-phase flow, is not well known or understood at present.

Certain dynamic effects of vibration on tanks, partially filled with liquid and pressurized with an ullage gas, have been investigated and explained previously, at least in a qualitative manner. The pressure oscillations within the fluid are dependent upon frequency, acceleration level, location in the tank or supply line, and structural rigidity. The stability of the interface between the liquid and the ullage gas in the tank is dependent upon the same parameters. Under certain specific conditions, considerable gas entrainment occurs at this interface resulting in large conglomerations of gas bubbles which subsequently become located at low pressure regions within the fluid. As the liquid level in a tank drops during discharge, the dynamic response of

the tank changes such that the bubble agglomerations either rise to the surface and dissipate into the ullage gas region, or are discharged into the supply line to be subsequently passed on to a pump, and perhaps also to the combustion chamber of the rocket motor. This type of two-phase flow is different from the cavitation phenomena described earlier since this occurs when the ullage gas is a permanent foreign gas which does not undergo a phase transformation to a liquid. The resulting liquid-gas flow is more properly defined as two-phase, two-component flow.

The entrainment of ullage gas into the liquid and the subsequent two-phase conditions can have a very serious effect on the propellent flow rate. The trapped ullage gas bubbles act as nuclei for large scale severe cavitation to develop. So significant is the effect of these nuclei on cavitation that extensive experimental work has been performed on cavitation resulting from longitudinal vibration in liquid-filled containers in the absence of flow. The implications of cavitation in a "no-flow" situation are significant since cavitation is usually associated with high velocity flows. How the effect of longitudinal vibration of a simulated discharge line affects cavitation inception during flow through the line has not been thoroughly investigated previously.

Experiments have shown that localized flashing can occur in a liquid container which is vibrated on an

electro-dynamic shaker at various frequencies and acceleration levels. It has also been shown that gravity driven discharge rates from containers exposed to vibration are reduced. The subsequent questions raised by these experiments are: What effect does vibration have on the single phase liquid flow through a discharge line? What effect does vibration have on choking and two-phase conditions within a discharge line, and how do these conditions affect the propellent transfer rates in a rocket system?

The answers to the above questions necessarily require a thorough knowledge of the phenomena which are occurring. To determine the current state of knowledge with regard to the phenomena involved in liquid fuel rocket technology and discussed in this chapter, a literature survey was conducted. A description of the pertinent contributions in this area is given in Chapter 4.

CHAPTER 4

LITERATURE SURVEY

An extensive research effort has been devoted to the field of two-phase flow in the past two decades. Numerous papers have been published covering the multitude of problems associated with cavitation, acoustic velocity, critical flow, boiling, mathematical modeling and many other topics not directly associated with this investigation. The references in these areas which are pertinent to the present study are discussed briefly in this chapter. Phenomena associated with a vibrating environment are of a more special nature, and these are reviewed subsequent to discussion of literature pertaining to two-phase flow.

Streeter (1)*, Shames (2), and Kenyon (3), describe the contributions of many past investigators in the science of fluid mechanics, and material from these well known texts formed the starting point for the single phase liquid analysis in the present study. The classic relations of fluid mechanics not only were useful for the liquid flow problem, but also served as the basis from which extensions to two-phase flows were made.

---

* Numbers in parenthesis represent references listed in the Bibliography.

Some of the very early contributions to the two-phase flow literature were associated with jet flow analysis of the situation in which a non-viscous fluid of large density was discharged into a second non-viscous fluid of much lower density. A review of work in the jet flow field was presented by von Mises (4) who also described his own derivation for the two dimensional slot flow solutions he collected. The most recent significant contribution to jet flow theory was made by Gurevich (5) who has included many references not previously available to free world researchers. This text also illustrates the use of complex analysis in solving certain types of fluid flow problems in two and three dimensions.

An experimental investigation by Rouse and Abul-Fetouh (6) was very pertinent to the present research. Their work on jet flows for axisymmetric geometries utilized an electrohydrodynamic analogy. The resulting experimental solution to an axisymmetric jet flow problem was shown to be in agreement with the two dimensional slot flow analysis performed by von Mises (4). It was shown that the two different geometric solutions presented in References (4) and (6), two-dimensional and axisymmetric respectively, yield the same numerical value of the contraction coefficient when the ratio of orifice size to tank size is the same. Thus, the two-dimensional analysis was extended to provide solutions for axisymmetric flow problems. Contraction coefficients

determined by Rouse and Abul-Fetouh (6) were used in the present investigation for analytically predicting choking conditions (Chapter 8).

A sizable compilation of many of the major references in two-phase flow has been given by Gouse (7) who lists thousands of papers in three sections for organizational purposes. There was no attempt by the author to discuss material within each individual paper, however. Rather, cross referencing by title, subject, and author was provided to facilitate the usefulness of the collection as a very desirable aid to research in two-phase flow.

Among the more specific research investigations of importance was that of Frinhard and Stephenson (8) which was directed at temperature and scale effects of cavitation in two types of jets. Incipient and desinent cavitation numbers were presented and a correlation between superheat, jet area, and flashing was given. Similar research was performed by Numachi, et. al. (9) who present data on effects of cavitation on the discharge coefficient for sharp-edged orifice plates. Kobayashi (10) performed a study similar to that described in Reference (9); however, his work on discharge coefficients and cavitation was performed using standard ASME long-radius flow nozzles and ISA flow nozzles. Gorinda Rao, et. al. (11) investigated cavitation in quadrant-edged orifices similar to those used by Numachi (9, 12). The researchers of Reference (11) were concerned with the

applications of graphical correlations between the cavitation number and coefficient of discharge for standard orifice meters.

The problem of scale effects in cavitating systems has been described extensively by Hall and Wislicenus (13). Some of the modeling parameters were tabulated by these investigators, and their effects were illustrated by using the similarity principle. A significant conclusion was that further experimentation and analysis should be conducted. A similar treatment of scale effects of cavitation has been given by Oshima (14). This study was restricted to the special case of axisymmetric bodies. Experimental data of Kermeen, et al. (15) and an analytical solution by Knapp (16) are included in Reference (14). The main interest in these papers lies in the proof of validity of applying the cavitation number to different geometric systems. The application of similarity conditions to cavitation is discussed in References (14-16), and its validity is supported on the basis of experimental results.

Hall (17) has noted a distinction between the appearance of cavitation under a diminishing pressure and the disappearance of cavitation under increasing pressure. Thus, he has defined the incipient and desinent cavitation numbers. Kermeen (15) and Hall and Treaster (18) came to similar conclusions concerning the significance of the previous history of the fluid in regard to incipient and desinent cavitation.

Kamiyama (19) found that the longer a region of liquid was subjected to a low pressure, the easier became the inception of cavitation.

The existence of dual cavitation numbers prompted Hall and Treaster (18) to consider the incipient and desinent cavitation numbers as being indicative of a hysteresis effect with a measurable cavitation-delay time. Unfortunately, the complexities of the problem allowed for only a qualitative, explanatory investigation of this effect. However, it was found in the present investigation that the existence of a measurable response time is an important consideration in the analytical treatment of cavitation in an oscillating pressure field.

In addition to the problem of cavitation, it is appropriate to consider the significance of other two-phase flow phenomena. Perhaps the most useful existing reference of a general nature is that provided by Collier and Wallis (20). This reference covers all aspects of two-phase flow, and many model formulations and specific analyses are included. The definitions and experimental and analytical relations were compiled in a systematic representation in this reference.

A one-dimensional solution for homogeneous flow presented by Collier and Wallis (21) illustrates the advantages of applying the pseudo fluid concept. Pressure drop relations and the one-dimensional Mach number for two-phase flow were used in order to analytically predict two-phase choking. The

general analytical formulations for two-phase flow noted in Reference (21) were used in the present study in the development of the analyses given in Chapters 6-8. In particular, the influence coefficient method of evaluating and describing the pressure gradient has been utilized in Chapter 8 to discuss a choking condition for two-phase flows.

The relationship between the choking phenomenon and the fluid acoustic velocity for single phase flows has been well described by Shapiro (22). An extension to the two-phase flow situation was given by Fouse (23), whose survey reports surprisingly low values for two-phase acoustic velocities. Several analytical flow models and their associated acoustic velocities have been discussed by Smith (24). Most of Smith's research was directed towards cryogenic fluids.

A study of critical flow of a non-cryogenic fluid has been performed by Levy (25). For the analytical model proposed by Levy, the velocity of each phase is represented by a mean value, and frictional and hydrostatic losses are neglected. Comparison of the predicted values with available measurements showed that these analytical predictions were in close correlation with the data. The advantage of this particular analysis lies in the fact that the predicted acoustic velocity is not dependent on the void fraction. Fauske (26) has used an annular type model for a critical flow analysis. The same model was used by Moody (27). Moody treated the local quality as an independent parameter

in his analysis. In a later publication by Moody (28), the existing flow models were used to predict the maximum flow rate for given upstream stagnation conditions. The effects of pipe resistance were accounted for in this analysis. An analytical model based upon flow parameters in the operating region approaching the critical flow condition has been presented by Nahavandi and von Hollen (29).

Collier and Wallis (30) list several references which report the use of a single phase flow equation for flow through a sharp edged orifice (31-34). They note that considerable uncertainty exists as to the application of the single phase equation when flashing occurs upstream. Zaloudek (33) has extended the single phase equation to apply to an application involving entrance choking for the situation in which the downstream pressure is the vapor pressure of the liquid corresponding to the upstream temperature. The correlation presented by Zaloudek (33) was noted as being valid for long pipes (L/d>10) with sharp edged entrances, as discussed by Collier and Wallis (30). A solution which is very similar to the choking expression of Zaloudek was used successfully in the present investigation in treating the choking of a flashing flow. The details of this treatment are discussed further in Chapter 8.

Research by Fauske (33, 34) on the "critical" pressure for short discharge pipes and subsequent modeling for this problem by Silver (35) were discussed further by Collier and

Wallis (30). The question of whether vaporization occurs on the surface of the liquid core, or nucleation occurs within the core of liquid, is also discussed in Reference (30).

The existence of a critical rate implies that the flow achieves its sonic velocity with the possible existence of a shock wave. Some research in this area has been performed by Eddington (36) who presented descriptions for normal and oblique shock phenomena in a homogeneous two-phase two-component system at high pressures. An analysis was performed for isothermal conditions, and the similarity between the two-phase analysis and a single phase compressible flow analysis was discussed. Other remarks relating to the existence of normal shocks have been made by Muir and Eichorn (37) and also by Elliott et al. (38). To the best knowledge of the author, there has been no previous research on shock waves in low pressure, two-phase, single component flashing flow. However, the basic approaches utilized in the analyses described above were most useful in the present study for formulating the equations governing a shock in flashing flow. These equations are presented in Chapter 8.

The extension of two-phase flow research to include vibrational effects has been very limited in scope so far. Most investigations in this area have dealt with liquids confined in vibrating systems, and have been primarily directed toward the stability of the liquid-gas interface and the dynamic interaction between the liquid and its

container. Typical of work in this field is the contribution of Bleich (39) which consisted of an analytical solution to the problem of a flexible, liquid-filled tank exposed to longitudinal forced vibration. Boundary conditions for both rigid and flexible tank bottoms were considered together with the effects of the compressibility of the liquid. Bleich later extended the analysis to include prediction of the motion of gas bubbles in a liquid subjected to longitudinal vibration (40). The results have considerable significance with regard to propellant supply systems of liquid fuel rockets. Additional studies of the motions of small gas bubbles in vibrating liquids have been performed by Baird (41) and Buchanan, et al. (42). Pounder, et al. (43) developed an analytical method to predict both inception and growth rates for gas and vapor bubbles in longitudinally vibrated tanks.

Schoenhals and Overcamp (44) presented an analysis of the periodic pressure variations in a longitudinally vibrated liquid-filled flexible container. Their prediction of the oscillating pressure distribution was extended in the present research to yield a modified cavitation number (Chapter 7).

Schoenhals, Winter, and Griggs (45) have presented measurements which show the effect of vibration on the liquid discharge rates from tanks subjected to longitudinal vibration. A flow retardation was found to exist due to the vibratory conditions. Pesar (46) provided further experimental

verification of the retardation effect first noted in Reference (45). The retardation was attributed primarily to a lower average pressure in the discharge tube inlet.

Research described in References (45) and (46) was concerned only with gravity discharge of simulated propellant tanks. However, these results naturally led to the expectation that a flow retardation could also occur under vibratory conditions in the case of forced flow due to a pressure drop, and this topic was investigated in the present study (Chapters 6-8).

The literature discussed up to this point has dealt with the various phenomena as if they were separate and independent physical processes. It is now appropriate to discuss the literature describing the effects that these combined phenomena can produce in a total system such as a liquid fuel rocket, for example. The problems associated with a rocket system are necessarily dependent upon many factors which can be included in an analysis if each of these factors can be accurately described.

Fashbaugh and Streeter (47) performed a transient flow analysis of a liquid feed system for a liquid propellant rocket subjected to longitudinal vibration. This paper is of considerable interest in that effects of cavitation (onset of two-phase flow) in the pump inlet were estimated from experimental data. Also, the analysis was directed towards a specific system, and correlation between theoretical

predictions and experimental data are included. The longitudinal vibrations of the system were modeled as being part of the POGO effect. (The dynamic interaction of the rocket system with the unsteady combustion in the motors is referred to as the "POGO effect".)

An analysis by Licht and Park (48) was performed to determine if POGO oscillations could develop in the Saturn V second stage due to interaction between the propulsion system and the longitudinal modes of vibration. A linear mathematical model was used. The stability (lack of POGO vibrations) was shown to be dependent upon pump compliance, line inertance, and structural damping. The dependence of the POGO effect on the parameters mentioned above was also considered in Reference (48). Since the total system was treated as a closed loop, each segment of the loop affected the performance of the total system. If conditions for two-phase generation develop in the line, the line inertance can change; and as a result, the overall performance of the loop can be affected.

An analog simulation of the dynamic characteristics of a rocket propulsion system was used by Lehner (49). In this work, parameters such as pump inlet cavitation compliance were studied so that their influence on the total system performance was determined, and the characteristic contributions of each specific phenomena to the instability problem were obtained.

It should be noted that the investigations described above were concerned with the total rocket system, and that the characteristics of each segment in the system can affect the behavior of every other segment. For example, the extent of pump inlet cavitation is partially dependent on the magnitude of the combustion instabilities in the rocket motor. And conversely, the combustion instabilities are partially dependent on the extent of the pump inlet cavitation.

The research conducted in the present investigation was concerned with two-phase generation and its interaction with a vibrating discharge line. The flow retardation effect described in References (45) and (46) prompted, in part, the initiation of the experimental program. The following chapter describes the experimental facility which was constructed for studying this effect and for observing the several other phenomena previously mentioned.

CHAPTER 5

EXPERIMENTAL INVESTIGATION

5.1 Description of Flow Facility and Equipment Specifications

The experimental facility was developed with the objective of simulation of a propellant tank discharge line which could be subjected to a wide range of operating conditions. Variables such as stagnation pressure and temperature, flow rates, pressure losses and gradients for pure liquid flow and for two-phase flow were to be measured and recorded. Also, those parameters not dependent on the geometry had to be sufficiently controllable in order to systematically cover the desired experimental combinations of flow variables. The geometry of the discharge line was an independent parameter.

A closed loop fluid flow system was designed and constructed. A schematic diagram of the resulting facility is shown in Figure 2. The test fluid is recirculated continuously through the system, thus assuring that the properties can be kept constant. The prime mover is a Roth two-stage turbine pump, Model #3751, driven by a fifteen horse-power U.S. Electric motor.

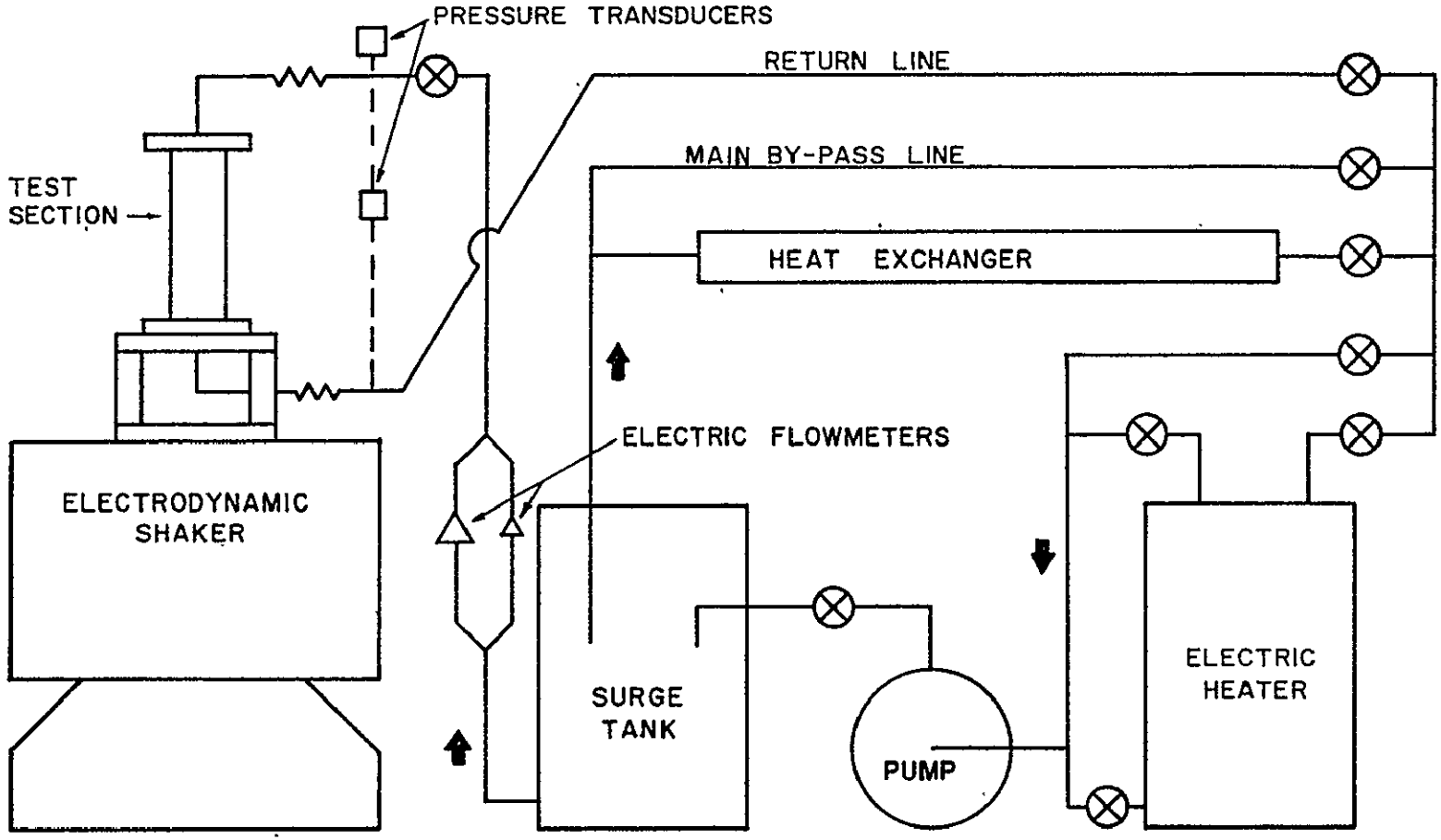

Figure 2. Schematic Diagram of Closed Loop Fluid Flow Facility.

The fluid is discharged by the pump into a glass lined surge tank and then flows either through a by-pass loop or through the main line to the test section. The ullage pressure in the surge tank is variable and is controlled by a National dual-meter pressure regulating valve attached to a high pressure nitrogen tank. The pressure can be increased by means of the reducing valve, and the bleed valve is used to reduce the pressure when desired.

The amount of flow through the test section main delivery line and through the by-pass line, respectively, depend upon the relative settings of the nine control valves in the system. All the valves shown in Figure 2 are teflon lined ball valves manufactured by Jenkins.

The main by-pass line consists of two inch galvanized steel pipe. The flow in the by-pass system can be controlled so that any desired portion of it is caused to pass through a Dupont shell and teflon tube heat exchanger. The flow rate through the exchanger is adjustable from zero to a maximum of 50 gpm at 150 psi. The coolant side of the heat exchanger is connected to a building main water line with a nominal average temperature of 55° F. It acts as a variable heat sink to control the temperature of the test fluid.

Once the by-pass fluid has traversed the heat exchanger and main by-pass, respectively, it can either flow through a glass lined electric heater or through another by-pass line around this heater. If the test loop is being operated

at elevated temperatures, varying amounts of the test fluid can be passed through the thermostatically controlled heater to maintain the proper temperature in the liquid in spite of free convection losses from the piping. Finally the by-pass fluid returns to the inlet of the pump.

The test section delivery line is also connected to the surge tank described above. A Fischer-Porter Model 10C1505 dual turbine flow metering system with automatic switching is located in a segment of straight pipe in this line. The meter serves as a continuous monitor of the fluid flow through the test section. Two one foot long flexible sections of steam hose serve as connectors between the delivery pipe and the test section. The flexible connectors are required in order to allow the test section to be vibrated on the electrodynamic shaker. The fluid passing through the test section is returned to the manifold system upstream of the pump inlet where it joins the fluid flowing in the by-pass system.

The shaker on which the test section is mounted is part of the vibrational facility shown schematically in Figure 3. The Calidyne Model 177A Electrodynamic Shaker is powered by a Westinghouse Industrial Audio Amplifier, Type FG-11. The control console consists of a combination of Calidyne Model 231 and Model 232 systems with a Bruel and Kjaer Audio Oscillator. A feedback loop consisting of a Bruel and Kjaer type 4334 crystal accelerometer and an Unhlotz-Dickie Model 608PS-1

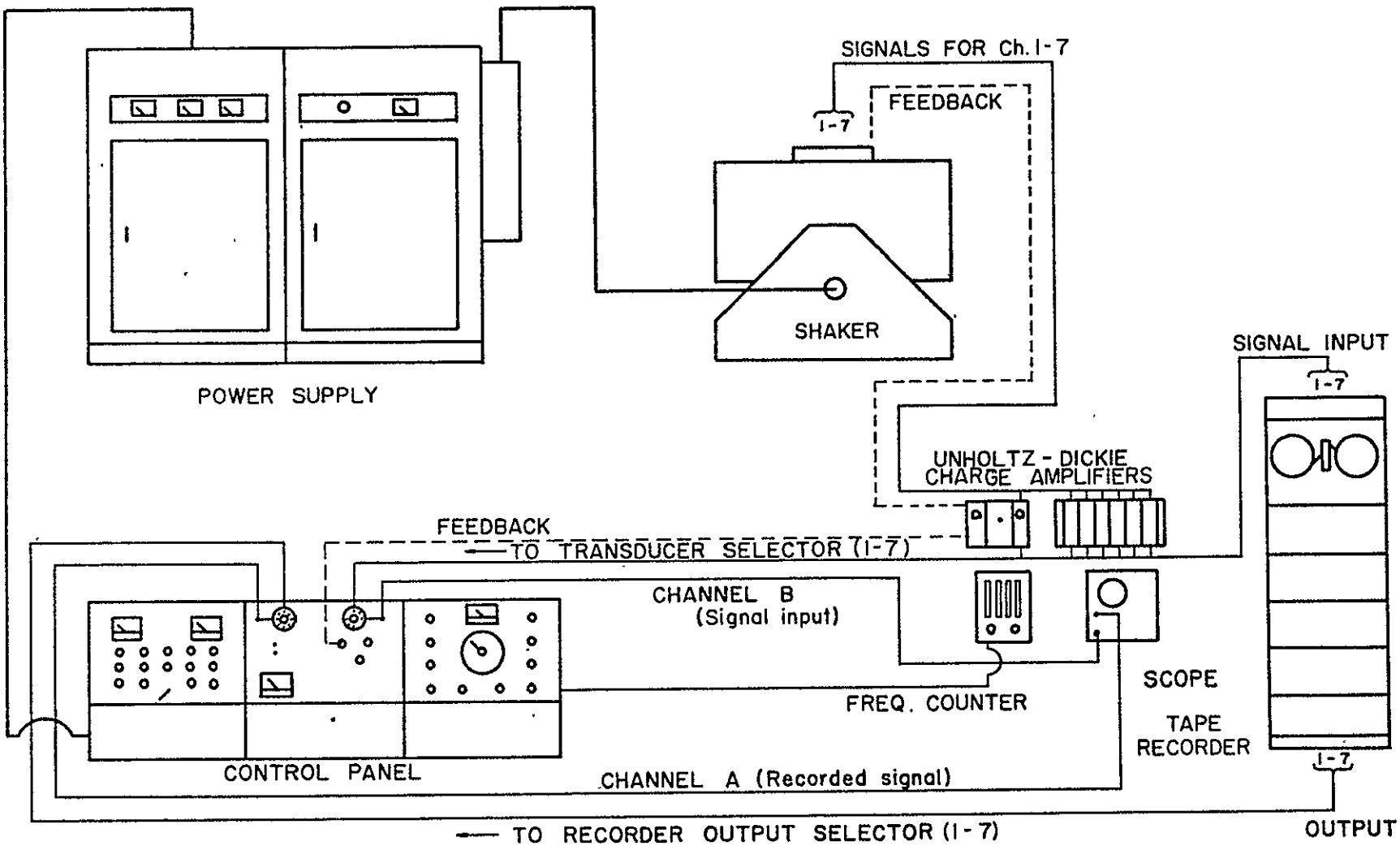

Figure 3. Shaker Facility Used in Experimental Investigation.

charge amplifier for signal conditioning are used to continuously monitor the vibrational conditions of the shaker table and to provide for the automatic functioning of the entire system. A CMC Model 226A Universal Counter-Timer is used to measure the frequency output of the Automatic Vibration Exciter Control. The facility provides excitation at frequencies from 10 to 2000 cycles per second and delivers forces up to a maximum of 5000 pounds.

Two pressure transducers are installed permanently in the main delivery line to the test section. The upstream transducer is a Pace Model P1A (0-100 psia), and the other is a Pace Model P7D (0-100 psid) differential transducer. Signal conditioning for both transducers is accomplished with a set of Carrier Demodulators Model CD10. The absolute transducer measures the static pressure in the delivery line. The upstream stagnation pressure is obtained by correcting for the dynamic pressure associated with the flow which is calculated using the measured flow rate. The differential transducer is used to measure the stagnation pressure loss across the test section. This setup is shown schematically in Figure 4.

Additional instruments permanently installed in the flow loop are a Fischer-Porter Model 1842 Industrial Rate Indicator (which serves as a readout device for the turbine flow meters) and a Leeds and Northrup multiple range potentiometer indicator (which is used together with an

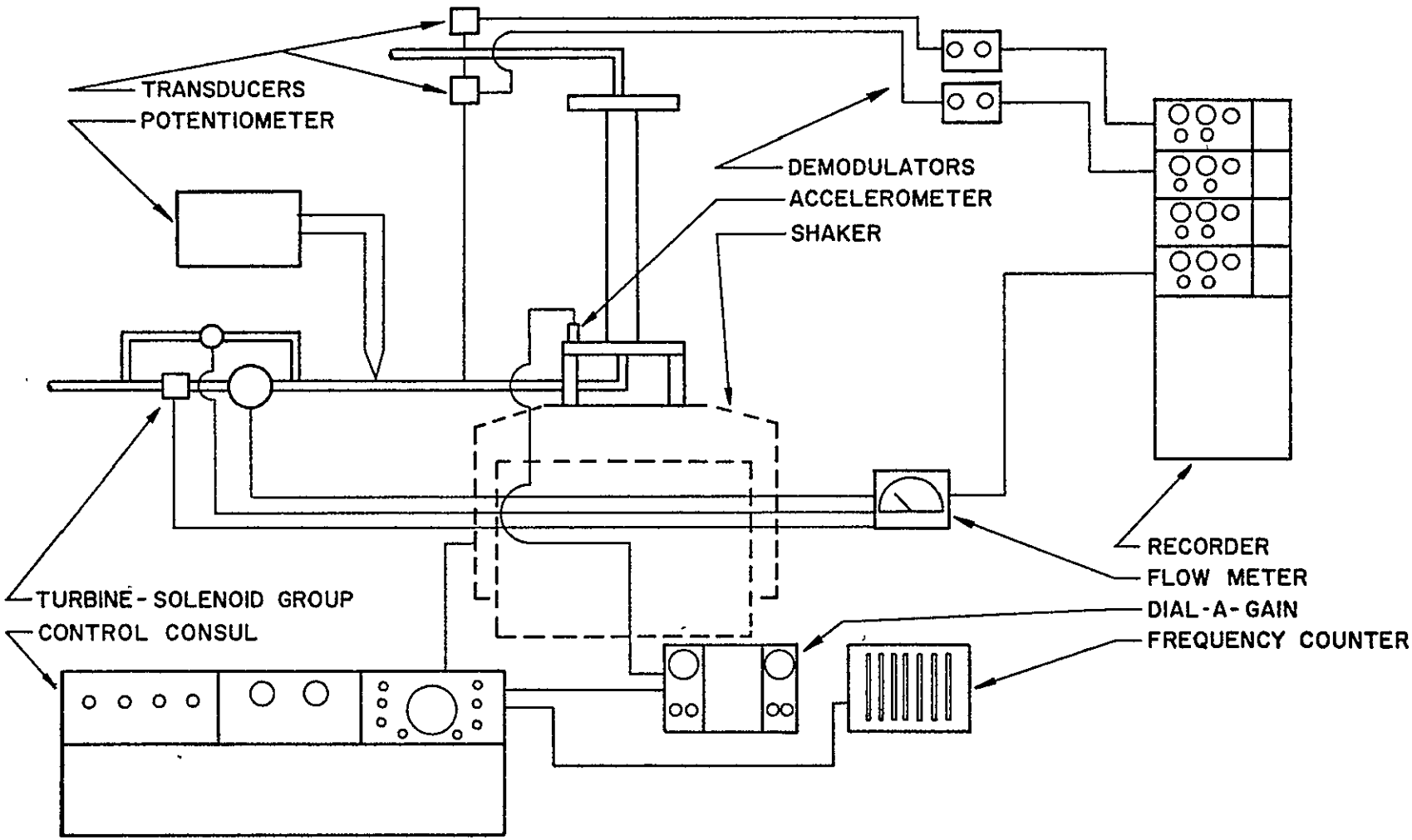

Figure 4. Permanent Instrumentation of the Combined Fluid Flow and Shaker Facility.

iron-constantan thermocouple to measure the fluid temperature).

Two different test section configurations were used in the experimental work. Both were constructed of plexiglass since visual observation of the test fluid required a transparent test section both for cavitation studies and for observations of two-phase choking. Plexiglass was chosen because of its transparency as well as its availability and relative ease of machining and fabrication. Several different sizes of cylindrical plexiglass tubes were used in order to achieve various geometries for the simulated discharge line. The disadvantages of this material were associated with its upper temperature limit of 174° F, a relatively low high pressure limit, and the lack of structural rigidity of the test section.

The more specific measurements associated with variables such as oscillating pressures and pressure gradients were obtained with the test configuration shown in the schematic diagram of Figure 5. Pressure taps located along the discharge line enabled the measurement of the static pressure along the wall. Data for frictional losses and pressure gradients in flashing flow were obtained using this test section. A Kistler Model 701A pressure transducer was used for measurement of the pressure fluctuations in the fluid when the test section was being longitudinally vibrated. This was mounted in the test section with the pressure tap

Figure 5. Schematic Cross-Sectional View of Specific Test Section.

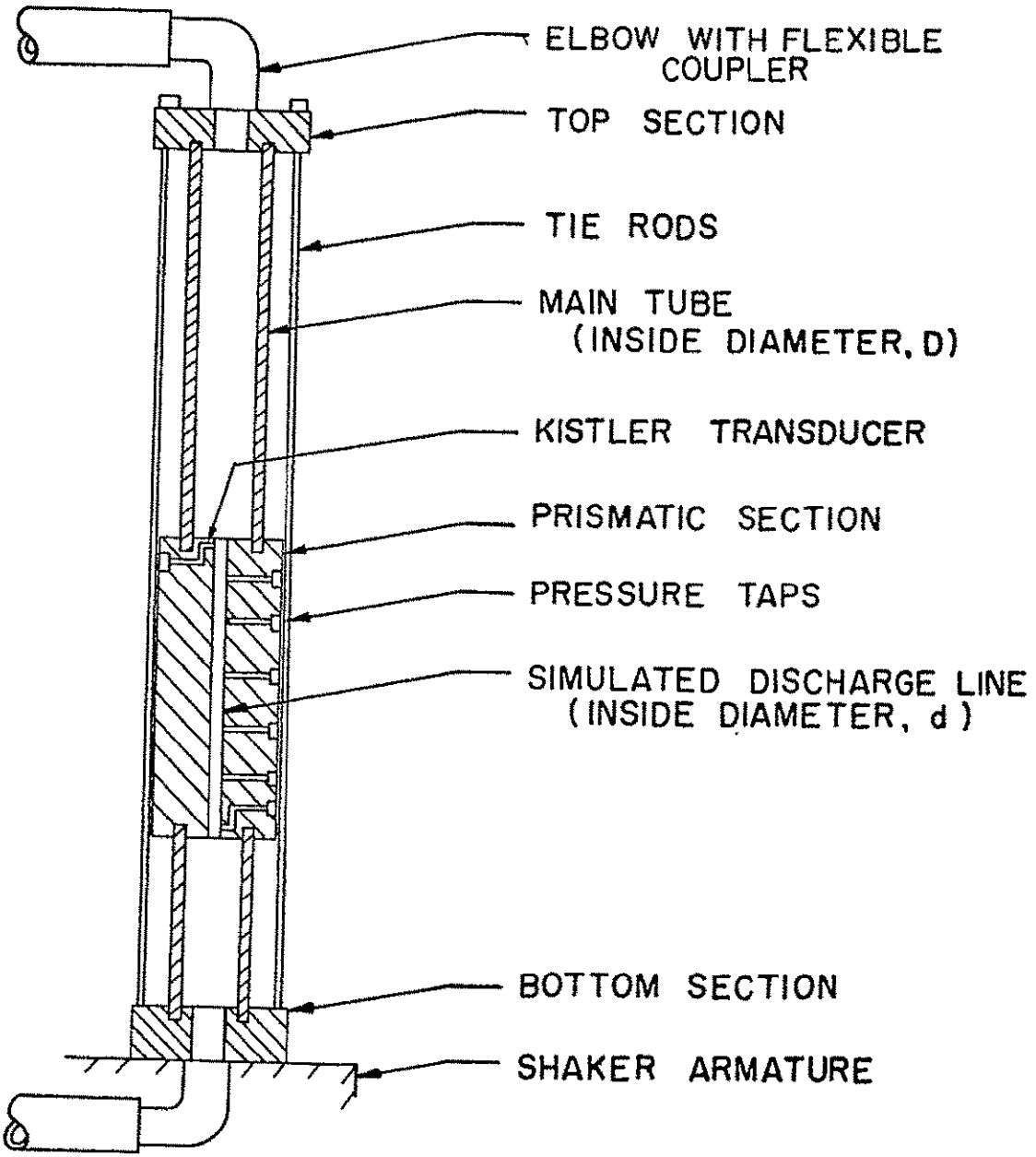
ELBOW WITH FLEXIBLE COUPLER
TOP SECTION
TIE RODS
MAIN TUBE (INSIDE DIAMETER, D)
KISTLER TRANSDUCER
PRISMATIC SECTION
PRESSURE TAPS
SIMULATED DISCHARGE LINE (INSIDE DIAMETER, d)
BOTTOM SECTION
SHAKER ARMATURE

Figure 5

located 0.125 inch from the sharp edged entrance of a 0.375 inch diameter discharge line. The transducer signal was conditioned by a Kistler SN 1911 Charge Amplifier and was displayed on a Tektronic Type 502A dual beam oscilloscope. The faces of the test section were made flat and were highly polished to allow for undistorted flow visualization. A photographic study was also conducted with this test section.

A second and more comprehensive test section, illustrated in the schematic diagram of Figure 6, was used to investigate other geometric configurations. No additional instrumentation for this test section was necessary since all data were obtained with the permanent instrumentation of the fluid flow loop.

Two Sandborn Model 150 Recorders were used for the simultaneous recording of pressures and flow rates as functions of time. Each unit contained four Model 150-400 Power Supplies and Model 150-100 AC-DC Preamplifier units with a Model 154-100 B Four Trace Recorder.

Visual observation of the flow in the discharge line under vibrating conditions was made possible with the aid of a Bruel and Kjaer Stroboscope Type 4910. This stroboscope is syncronized with the motion of the shaker table by adjusting the frequency signal of the Audio Oscillator installed in the control consol. The unit has allowance for an adjustable phase angle deviation from the motion of the shaker table. To the eye of the observer, the test section appears

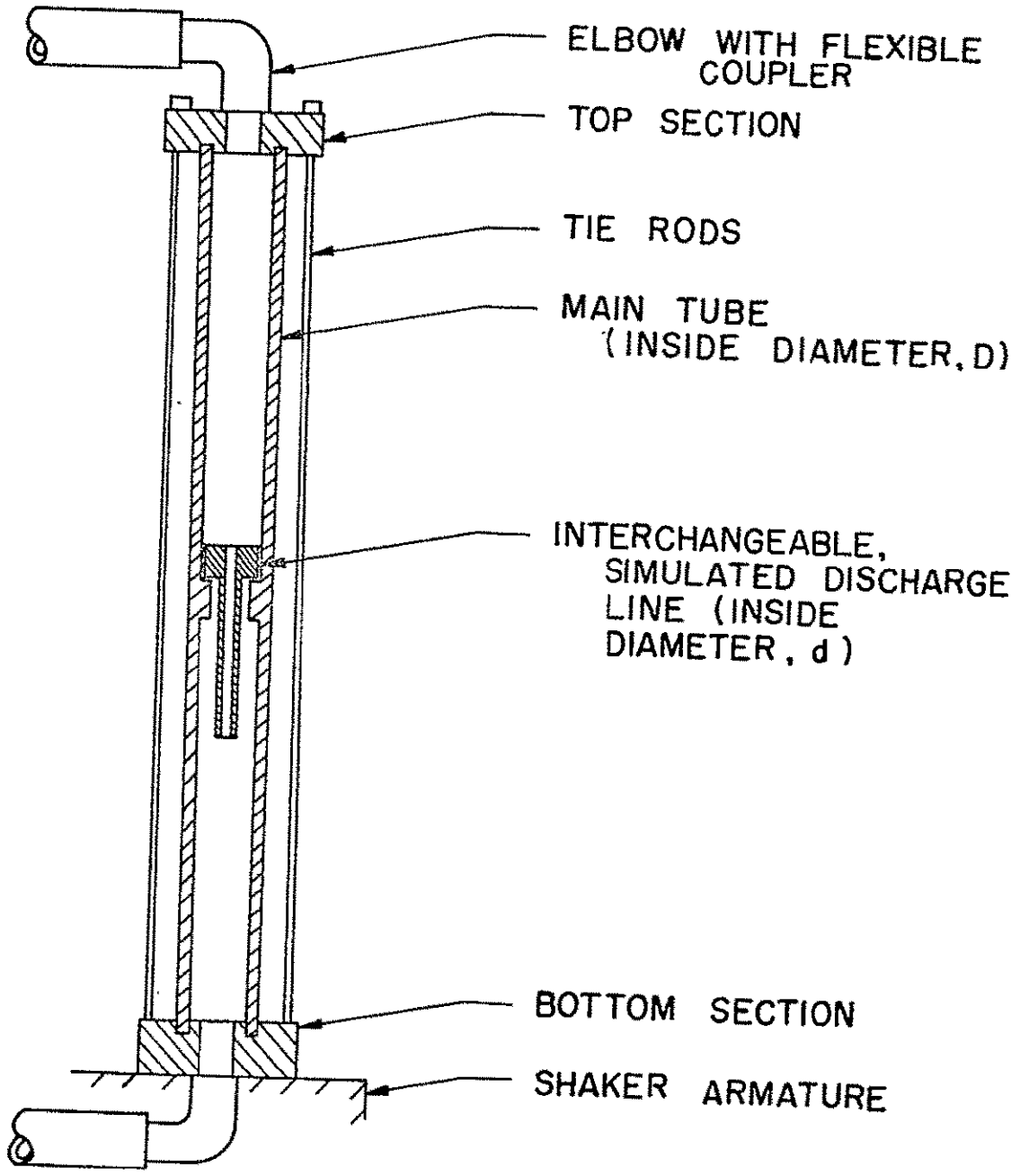

Figure 6. Schematic Cross-Sectional View of Variable Geometry Test Section.

stationary at any chosen position along its sinusoidal displacement path.

The test fluid used in the flow loop was water which was filtered in order to remove particles having diameters larger than four microns. Measurements of the surface tension were made periodically with a Fischer Porter Surface Tensiomat to check the water condition in the flow loop.

5.2 Description of Experimental Procedure

The first step, preceeding experimental measurements, involved calibration of the measuring instruments. Both Pace transducers were calibrated by means of a dead-weight tester and a standard pressure gauge of sufficiently high accuracy. The flow meters were provided with an internally adjustable calibration circuit which was installed within the rate indicator.

A typical liquid flow experiment was initiated by mounting the appropriate test section on the shaker table. The flow loop was then filled with water which was brought to the desired temperature. Finally all instrumentation was checked for proper operation.

All flow control valves were initially set in the full open position, and the pump was started. By proper adjustment of the valves, the fractions of the total pump flow through the by-pass line and the test section could be precisely regulated. Restriction of fluid flow through the by-pass line increased fluid flow through the test section

and vice-versa. The pressure in the test section could be controlled in two different manners. The first control was achieved by simply changing the ambient pressure in the surge tank by regulating a pressure reducing valve which was connected between the surge tank and the high pressure nitrogen bottle. In the second method, use was made of the various valves located in the loop. Proper adjustment of individual control valves permitted the selection of an appropriate stagnation pressure in the main delivery line for any desired flow rate. With both the stagnation pressure and the flow rate adjustable, many different types of experiments could be carried out within the performance range of the pump.

In a typical cavitation experiment, the stagnation pressure was held constant, and the flow velocity was increased until cavitation appeared. The stagnation pressure was then changed and the same operation was repeated for this new stagnation pressure value. If the test section was vibrated during a test run, the observer used the stroboscopic light to observe the cavitation, and the test section then appeared as a stationary object.

A typical choking experiment was conducted in a very similar manner. First, choking of the flow was induced at a given upstream stagnation pressure by reducing the exit pressure to a limiting value beyond which no further increase in the volumetric flow rate was observed. Although a normal

shock could occur at various locations in the discharge line, the exit pressure was always adjusted to a value which would drive the shock into the exit plane of the discharge line. The stagnation pressure was then increased with a simultaneous adjustment in flow rate to maintain the two-phase shock in the exit plane of the discharge line. In this manner many different combinations of flow rates and stagnation pressures were obtained. Choking experiments were performed in exactly the same manner when the test section vibrated.

The following three chapters contain the results of the experimental work, and they also include the corresponding analytical predictions for most of the cases investigated.

CHAPTER 6

SINGLE PHASE LIQUID FLOW IN A DISCHARGE LINE

6.1 Flow in the Absence of Vibration

The classical one-dimensional relations defining liquid flow in a circular pipe were used to predict static pressures and stagnation pressure losses in the discharge line. The objective of this investigative phase was to obtain a comparison with experimental data which would serve as a criterion for the reliability of the facility.

It follows from Streeter (1) that the static pressure in a pipe for one-dimensional flow of a single phase liquid is given by the relation,

$$p_n = P_s - \Delta P_{entrance} - \Delta P_{friction} - P_{dynamic} + \rho_f g z \cos \phi \tag{6.1}$$

where

$\Delta P_{entrance}$ = stagnation pressure loss due to vena-contracta

$\Delta P_{friction}$ = stagnation pressure loss due to friction in the pipe

$P_{dynamic}$ = dynamic pressure of liquid due to liquid motion

p_n = static pressure at location "n" along discharge line

ϕ = angle of inclination from the vertical

The definitions given by Streeter (1) are listed below using the parameter defined as V_f^*, the apparent liquid velocity. This term is used throughout the analysis, and it is carefully defined to prevent misunderstanding. The apparent liquid velocity is defined as the volumetric liquid flow rate measured by the turbine flow meters in the delivery line, divided by the cross sectional area of the discharge line. This means that when single phase liquid is flowing through the discharge line, the average liquid velocity in the discharge line equals the apparent liquid velocity. However, when a two phase (liquid and vapor) mixture is flowing in the discharge line, the average flow velocity does not equal the apparent liquid velocity but is a function of the void fraction and the term V_f^*. Thus for the single phase liquid, the definitions from Streeter (1) are

$$\Delta P_{entrance} = K\left(\frac{1}{2}\rho_f V_f^{*2}\right) \tag{6.2}$$

where $K = 0.5$ for the geometry investigated.

$$\Delta P_{friction}\Big|_0^z = \frac{fz}{d}\left(\frac{1}{2}\rho_f V_f^{*2}\right) \tag{6.3}$$

$$P_{dynamic} = \frac{1}{2}\rho_f V_f^{*2} \tag{6.4}$$

Substitution of the definitions into equation (6.1) results in the one dimensional equation governing the static pressure

in the discharge line.

$$p_n = P_s + \rho_f g z \cos \phi - \left(\frac{fz}{d} + 1.5\right) \frac{1}{2} \rho_f V_f^{*2} \qquad (6.5)$$

Friction was considered to be important not only for the single phase analysis but also for the two-phase analysis to be discussed later. Shames (2) presents friction factors in a Moody diagram. Representative values for a very smooth pipe are listed in Table 1.

Table 1

Friction Factors

V_f^* (ft/sec)	Reynolds No.	f
10	33,800	0.0222
20	67,600	0.0195
30	101,400	0.0178
40	135,000	0.0170
50	109,000	0.0163
60	202,500	0.0159
70	236,000	0.0154

An experimental verification of these values was performed. Two different pressure transducers were connected to pressure taps numbers 2 and 3, and numbers 3 and 4 respectively as shown in the schematic diagram, Figure 7. The pressure difference between the stations under flow conditions

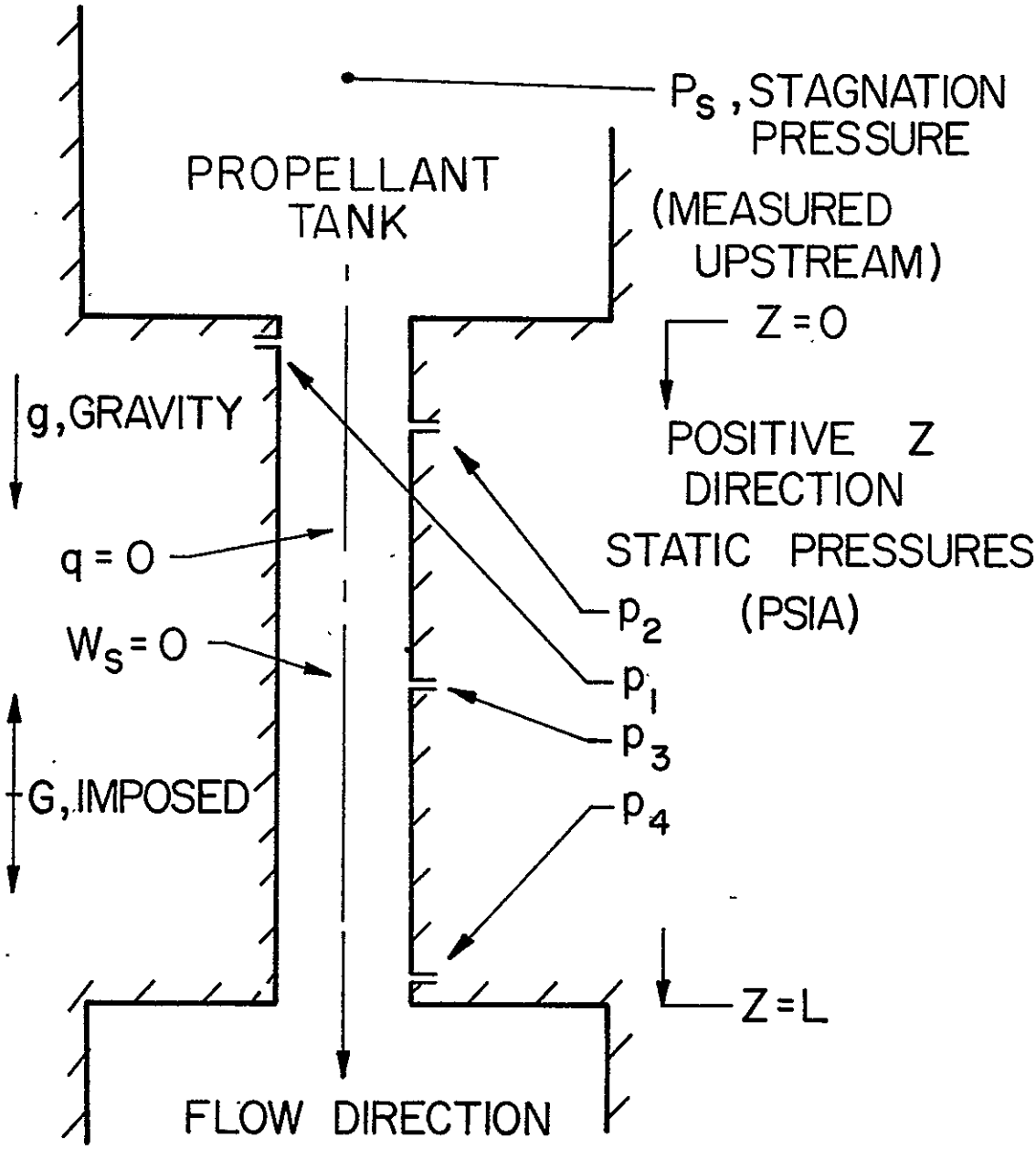

Figure 7. System Configuration of "Specific" Discharge Line and Propellant Tank.

represented the frictional pressure loss. A comparison between experimental data and predictions generated with equation (6.3) using friction factors from Table 1 is shown in Figure 8. The results of the one dimensional equation yielding static pressures in the discharge line, equation (6.5), are compared with experimental data in Figure 9, where the static pressures p_n, n = 1, 2, 3, 4, (the subscripts 1, 2, etc. define locations along the discharge line) are as illustrated in Figure 7. The value for the Reynolds number listed in Table 1 was obtained by using property values for water at 80° F. The majority of experiments for this initial phase of the investigation were conducted at this temperature.

An important feature of the geometric configuration illustrated in Figure 7 is the stagnation pressure loss caused by the sudden expansion of the single phase fluid as it discharges from the simulated discharge line. The flow pattern during expansion is shown schematically in Figure 10 which was taken from Kenyon (3). Streeter (1) derives an expression for the stagnation pressure loss due to a sudden expansion for the stagnation pressure loss due to a sudden expansion in terms of characteristic diameters which are indicated in Figure 10. The expression for the expansion pressure loss is noted subsequently.

$$\Delta P_{expansion} = \text{stagnation pressure loss due to sudden expansion}$$

$$\Delta P_{expansion} = \left(1 - d^2/D^2\right)^2 \frac{1}{2} \rho_f V_f^{*2} \qquad (6.6)$$

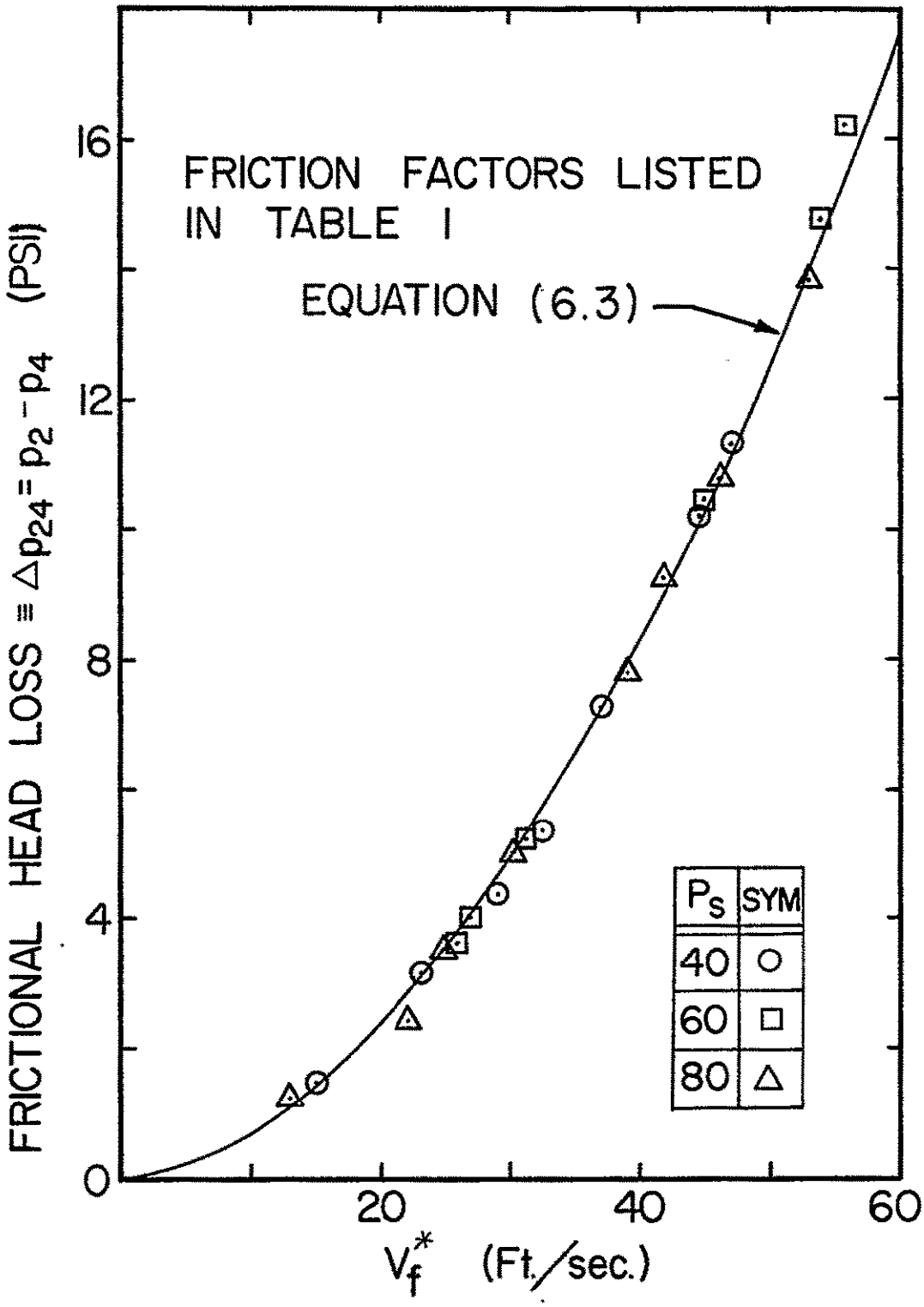

Figure 8. Illustration of Measured Frictional Head Loss as a Function of Apparent Liquid Velocity.

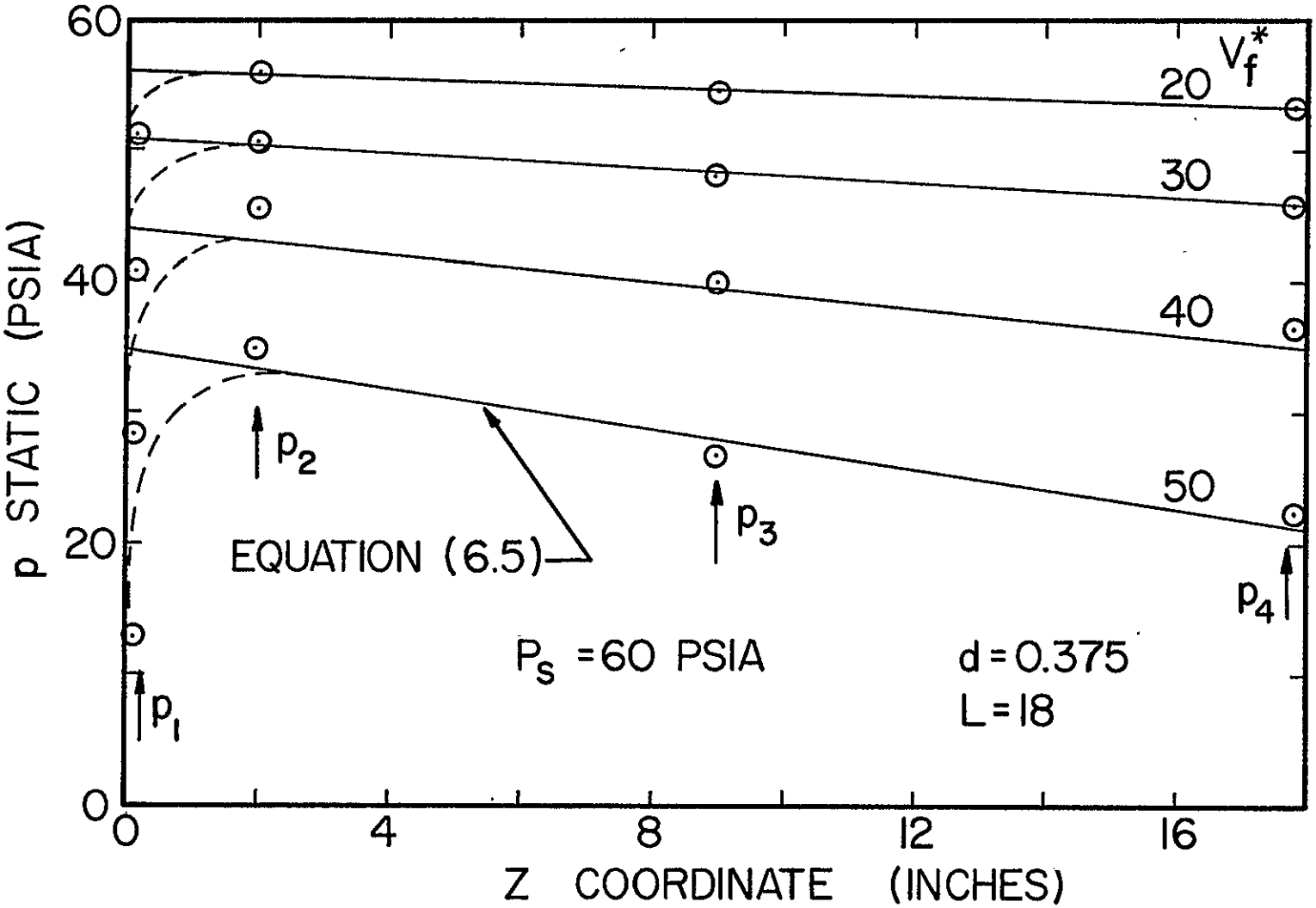

Figure 9. Illustration of Static Pressure Distribution Along Discharge Line Wall with Different Apparent Liquid Velocities at One Constant Stagnation Pressure.

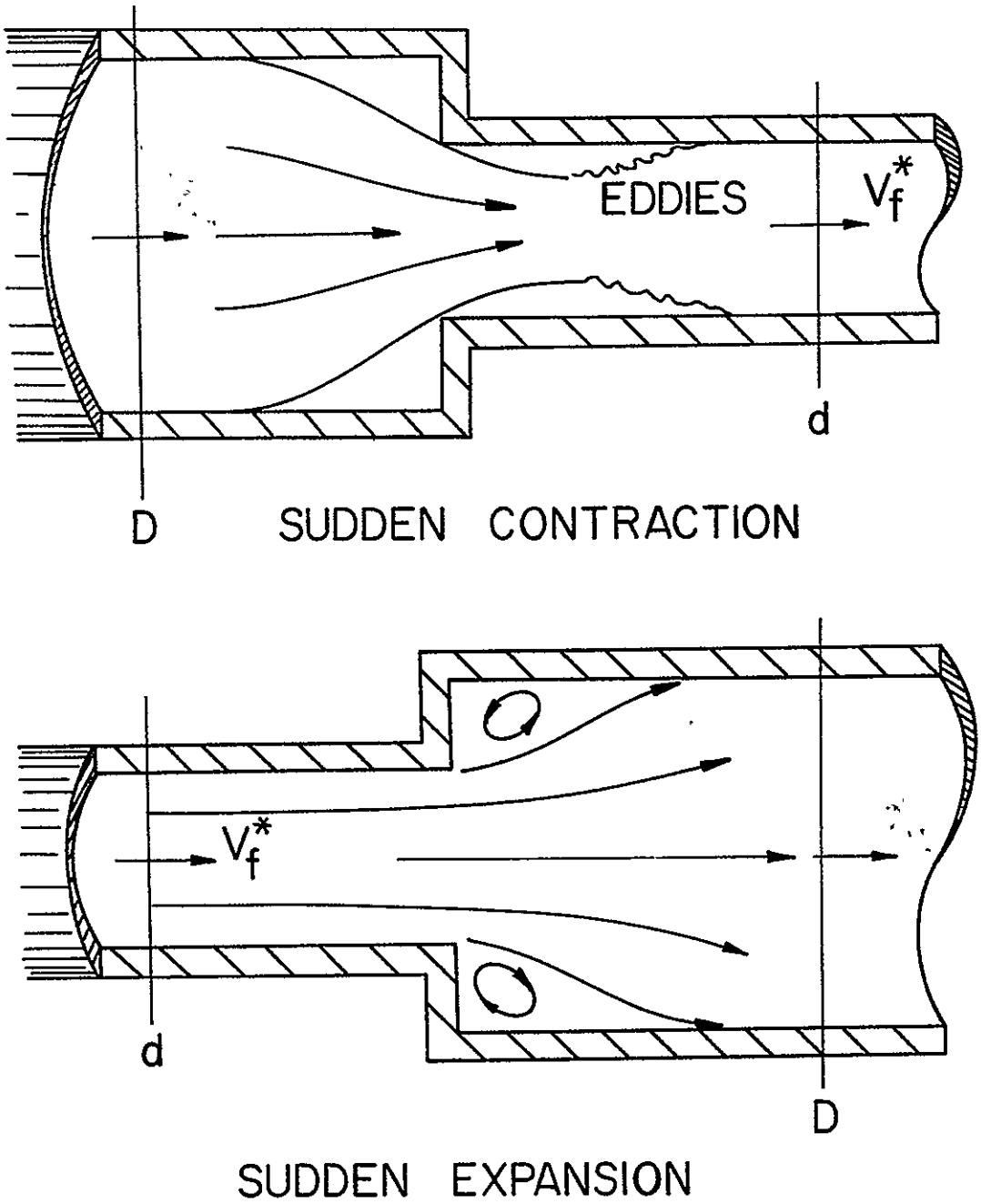

Figure 10. Single Phase Liquid Flow Through Sudden Area Changes from Kenyon (3).

The total sum of all stagnation pressure loss terms represents the irrecoverable pressure lost by the fluid flowing through the discharge line.

$$\Delta P_{loss} = \Delta P_{entrance} + \Delta P_{friction} + \Delta P_{expansion}$$

$$\Delta P_{loss} = \left[0.5 + \frac{fL}{d} + \left(1 - d^2/D^2\right)^2\right] \frac{1}{2} \rho_f V_f^{*2} \qquad (6.7)$$

This pressure loss was measured by the differential pressure transducer connected to the pressure taps located between the test section delivery line and exit line which are shown in Figure 4. The signal generated by the transducer was corrected for the losses caused by the elbows and the friction in the test section by measuring these losses without a discharge line present in the system. A comparison of experimental data for the stagnation pressure loss across the discharge line with the results of equation (6.7) is presented in Figure 11 for several different geometries.

The expansion pressure loss relation is assumed to be valid for the discharge line configuration shown in Figure 6 as well as for that configuration shown in Figure 5. This assumption is valid because of the nearly identical values of the loss coefficient,

$$\left(1 - d^2/D^2\right)^2 \approx 1.0 \qquad (6.8)$$

The condition of $d \ll D$ permitted the flow to be treated as that of a free jet expansion problem.

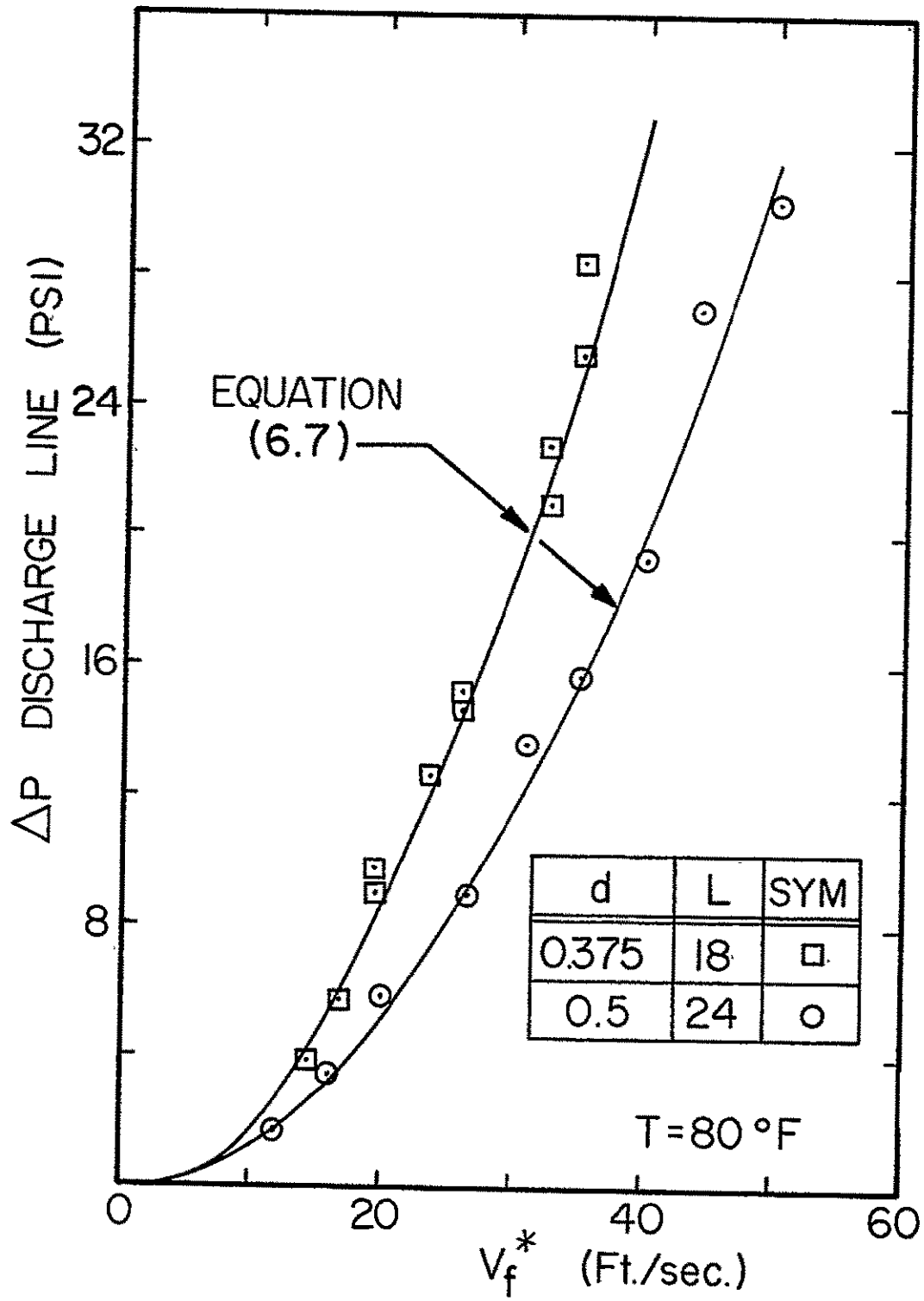

Figure 11. Stagnation Pressure Loss Versus Apparent Liquid Velocity for Different Liquid Flow Geometries.

The one-dimensional analysis for the static pressure distribution presented above becomes inadequate in the proximity of the sharp edged corner of the entrance to the discharge line. The experimental values of the static pressure, p_1, shown in Figure 9 were found to be very different from the values predicted by equation (6.5). The reason for this discrepancy was obviously the vena-contracta effect illustrated in Figure 10. In order to predict the static pressure, p_1, at the entrance to the discharge line and the local static pressure across the entrance plane, a three-dimensional analysis would have to be performed. Order of magnitude calculations demonstrated that the predictions obtained for a one-dimensional model differed by an order of magnitude from the experimentally determined pressures.

Since no three-dimensional solution to this problem was found in the literature and since a solution of this nature was beyond the scope of this investigation, it was decided to employ a less sophisticated two-dimensional model. The method of conformal transformation could have been applied to this type of two-dimensional flow problem. However, this method of solution was not considered. A conformal transformation flow solution to the geometry of the discharge line necessarily required negative pressure values at the sharp edged entrance. It also required that the fluid did not separate from the physical boundary. The vena-contracta

effect combined with the physical reality of having a finite pressure at the corner were powerful arguments against using a boundary mapping solution for the velocity and pressure fields.

A free-streamline model was considered as being more representative of the fluid flow near the corner. Although the free streamline concept is usually applied to a liquid in contact with a fluid of much lower density, nevertheless the free streamline was considered adequate for the description of the flow in the region at the entrance to the discharge line. This assumption was based on two arguments:

1. The area ratio $(d/D)^2$ was always very small, and the flow rates were usually high enough to cause significant acceleration forces on the fluid flowing into the discharge line.
2. The region of application was very limited in size.

Since the theory of the free-streamline can be found in many textbooks, it is not rederived here. For a general solution to the problem of flow from a vessel, von Mises (4) showed that most flow situations were particular cases of a well defined problem. This problem is illustrated in Figure 12 which was taken from von Mises (4). For the problem under investigation, shown in Figure 13, the constants used by von Mises are given below.

The values of von Mises' constants are:

$$K = 1/2 \ .$$

$$\beta = 0$$

$$a = b$$

$$j = D/2$$

A and E coincide

The free streamline analysis lead to the determination of the contraction coefficient which is defined by the asymptotic width of the resulting jet.

$$C_c \equiv \text{contraction coefficient}$$

$$C_c \equiv \frac{\text{asymptotic area of free jet}}{\text{area of orifice}}$$

$$C_c = \beta/b \text{ in Figure 13} \qquad (6.9)$$

Since the velocity along the free streamline is constant and the final flow area is known, the pressure along the free streamline can be determined immediately from Bernoulli's equation.

Table 2 represents the tabulations of contraction coefficients arrived at by the solutions of the two-dimensional problem posed in Figure 13 and cited by Gurevich (5).

Table 2

Contraction Coefficients

b/B	C_c	b/B	C_c
0.0	0.611	0.5	0.644
0.1	0.612	0.6	0.622
0.2	0.616	0.7	0.687
0.3	0.622	0.8	0.722
0.4	0.633	0.9	0.781

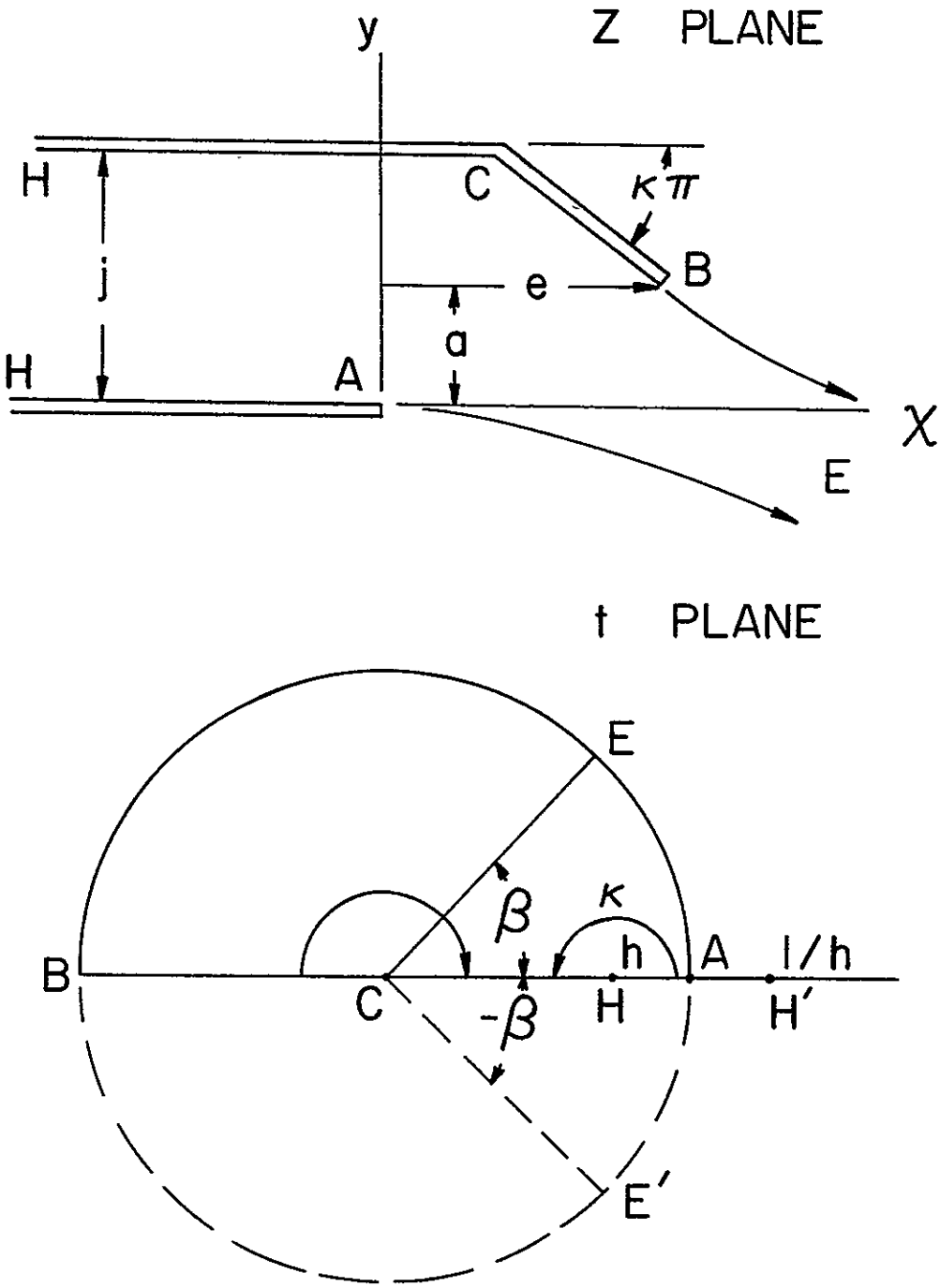

Figure 12. General Free Streamline Liquid Flow Problem and Method of Solution from von Mises (4).

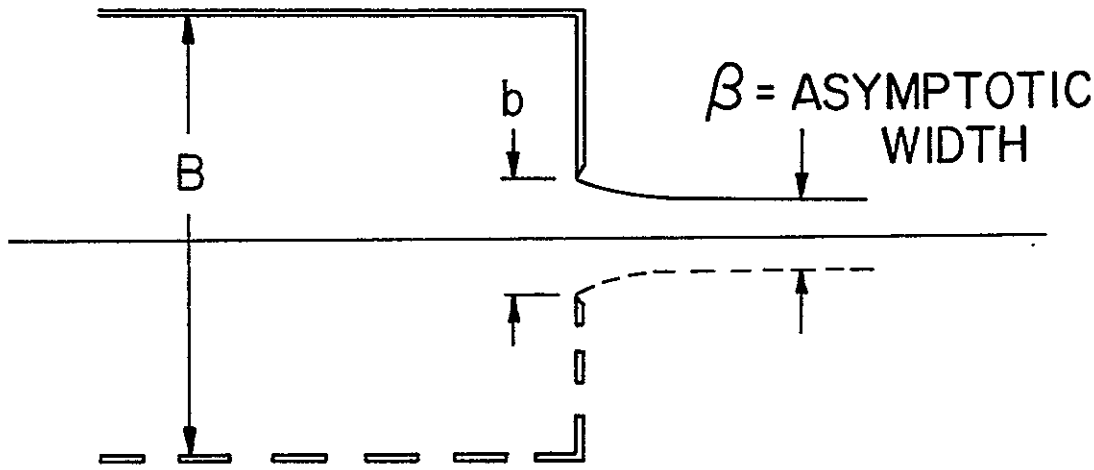

Figure 13. Two-Dimensional Liquid Flow Problem from von Mises (4).

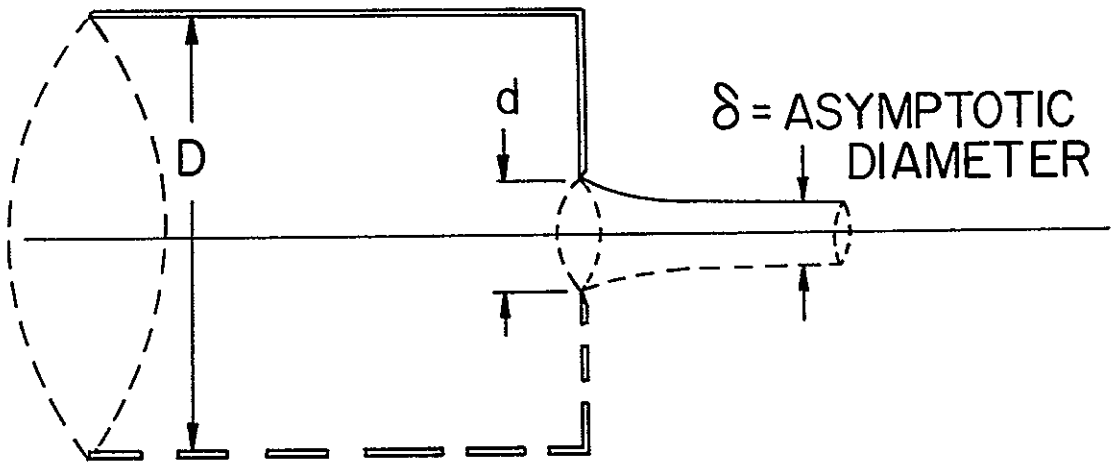

Figure 14. Axisymmetric Liquid Flow Problem from Rouse and Abul-Fetouh (6).

The tabulations of von Mises are solutions for two-dimensional problems only. The problem on hand is a special case of a three-dimensional flow, namely axisymmetric flow. An axisymmetric flow problem is formulated below.

$$\frac{\partial \phi}{\partial z} = \frac{1}{r} \frac{\partial \psi}{\partial r} = V_z \tag{6.10}$$

$$\frac{\partial \phi}{\partial r} = - \frac{1}{r} \frac{\partial \psi}{\partial z} = V_r \tag{6.11}$$

where ϕ = potential function

ψ = stream function

r = radial coordinate

z = longitudinal coordinate

Θ = angular position coordinate

By differentiating and combining equations (6.10) and (6.11), Laplace's equations for axisymmetric flow are obtained

$$\frac{\partial^2 \phi}{\partial z^2} + \frac{\partial^2 \phi}{\partial r^2} + \frac{1}{r} \frac{\partial \phi}{\partial r} = 0 \tag{6.12}$$

$$\frac{\partial^2 \psi}{\partial z^2} + \frac{\partial^2 \psi}{\partial r^2} - \frac{1}{r} \frac{\partial \psi}{\partial r} = 0 \tag{6.13}$$

The hydrodynamic problem is solved when the functional relationship of either $\phi(r,z)$ or $\psi(r,z)$ is determined. Along the free streamline, the boundary conditions are known.

$$\frac{\partial \phi}{\partial n} = 0 \tag{6.14}$$

$$\psi = \text{constant}$$

where $n \equiv$ outward drawn normal

The solution of the above equations leads to great mathematical difficulties. While the only known three-dimensional solutions are given for axisymmetric jet flows, Gurevich (5) points out that papers dealing with axisymmetric jet flows either describe theorems of a general or qualitative nature or present solutions which are at best numerical or approximate.

An analogue solution of the problem illustrated in Figure 14 was given by Rouse and Abul-Fetouh (6). These authors used an electrohydrodynamic analogy to solve the problem of flow of a circular jet from an infinitely long circular vessel. Rouse and Abul-Fetouh (6) have tabulated the contraction coefficients of the axisymmetric flow problem which was solved earlier for a two-dimensional model by von Mises (4). The coefficients are listed in Table 3.

Table 3

Comparison of Contraction Coefficients for Slots and Orifices. (Taken from Rouse and Abul-Fetouh (6) and von Mises (4).)

$(b/B)^2 = (d/D)^2$	C_c, Slot von Mises	C_c, Orifice Rouse and Abul-Fetouh
0.00	0.611	0.612
0.25	0.644	0.644
0.50	0.689	0.691
0.75	0.757	0.757
1.00	1.000	1.000

At equal values of the ratios describing the geometries of the problems,

$$\left(\frac{b}{B}\right)^2 = \left(\frac{d}{D}\right)^2 \tag{6.16}$$

the contraction coefficients are equal.

Using the theory of free streamline flow and the fact that the contraction coefficient yields an effective flow area, the static pressure in the area between the free streamline and the wall of the discharge line geometry illustrated in Figure 10 can be approximated. Since the pressure and velocity along this particular streamline are constant from its starting point at the sharp-edged entrance to its final point of deterioration, Bernoulli's equation can be used to obtain the value of the static pressure along this streamline.

Neglecting the gravity force for the liquid within the small entrance region, the total pressure along the streamline is defined as:

$$P_s = p' + \frac{1}{2} \rho_f V'^2 \tag{6.17}$$

where p' ≡ static pressure along the free streamline

V' ≡ constant velocity along the free streamline

Using the contraction coefficient and the continuity equation with equation (6.17) the static pressure equation was obtained as follows.

Continuity: $$\rho_1 A_1 V_1 = \rho_2 A_2 V_2 \tag{6.18}$$

$$\rho_f V_f^* A_d = \rho_f V' A_{jet} = \rho_f V' C_c A_d \tag{6.19}$$

$$\text{or} \quad V' = V_f^*/C_c \tag{6.20}$$

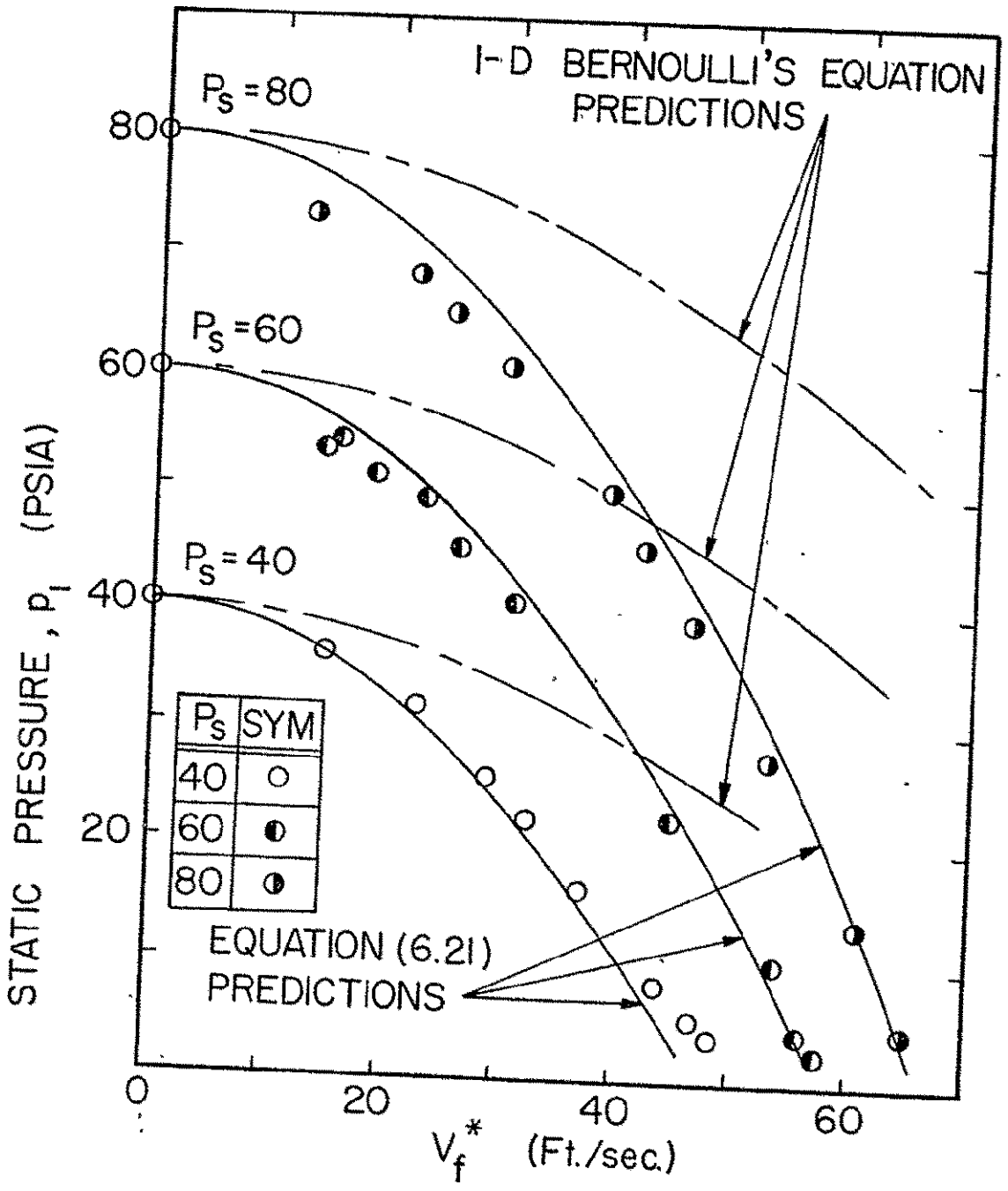

Figure 15. Static Pressure as a Function of Apparent Liquid Velocity 1/3 Diameter Downstream from the Sharp Edged Entrance in the Discharge Line Under Various Stagnation Pressures.

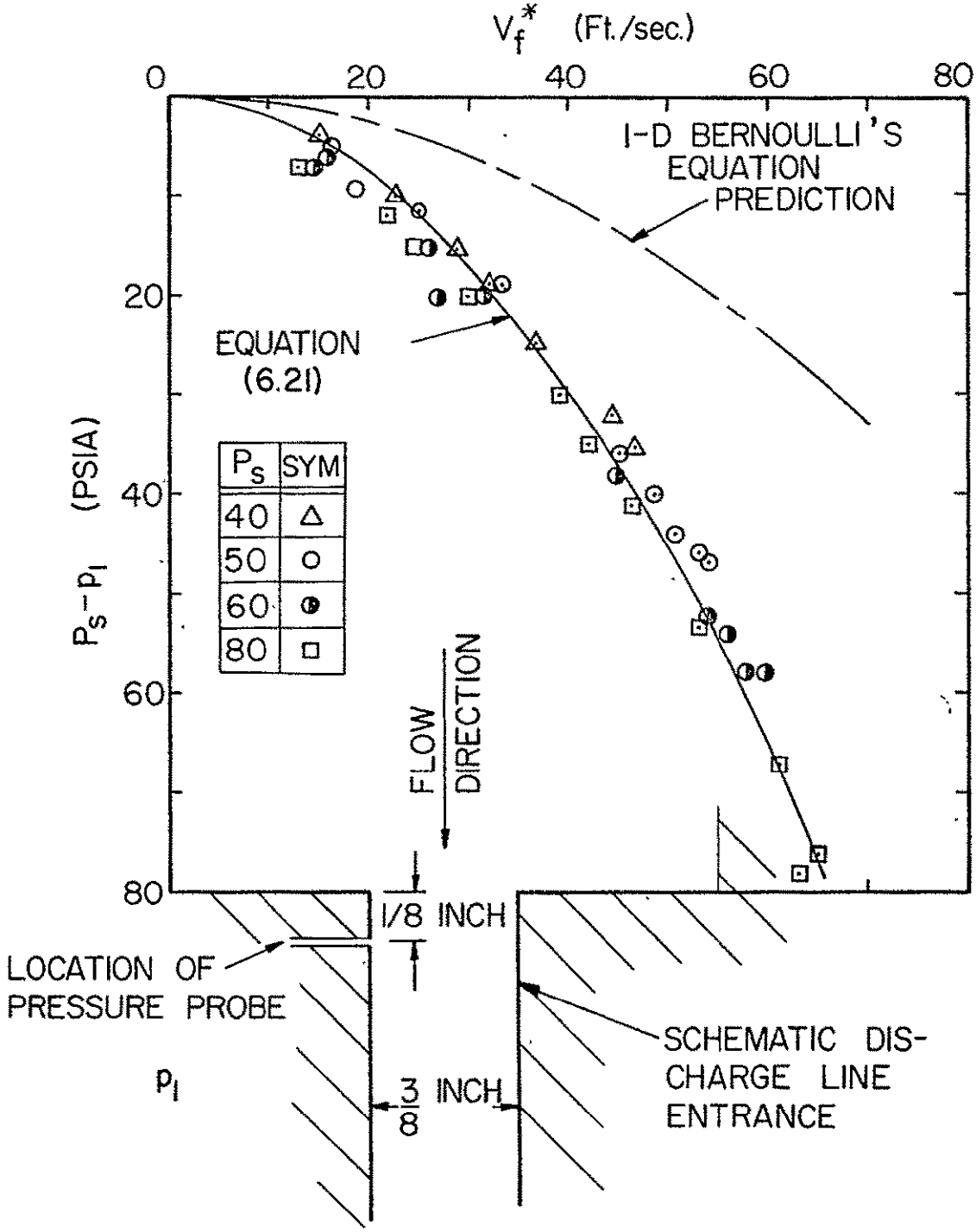

Figure 16. Dynamic Pressure as a Function of Apparent Liquid Velocity 1/3 Diameter Downstream from the Sharp Edged Entrance in the Discharge Line Under Various Stagnation Pressures.

Therefore

$$p' = P_s - \frac{1}{2} \rho_f \left(V_f^*/C_c\right)^2 \qquad (6.21)$$

Equation (6.21) describes the static pressure along the free streamline only as long as the jet persists. The region noted as "eddies" in Figure 10 represents the limit of the applicability of equation (6.21). The static pressure in the fluid in the eddy flow region is very difficult to predict analytically.

Data taken by a static pressure probe located 0.125 inch downstream from the entrance of a 0.375 inch diameter discharge line are compared in Figures 15 and 16 with the analytical predictions obtained by solving equation (6.21). Note that in these figures, the relation (6.21) is compared to a one-dimensional Bernoulli's equation. The only factor considered in the one-dimensional equation was the area change in going from the flow area with diameter, D, to the discharge line with diameter, d.

6.2 Single Phase Flow in the Presence of Longitudinal Vibration

In order to study the influence of vibration on the single phase flow in a discharge line, an experimental investigation was conducted. The influence of frequency and acceleration level was measured for various flow rates and geometric flow configurations of the discharge line. While

vibrations in a real situation are usually random in nature, the correlation between frequency and acceleration and physical flow effects could best be determined for a sinusoidal vibration situation. This restriction to sinusoidal vibrations was also necessitated by the lack of random vibration capabilities of the vibrator facility.

Initial data were taken for the pressure loss across the test section with the discharge line removed. In this calibration procedure the pressure losses caused by the elbows and other fittings in the test section were determined. Thus data obtained with the discharge line installed in the test section could be corrected for the pressure losses not directly associated with the discharge line.

Data obtained for the stagnation pressure loss across the test section in the absence of vibration with the discharge line removed are presented in Figure 17. A comparison for cases where frequency and acceleration are independent variables is illustrated in Figure 18. Data are shown and a comparison with the best fit curve for the non-vibratory situation (F = 0) is included in these plots.

The obvious conclusion is that the stagnation pressure loss increases where vibration is present. For a given frequency, the pressure loss increases with increasing acceleration level. This is consistent with the fact that at higher acceleration levels for a given frequency the displacement amplitude is larger than at lower acceleration

levels. Thus the larger magnitude of vibration would cause a larger loss in stagnation pressure.

The results obtained in the experimental investigation of the stagnation pressure losses across the test section with the discharge line installed are similar to those described above. A vibrated test section where the discharge line was installed showed an increase in the stagnation pressure loss. However a significant difference was noted when the data was corrected to represent the stagnation pressure losses only across the discharge line rather than the combination of the line plus test section. When the values for the pressure losses across the test section without discharge line present were subtracted from the pressure losses across the test section with the discharge line installed, the pressure loss values were lower for the cases where vibration was present than for the non-vibrating case. This can be stated in a different manner by saying that the pressure loss increase for the test section without the discharge line was greater than the pressure loss increase for the test section with the discharge line installed under the same conditions of flow rate, vibrational frequency, and acceleration level. These data are presented in Figures 19 and 20 for various vibration conditions and geometries.

The fact that vibration of a discharge line retards the flow has been noted previously by Pesar (46) and in reference (45). This corresponds to having a larger pressure loss at

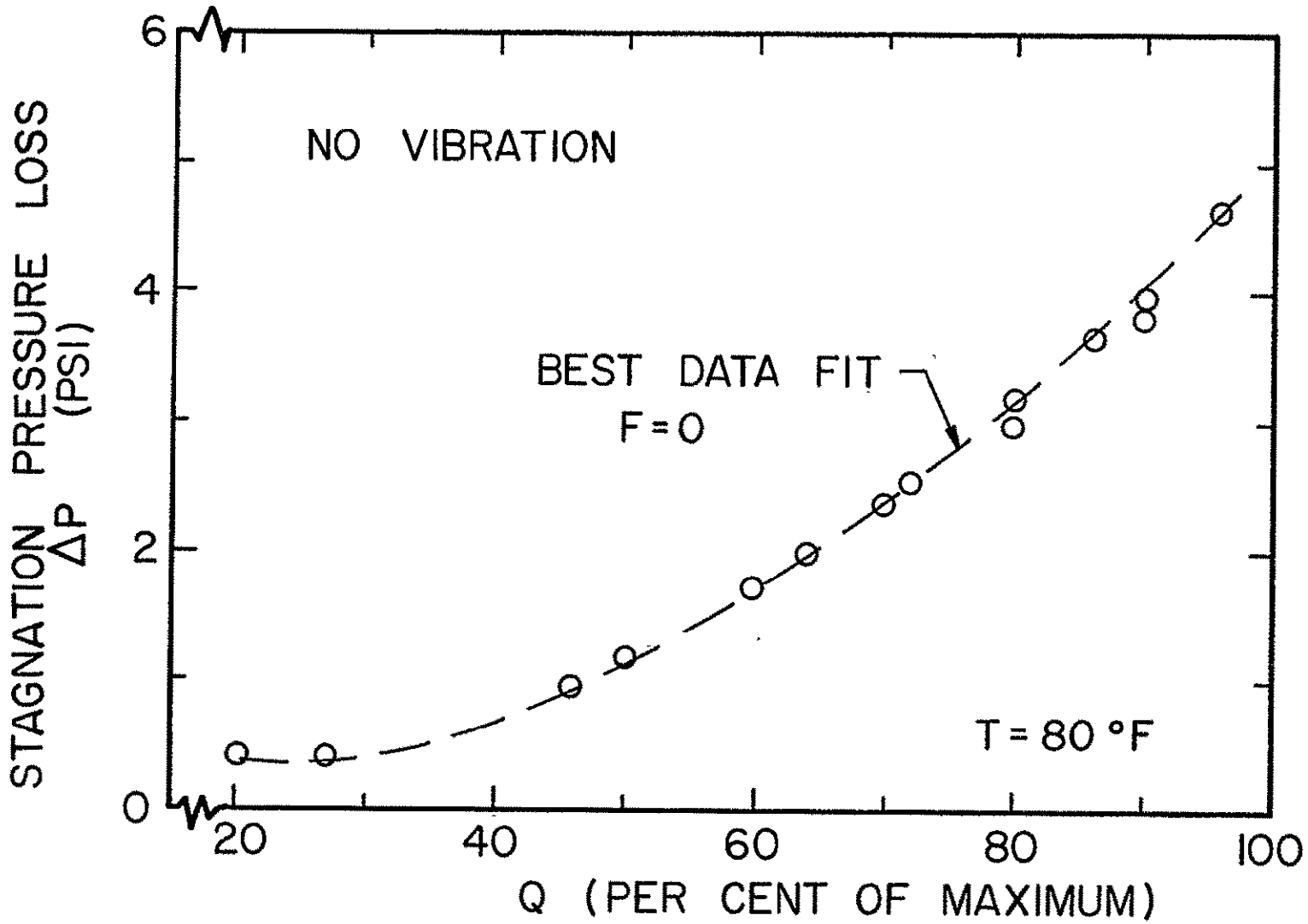

Figure 17. Stagnation Pressure Loss Across the Test Section in Absence of Discharge Line Given as a Function of the Volumetric Flow Rate, $Q(Q_{max} = 45$ GPM).

Figure 18. Stagnation Pressure Loss Across the Test Section in Absence of Discharge Line Given as a Function of the Volumetric Flow Rate, $Q(Q_{max} = 45$ GPM), for Various Vibrational Conditions.

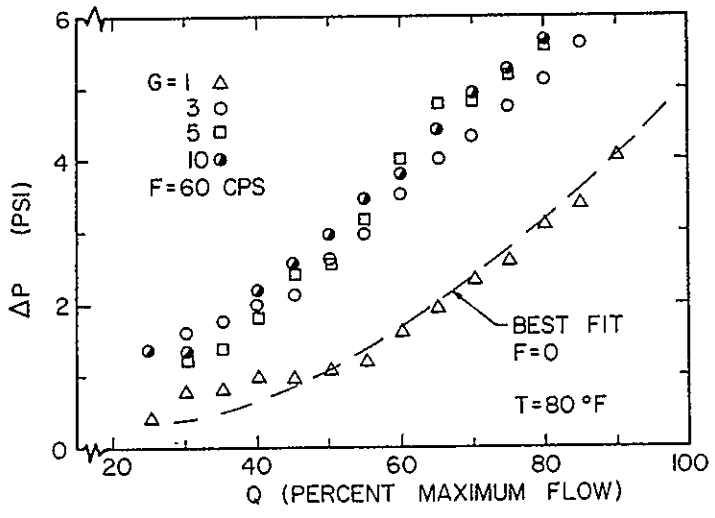
G=1
3
5
10
F=60 CPS
BEST FIT
F=0
T=80 °F
ΔP (PSI)
Q (PERCENT MAXIMUM FLOW)

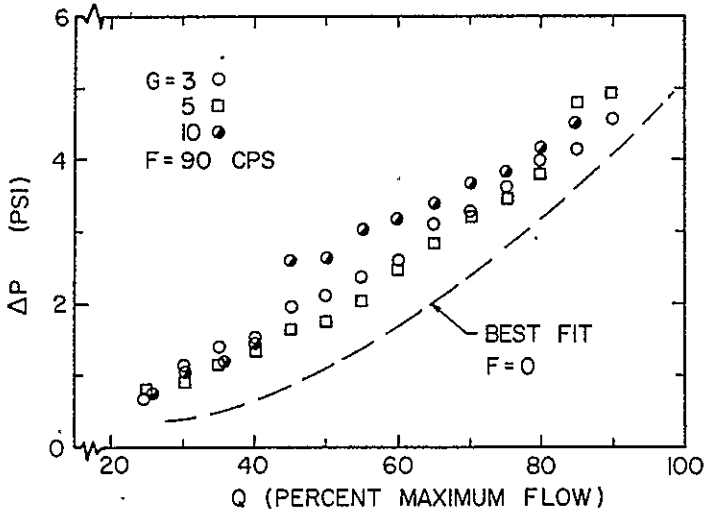
G=3
5
10
F=90 CPS
BEST FIT
F=0
ΔP (PSI)
Q (PERCENT MAXIMUM FLOW)

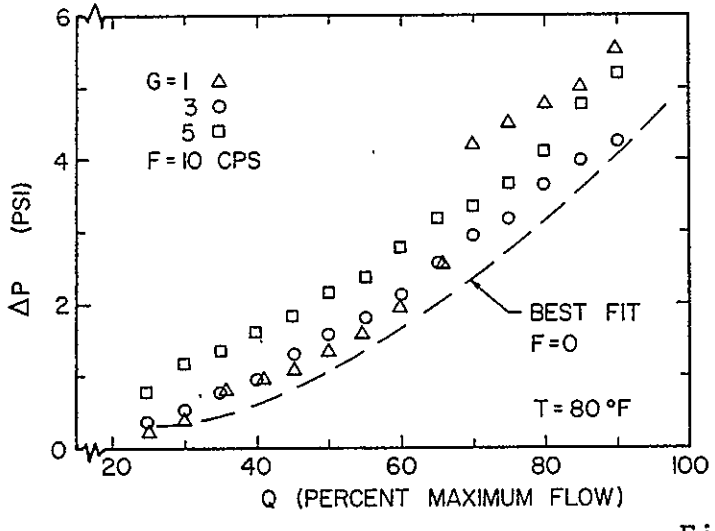
G=1
3
5
F=10 CPS
BEST FIT
F=0
T=80 °F
ΔP (PSI)
Q (PERCENT MAXIMUM FLOW)

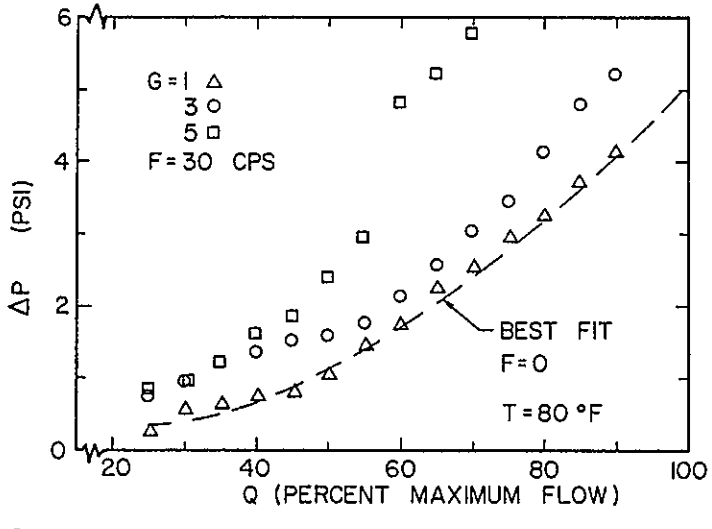
G=1
3
5
F=30 CPS
BEST FIT
F=0
T=80 °F
ΔP (PSI)
Q (PERCENT MAXIMUM FLOW)

Figure 18.

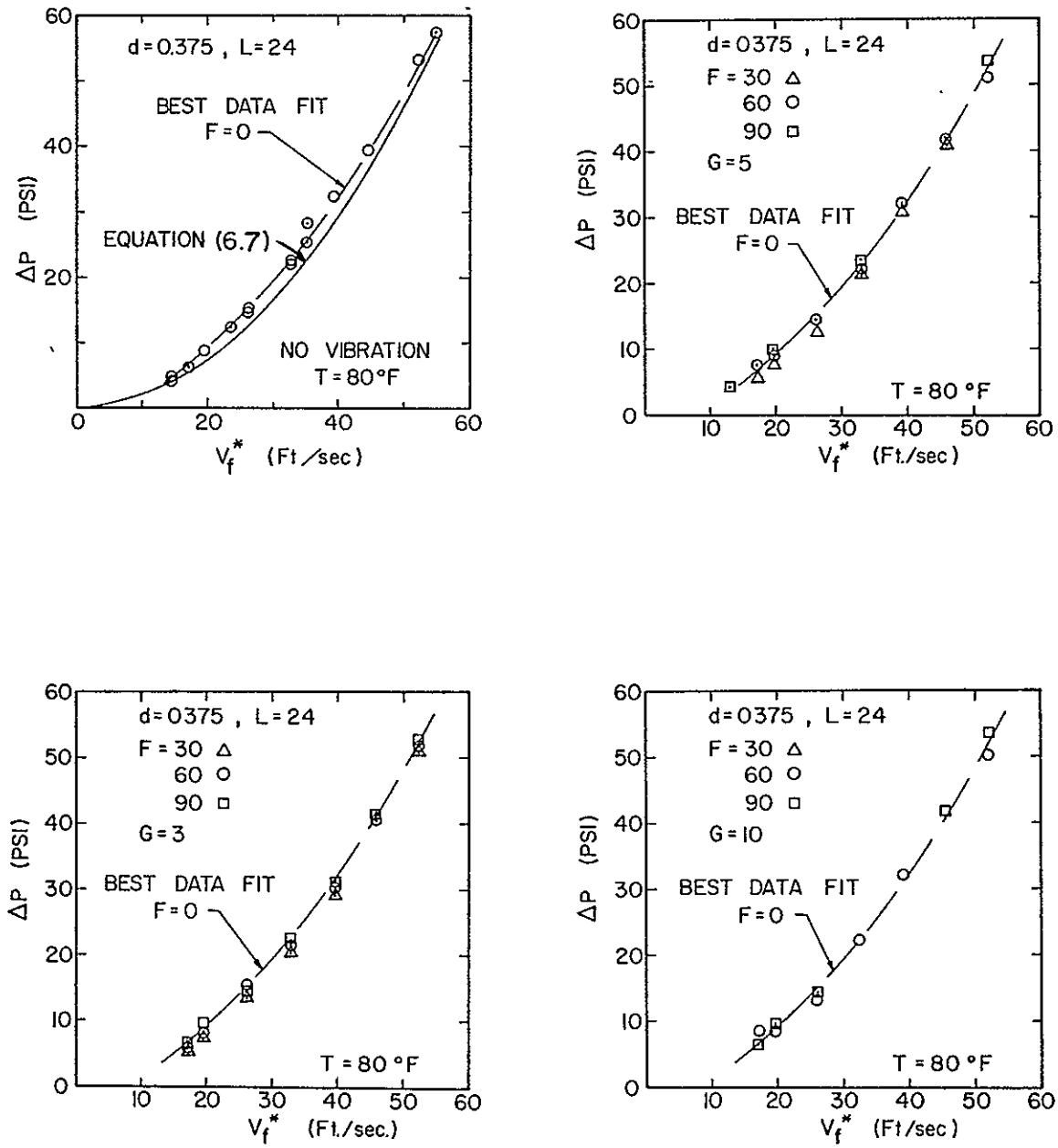

Figure 19. Stagnation Pressure Loss Across the Discharge Line for Various Vibratory and Non-Vibratory Conditions as a Function of Apparent Liquid Velocity (d = 0.375 in., L = 24 in.).

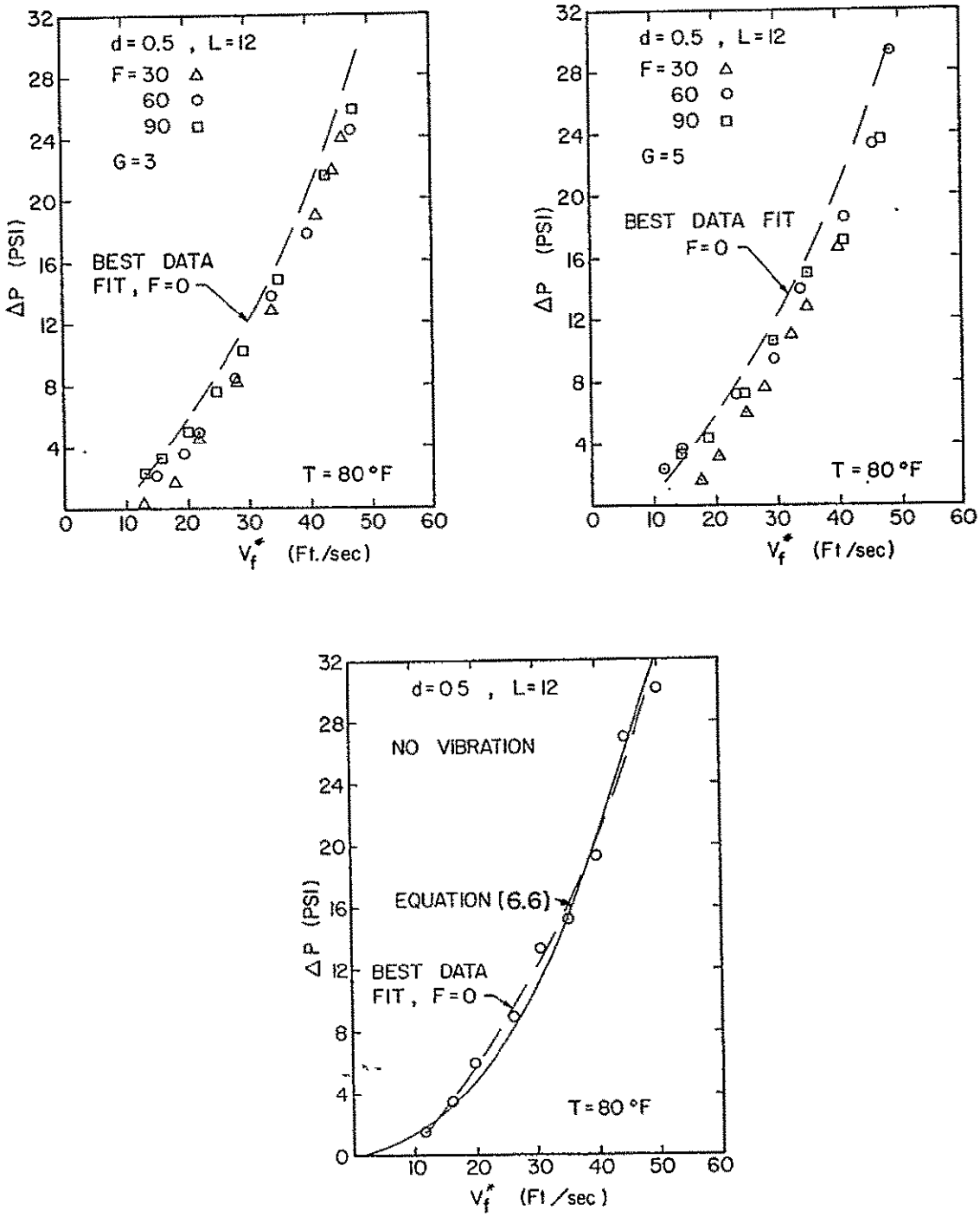

Figure 20. Stagnation Pressure Loss Across the Discharge Line for Various Vibratory and Non-Vibratory Conditions as a Function of Apparent Liquid Velocity (d = 0.375 in., L = 12 in.).

a given flow rate which indeed the data presented in Figure 18 demonstrate.

6.3 Conclusions

At this phase of the investigation, the check-out of the experimental facility was completed. The experimental facility was proved capable of providing those fluid flow conditions necessary to investigate high speed liquid flow in a simulated discharge line. Comparison of experimentally obtained data with the well known predictions for single phase fluid flow showed excellent agreement. The one-dimensional flow equation, (6.21), for the stagnation pressure loss across the discharge line evidently described the flow to a high degree of accuracy as exhibited by the comparisons with the experimental data.

The objective of finding a model describing accurately the multi-dimensional flow pattern in the entrance of the discharge line was achieved by the application of the free streamline theory. The theory of free jets combined with the axisymmetric solution presented by Rouse and Abul-Fetouh (6) enabled a one-dimensional analytical model to be developed which was verified by experimental results.

The experimental investigation of single phase fluid flow subjected to the influence of longitudinal vibration showed that stagnation pressure losses increased with increasing acceleration levels. The frequency influence was less pronounced; however, in the high frequency range, the

pressure losses tended to decrease in magnitude. An analytical solution to this problem was not attempted.

The inconsistency of having smaller stagnation pressure losses across the discharge line can be attributed, perhaps, to difficulties in proper instrumentation and signal conditioning in the pressure transducers. Resonances within the tubing leading to the sensing elements inside the transducers could have produced errors not readily noticeable or easily eliminated.

Both the one-dimensional and the multi-dimensional solutions derived for single phase flow in discharge lines were now extended into two-phase flow situations. This is discussed in the next chapter.

CHAPTER 7

CAVITATION INCEPTION IN A DISCHARGE LINE

7.1 The Flow Problem in the Non-Vibrating Case

Cavitation is defined as the formation of vapor filled voids in a liquid caused by a local pressure reduction as a result of the dynamics of the flow situation. Potential flow theory for a pure liquid predicts that a minimum pressure will occur on a solid boundary. Cavitation in a pure liquid will occur at some given value of the ratio,

$$\sigma = \frac{p_0 - p_{minimum}}{\frac{1}{2} \rho_f V_0^2} \tag{7.1}$$

where p_0 = reference static pressure

and V_0 = a reference velocity usually taken at the same point as p_0

For a liquid which generally can not support a tension, cavitation will take place when the minimum static pressure equals the vapor pressure. Thus the classical definition of the cavitation parameter can be formulated.

$$\sigma = \frac{p_0 - p_V}{\frac{1}{2} \rho_f V_0^2} \tag{7.2}$$

Similarity requires that the cavitation numbers in similar systems be identical at the point of incipient cavitation.

In a real liquid, consideration of the surface tension of the liquid leads to a modification of the assumption that cavitation appears as soon as the local pressure reaches the vapor pressure of the liquid. It should be noted that for a single spherical bubble (i.e. cavity), the concept of thermodynamic equilibrium has to be used in order to establish a criterion for the existence of a cavity. A balance of forces has to take into account the surface tension of the liquid. This balance leads to the well known relationship,

$$\pi r_0^2 (P_v - P_\ell) = 2\pi r_0 \gamma \qquad (7.3)$$

where r_0 = bubble radius

γ = surface tension

The resulting pressure difference between the liquid and the vapor is given by:

$$P_v - P_\ell = \frac{2\gamma}{r_0} \qquad (7.4)$$

Inspection of equation (7.4) shows that the pressure inside the bubble must be larger than that of the liquid for a bubble to exist. Since a basic assumption is that of thermal equilibrium, the liquid must be superheated to allow the vapor bubble to exist.

It follows from equation (7.4) that as the radius of curvature of the bubble becomes larger, the amount of superheat required for equilibrium becomes smaller. For a situation where the radius of curvature of the liquid vapor

interface could be considered very large, the pressure difference and amount of superheat both go to zero.

Application of the definition of the cavitation number as given in equation (7.2) leads to the conclusion that cavitation would occur under a well definable flow situation, provided this flow situation can be treated adequately with an analytical model. As discussed earlier, this prediction is quite difficult in the entrance region of the discharge line under investigation. If the flow velocity through the discharge line is increased while a constant upstream stagnation pressure is maintained, then cavitation will eventually occur when the static pressure along the free streamline reaches the vapor pressure of the liquid. Initially this cavitation begins at the sharp edge of the discharge line entrance. The analysis presented in Chapter 6 gives the value of the free streamline pressure as a function of the velocity, stagnation pressure, the geometric parameter and its resulting contraction coefficient.

Using the definition of the cavitation number given by equation (7.2), a modified cavitation number which is independent of the geometry of the discharge line was derived and used for this special type of problem. The modified cavitation number is being introduced in order to express the cavitation parameter in terms of the apparent liquid velocity, V_f^*, which proved quite useful earlier in the analysis and experiments. The continuity equation can be

expressed in terms of the flow at the reference section (i.e. the location where p_0 and V_0 are measured in the delivery line) and the flow inside the discharge line assuming a uniform velocity profile.

Continuity:

$$\rho_f A_0 V_0 = \rho_f A_d V_f^* \tag{7.5}$$

$$V_0 = \frac{d^2}{D_0^2} V_f^* \tag{7.6}$$

Substituting equation (7.6) into equation (7.2) leads to

$$\sigma = \frac{p_0 - P_v}{\frac{1}{2} \rho_f V_f^{*2} \left(d^4/D_0^4\right)} \tag{7.7}$$

Now the definition for the modified cavitation number, $\bar{\sigma}^*$, is stated.

$$\bar{\sigma}^* = \frac{d^4}{D_0^4} \sigma \tag{7.8}$$

Substituting the cavitation number, σ, as formulated in equation (7.7) into the above definition yields a simple relation for the modified cavitation number, $\bar{\sigma}^*$.

$$\bar{\sigma}^* = \frac{p_0 - P_v}{\frac{1}{2} \rho_f V_f^{*2}} \tag{7.9}$$

The values of $\bar{\sigma}^*$ are obtained experimentally from the static pressures, p_0, which are measured in the delivery line, and from the value of V_f^* which is obtained from the turbine flow meter.

The theoretical value for $\bar{\sigma}^*$ can be derived from the free streamline analysis presented in Chapter 6. Bernoulli's equation along a streamline at the reference location is written in terms of the stagnation pressure

$$P_s = p_0 + \frac{1}{2} \rho_f V_0^2 \tag{7.10}$$

The pressure along the free streamline was defined in equation (6.21) and is repeated here.

$$p_1 = P_s - \frac{1}{2} \rho_f \left(V_f^*/C_c\right)^2 \tag{6.21}$$

Given the constraints that the pressure along the free streamline equals the vapor pressure and cavitation occurs, then equating of equations (6.21) and (7.10) leads to the relation,

$$p_0 - P_v = \frac{1}{2} \rho_f \left[\frac{V_f^*}{C_c}\right]^2 - \frac{1}{2} \rho_f V_0^2 \tag{7.11}$$

Substituting equation (7.6) into the above equation yields

$$p_0 - P_v = \left[\frac{1}{C_c^2} - \frac{d^4}{D_0^4}\right] \frac{1}{2} \rho_f V_f^{*2} \tag{7.12}$$

Now substitution of equation (7.12) into equation (7.9) leads to the final form of the modified cavitation number, $\bar{\sigma}^*$.

$$\bar{\sigma}^* = \frac{1}{C_c^2} - \frac{d^4}{D_0^4} \tag{7.13}$$

Equation 7.13 is an exact relation. For systems where $D_0 >> d$, the approximation for the area ratio noted below is valid.

It becomes:

$$\frac{d^4}{D_0^4} << 1 \tag{7.14}$$

The constraint exemplified by equation (7.14) leads to a simplification of the modified cavitation number.

$$\bar{\sigma}^* = \frac{1}{C_c^2} \tag{7.15}$$

The validity of the approximation for the modified cavitation number shown in its final form by equation (7.15) is illustrated by using the contraction coefficient listed by Rouse (6) for the ratios of diameters used in the work.

For the following conditions,

$$\frac{d}{D} \leq 0.1$$

$$C_c = 0.611$$

the corresponding value for the modified cavitation number is

$$\bar{\sigma}^* \approx 3.72 \tag{7.16}$$

Since the contribution of the fourth power of the ratio d/D_0 is less than 2% over the entire range of delivery line geometries used in the investigation, its contribution to the modified cavitation number can be neglected. Thus the modified cavitation number becomes,

$$\bar{\sigma}^* = \frac{1}{C_c^2} - \left(\frac{d}{D_0}\right)^4 \approx \frac{1}{C_c^2} \tag{7.17}$$

Typical experimental data to compare with the theoretical prediction of (7.17) were obtained by keeping the upstream

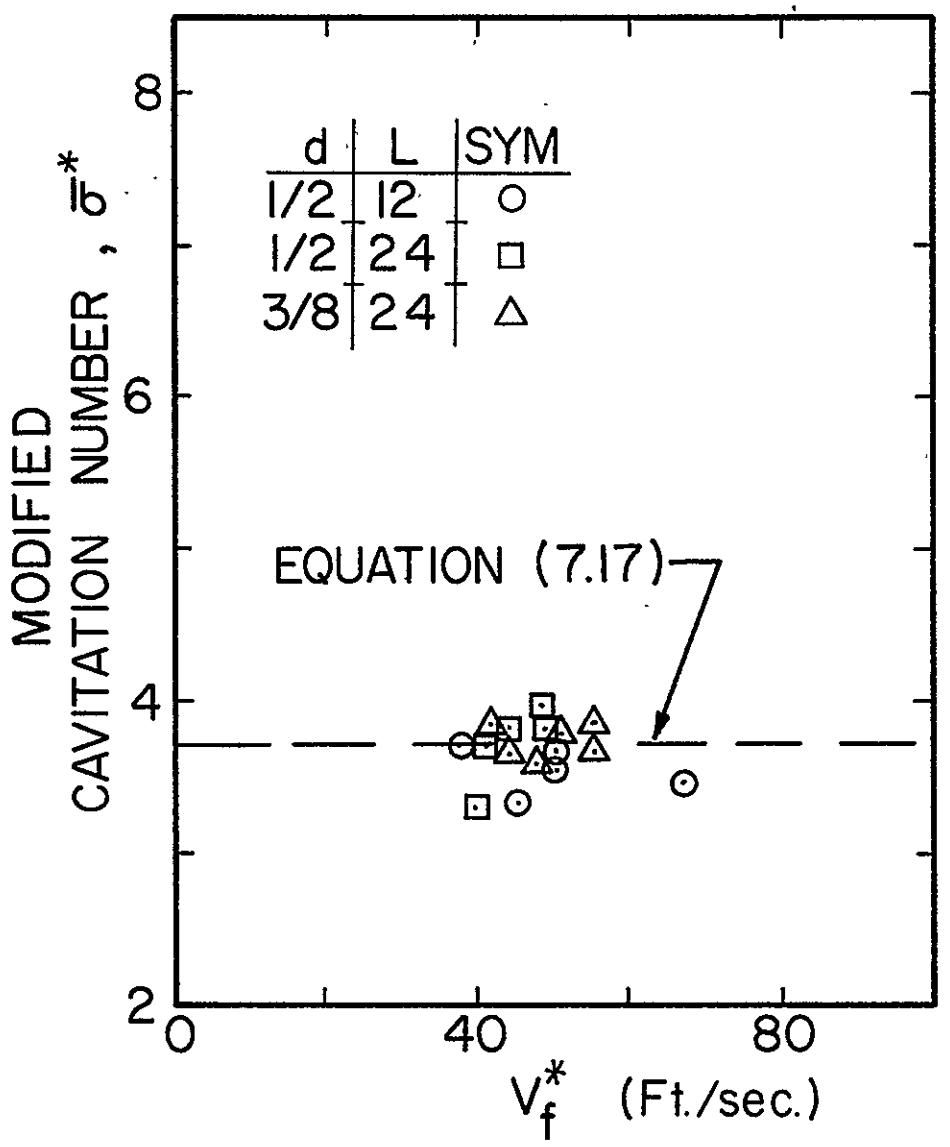

Figure 21. Modified Cavitation Number as a Function of Apparent Liquid Velocity for Various Discharge Line Geometries.

stagnation pressure constant and increasing the flow velocity until cavitation appeared. A more complete description of the experimental procedure used in this phase of the investigation is presented in Chapter 5.

A comparison between experimental data and a value calculated with equation (7.17) is illustrated for several geometries in Figure 21.

7.2 Cavitation Inception in a Discharge Line under the Influence of Longitudinal Vibration

It has already been shown that the inception of cavitation is a function of the local static pressure. An investigation by Schoenhals (44) of a flexible liquid-filled cylinder under the influence of longitudinal vibration proved that the local pressure oscillation could be predicted reasonably well. A schematic diagram of the system investigated in reference (44) together with a schematic diagram of the test section used in this investigation are shown in Figure 22. Referring to the schematic diagram for definitions an expression for the first natural frequency of the combined tank and liquid system was derived and presented by Schoenhals (44) to be

$$\frac{\omega \cdot \ell}{C} = \frac{\pi}{2} \qquad (7.18)$$

where $C \equiv$ acoustic velocity of the system.

Although Schoenhals (44) derived the above expression for a liquid filled closed container, it was applied successfully to the test section used in this investigation. This procedure was justified in the light of the results obtained in a

concurrent investigation by Pesar (46), who found that for small flow velocities, the natural frequency for a given system is independent of the flow velocity. The acoustic velocity, C, is dependent upon the structural parameters of the tank, the acoustic velocity in the water, C_L, and the bulk modulus of plexiglass of which the tank was fabricated. This derivation is presented in total in the reference; the final form of the expression is given below.

$$C = \frac{C_L}{\left|1 + \frac{B}{E} \cdot \frac{D}{S}\right|^{1/2}} \qquad (7.19)$$

Using equation (7.18), a resonant frequency of approximately 85 cps was calculated for the test section depicted in Figure 5. The length, ℓ, in the equation represents the distance from the top of the elbow on the top of the test section to the entrance plane of the discharge line. Under conditions of no flow, a comparison of analytical predictions given by Schoenhals (44) and experimental data obtained with the test section was made.

Pressure measurements were obtained with a Kistler transducer as indicated in the schematic diagram of Figure 5. A comparison of the experimental data obtained in this phase of the investigation with the theoretical prediction of pressure amplitudes as a function of frequency is shown in Figure 23. The data are somewhat scattered and are lower than the calculated values of the oscillating pressure amplitudes. However the prediction does give the trend and order of magnitude of the data.

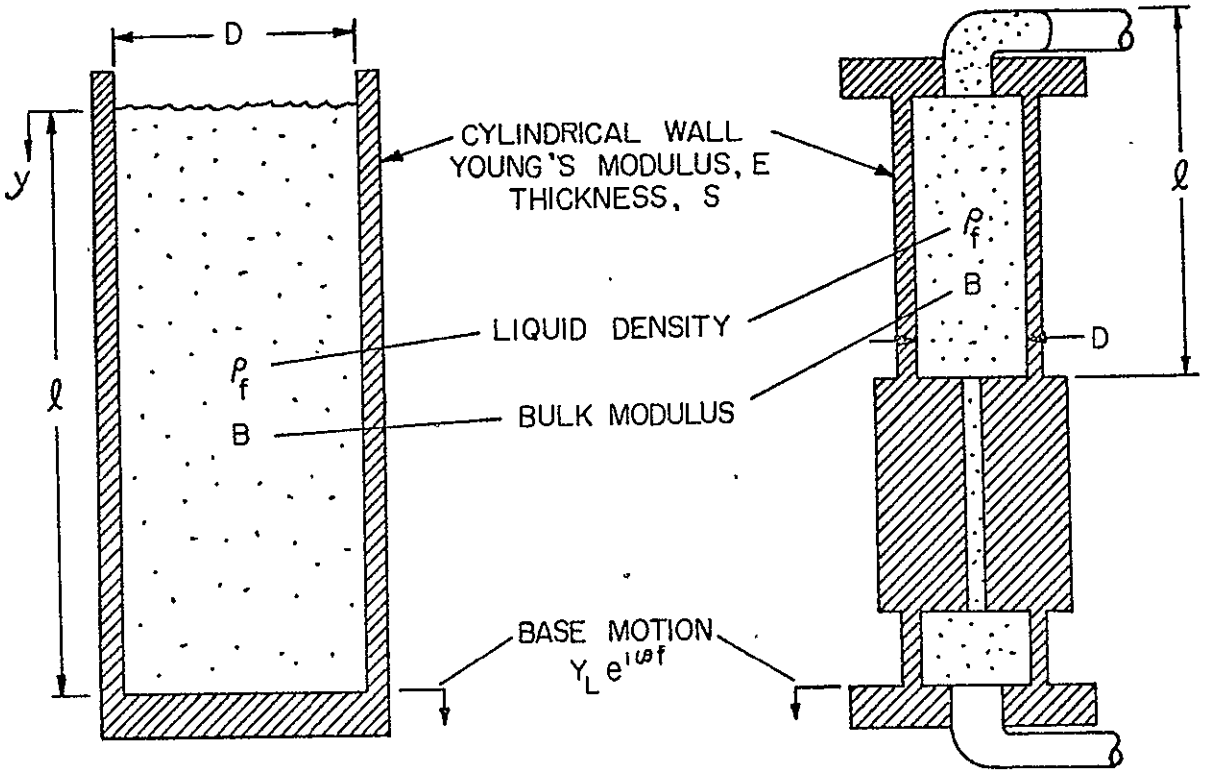

Figure 22. Schematic Diagram of Liquid Filled, Flexible Cylinder from Schoenhals (44) Compared to a Schematic Diagram of the Test Section Used in This Investigation.

In a subsequent investigation, data of pressure amplitudes were obtained for the same values of the stagnation pressure but now under moderate flow conditions, i.e. moderate apparent liquid flow velocities. Again the experimentally obtained pressure amplitudes as a function of frequency under various stagnation pressure conditions are compared with Schoenhals' theoretical prediction. Fairly good agreement of the experimental data with the theory, an observation which was also made by Pesar (46), is shown in Figure 24.

Under vibratory conditions, the stagnation pressure in the discharge line is composed of a steady state value upon which a pressure fluctuation is superimposed caused by the oscillating motion of the system. The instantaneous value for the stagnation pressure is given by,

$$P_s(t) = \overline{P}_s + \Delta P_s \cos \omega t \qquad (7.20)$$

where ΔP_s is a known function of frequency and acceleration level as given by Schoenhals (44). No phase angle relationship is shown in equation (7.20) since the discussion is concerned with the value of $P_s(t)$ at the entrance plane of the discharge line where the phase angle value would be zero if included. By using the expression for the static pressure, p', discussed in Chapter 6 as equation (6.21), the fluctuation $\Delta p'$ of the static pressure along the free streamline is shown to be equal to ΔP_s.

Neglecting the hydrostatic pressure term, Bernoulli's equation is valid along the free streamline in the entrance plane of the discharge line.

$$P_s = p' + \frac{1}{2} \rho_f \left[\frac{V_f^*}{C_c}\right]^2 \qquad (7.21)$$

This equation can be modified to account for the periodically oscillating pressure.

$$\overline{P}_s + \Delta P_s \cos \omega t = p'(t) + \frac{1}{2} \rho_f \left[\frac{V_f^*}{C_c}\right]^2 \qquad (7.22)$$

The above equation follows from the approximation that only the static pressure is subjected to periodic fluctuations.

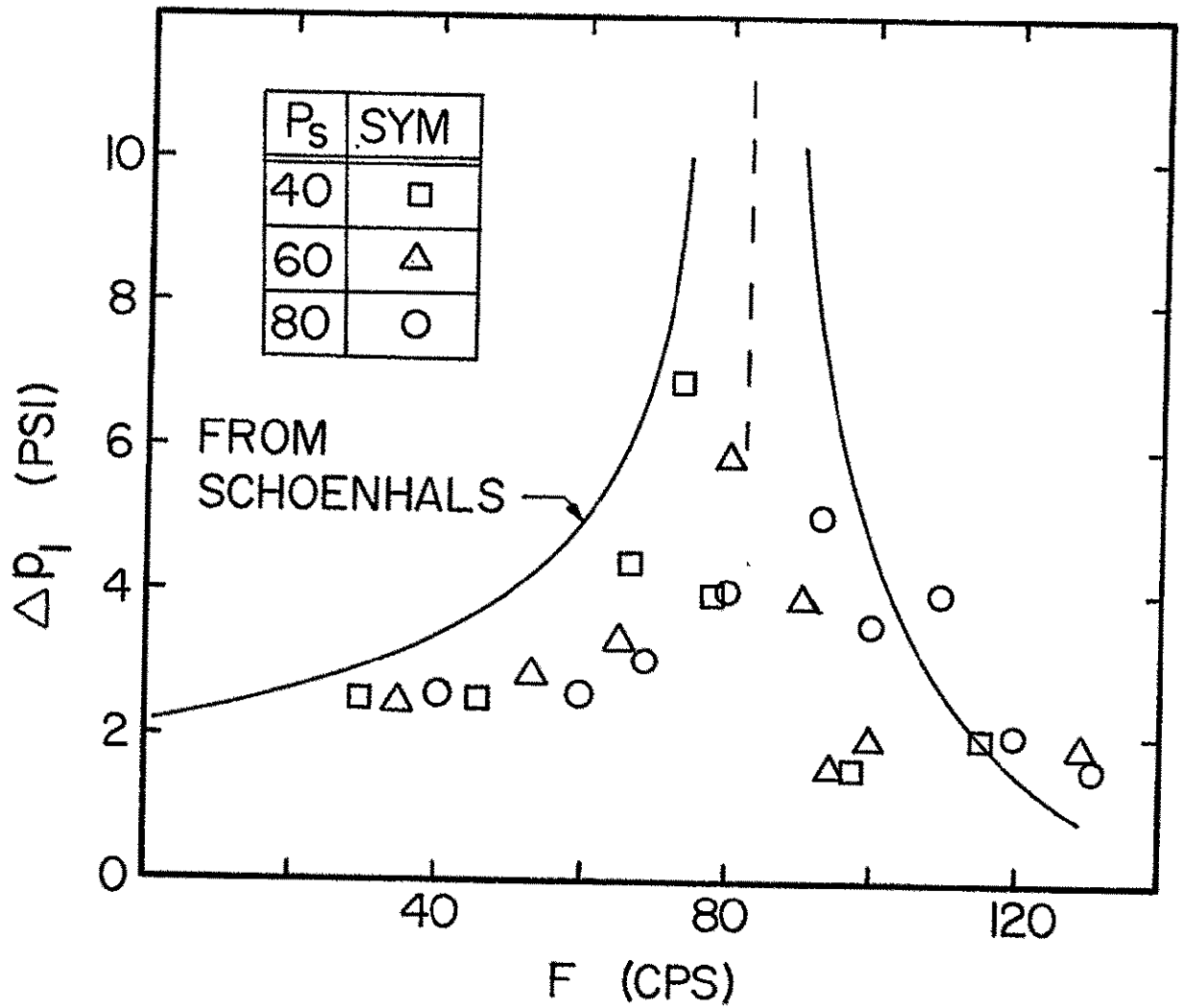

Figure 23. Pressure Oscillations in the Discharge Line Under No Flow Conditions Compared to the Prediction by Schoenhals (44).

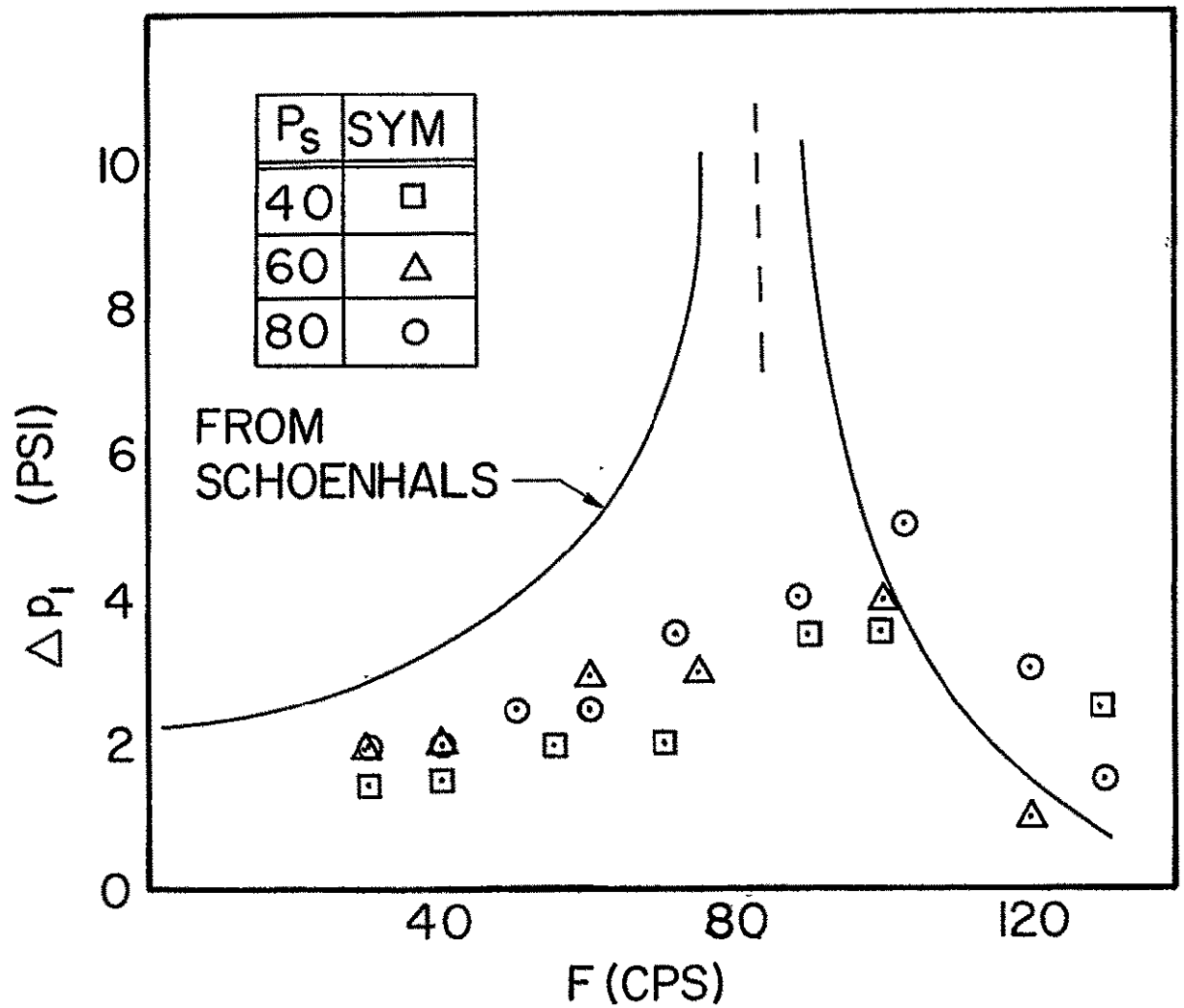

Figure 24. Pressure Oscillations in the Discharge Line Under Flow Conditions Compared to the Prediction by Schoenhals (44).

It will be shown that the periodic velocity fluctuations which are induced by the vibration are negligibly small. It follows from the base motion of the test section shown in Figure 22 that displacement, velocity, and acceleration of the system under consideration obey the relations noted as equations (7.23).

$$\begin{aligned} y(t) &= Y_L\, e^{i\omega t} \\ \dot{y}(t) &= Y_L i\omega e^{i\omega t} = ive^{i\omega t} \\ \ddot{y}(t) &= -\, Y_L \omega^2 e^{i\omega t} = -ae^{i\omega t} \end{aligned} \tag{7.23}$$

Considering the magnitudes of the velocity and acceleration expressions, the magnitude of the oscillating velocity is expressed as a function of acceleration and frequency.

$$|v| = |a/\omega| \tag{7.24}$$

The maximum value for the velocity magnitude at a given acceleration level occurs at the lowest frequency. For this investigation, this minimum frequency was 10 cps (20π rad/sec)

$$|v|_{max} = |a/\omega_{min}| = |a/20\pi| \tag{7.25}$$

A numerical evaluation of equation (7.25) illustrates why this oscillating velocity component can be neglected when compared with the minimum value of V_f^*. For example

$$\begin{aligned} &V_f^* = 30 \text{ ft/sec and } \bar{G} = 1 \Rightarrow |a| = 32.2 \text{ ft/sec} \\ &|v|_{max} = |32.2/20\pi| = 0.512 \text{ ft/sec} \\ &V_{f\,min}^* = 30 \text{ ft/sec} >> |v|_{max} = 0.512 \text{ ft/sec} \end{aligned} \tag{7.26}$$

With the above constraints, equation (7.22) implies the validity of the equation

$$p' \equiv p'(t) = \bar{p}' + \Delta P_s \cos \omega t \qquad (7.27)$$

Equation (7.27) can be used as an argument that the definition for the cavitation number in a non-vibrating flow can be used for this particular problem upon one modification. That is, the resulting expression must include a time dependent term accounting for the time dependency of the static pressure along the stream line under consideration. The second modified cavitation number, $\sigma^*(t)$, is therefore the time dependent function

$$\sigma^*(t) = \frac{1}{C_c^2} - \left(\frac{d}{D_0}\right)^4 + \frac{\Delta P_s \cos \omega t}{\frac{1}{2} \rho_f V_f^*} \qquad (7.28)$$

This expression can be rewritten by defining a $\Delta\sigma^*$ term.

$$\Delta\sigma^* = \frac{\Delta P_s}{\frac{1}{2} \rho_f V_f^*} \qquad (7.29)$$

Therefore the final form of the time dependent modified cavitation number is written as

$$\sigma^*(t) = \frac{1}{C_c^2} - \frac{d^4}{D_0^4} + \Delta\sigma^* \cos \omega t \qquad (7.30)$$

The term $\Delta\sigma^*$ needs to be discussed firstly in its implications on a hypothetical fluid and secondly for its implications on a real fluid.

Consider a hypothetical fluid which is not capable of sustaining a tension. Then for such a fluid it can be stated that the static pressure to which it might be subjected due to the dynamics of the flow process has to obey the relation

$$p_{static} \geq p_{vapor}$$

The static pressure in the fluid was measured at station 1 as indicated in Figure 6 and its measurements were displayed as a function of time. For given experimental conditions,

$$P_s = \text{constant}$$
$$F = \text{constant}$$
$$G = \text{constant}$$
$$\Delta P_s = \text{constant}$$

the flow rate was increased by lowering the exit pressure in the test section. The static pressures, p_1, and the apparent liquid velocity, V_f^*, are shown in Figure 25 as a function of time with the assumption that the fluid is hypothetical. A complete description of Figure 25 is given below:

Case (i) $$V_f^*(i) = 0$$
$$p_1(t) = P_s(t)$$

Under no flow conditions, the stagnation pressures and static pressures are identical.

Case (ii) $V_f^*(ii) > V_f^*(i) = 0$

$$p_l(\text{mean}) < P_s(\text{mean})$$

$$p_l(t) > P_v$$

The flow velocity causes a reduction in the mean static pressure. The reduction in the mean static pressure is not large.

Case (iii) $V_f^*(iii) > V_f^*(ii) > 0$

$$P_v < p_l(\text{mean}) < P_s(\text{mean})$$

$$\left(p_l(\text{mean}) - P_v\right) < \Delta P_s$$

The flow velocity has increased to a value such that cavitation would occur in part of the sinusoidal pressure cycle if the liquid could not sustain any tension whatsoever.

Case (iv) $V_f^*(iv) > V_f^*(iii) >> 0$

$$p_l(\text{mean})_{\text{theor.}} < P_v$$

$$\Delta P_s > \left(P_v - p_l(\text{mean})\right)$$

The flow velocity has increased to a value such that the theoretical mean static pressure is below the vapor pressure. This case was not observed experimentally. Cavitation occurs almost throughout the cycle except for a very small increment of time.

In order to discuss the significance of Figure 25, it is necessary to define an additional parameter which

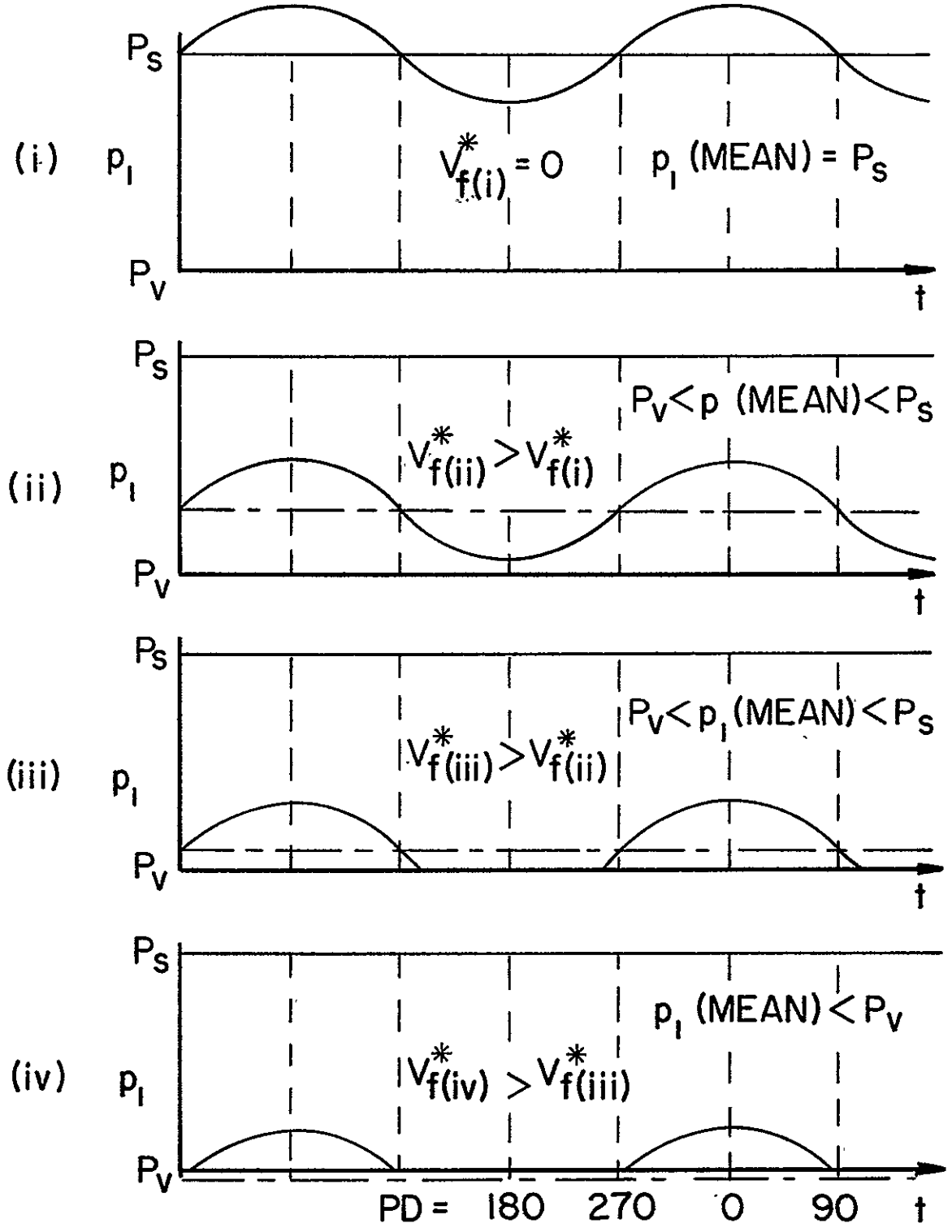

Figure 25. Pressure Oscillations in a Hypothetical Fluid as a Function of Time and Apparent Liquid Velocity.

references the point along the sinusoidal path of the shaker motion which is being considered. This reference parameter is called the phase deviation, and it is defined below.

PD = phase angle relationship of the shaker table when the strobe would flash.

PD = 0 is the lowermost position of the stroke.

PD = 90 is the neutral point on the path of the table with an upward velocity component

PD = 180 is the uppermost position of the stroke

PD = 270 is the neutral point on the path of the table with a downward velocity component

Utilization of this parameter, PD, is made when consideration is given to the pressure fluctuations noted in Figure 25.

The fact that the cavitation number obtained when viewing Case (iii) at PD =180 is different than the case of no vibration is obvious as the no vibration case would need a higher V_f^* before cavitation would occur. Similarly but in an opposite sense an observer would not detect cavitation in the oscillating test section if he were to observe the discharge line under Case (iv) at PD = 0 ; however, if the test section were not vibrating, cavitation would definitely be occurring.

At this point, reference should be made to the experimental procedure adhered to in the measurement of the inception of cavitation. The onset of cavitation was observed visually. A Breul and Kjaer Stroboscope Type 4910 with control unit was used for the investigation of cavitation. The features of the Stroboscope are too numerous to be

described here; however, one feature of which extreme use was made has to be mentioned. This was the phase deviation control which permitted synchronization of the flash from the lamp with the motion of the shaker table. In this manner, the shaker table and the test section mounted on it were visually static to the eye of the observer.

In these experiments, extensive use was made of an observer to detect the onset of cavitation in the discharge line. The operator manipulated the controls of the fluid flow loop and of the electrodynamic shaker while the observer concentrated his attention to the cavitation in the line. Data could be taken for only brief periods because of the strain on the eyes of the observer.

The data obtained for different PD values and presented in Figures 26 through 33 do not display a significant change in the value of $\sigma^*(t)$. The reference static pressure, p_0, for all conditions in these figures was kept at a constant value for each datum and ranged between 30 and 80 psia.

Cavitation measurements were performed in both test sections. Since the natural frequencies of the two test sections were expected to be different, an additional calculation of the magnitude of the pressure fluctuation was made for the second test section. The natural frequency for the test section shown schematically in Figure 6 was calculated to be 210 cps.

As described earlier, for all values of frequency well below this natural frequency, i.e. F<150 cps, the magnitude of the total pressure fluctuation should be relatively independent of the frequency and only a function of the acceleration level.

In order to obtain the value for the maximum excursions, the frequency dependent modified cavitation number, $\sigma^*(t)$, expressed in equation (7.28) was separated into two parts. The first part was the non-oscillating contribution defined earlier as $\bar{\sigma}^*$. The second part was the oscillating contribution having a magnitude defined by equation (7.29) with a frequency equal to the forcing frequency of the shaker table.

$$\sigma^* = \bar{\sigma}^* + \Delta\sigma^* \cos \omega t \tag{7.31}$$

The prediction of the magnitude of the pressure oscillations is given by

$$\Delta P_s = \rho_f g \ell \bar{G} \left| \frac{\sin \Omega (y/\ell)}{\Omega \cos \Omega} \right| \tag{7.32}$$

where $\Omega = \omega\ell/C$. Use of this expression gives rise to the frequency varying component $\Delta\sigma^*$:

$$\Delta\sigma^* = \frac{2g\ell\bar{G}}{V_f^{*2}} \left| \frac{\sin \Omega (y/\ell)}{\cos \Omega} \right| \tag{7.33}$$

At the entrance plane of the discharge line the ratio of y/ℓ equals unity. Therefore equation (7.33) reduces to

$$\Delta\sigma^* = \frac{2g\ell\bar{G}}{V_f^{*2}} \frac{\tan \Omega}{\Omega} \tag{7.34}$$

The magnitude of $\Delta\sigma^*$ will be large when the apparent liquid velocity is small. Therefore, for the data obtained in the experimental investigation this condition exists for the condition of $P_0 = 30$ psi. This can be explained by the fact that the velocity necessary to cause cavitation is lowest for the smallest reference pressure. A numerical solution for equation (7.34) in the frequency range

$$0 \leq F \leq 70 \text{ cps}, \quad \bar{G} = 1$$

gives the order of magnitude of $\Delta\sigma^*$ noted below

$$\Delta\sigma^* \approx 0.2 \tag{7.35}$$

Hence all effects of vibration on the cavitation parameter cause it to be confined to the range:

$$3.5 \lesssim \sigma^*(t) \lesssim 3.9$$

The limits of possible cavitation numbers are inscribed on Figures 26 and 27. It should be noted once again that the approximation of one value for the magnitude of the pressure oscillation due to the vibration is valid over only a limited frequency range. Thus the limits on $\sigma^*(t)$ are only inscribed over the frequency range where this approximation is valid, that is,

$$0 < F \leq 60 \quad \text{(cps)}$$

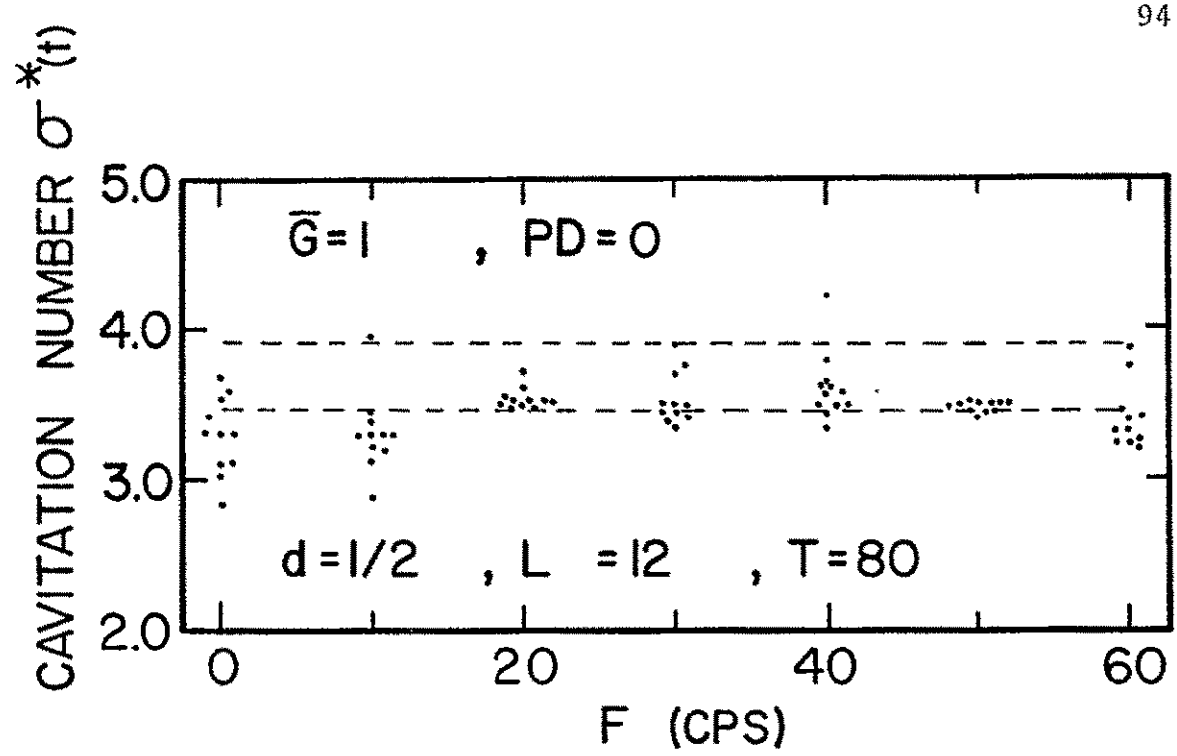

Figure 26. Time Dependent Modified Cavitation Number Compared to Approximated Limits for the Conditions, d = 1/2, L = 12, T = 80°F, PD = 0, $\bar{G}$ = 1.

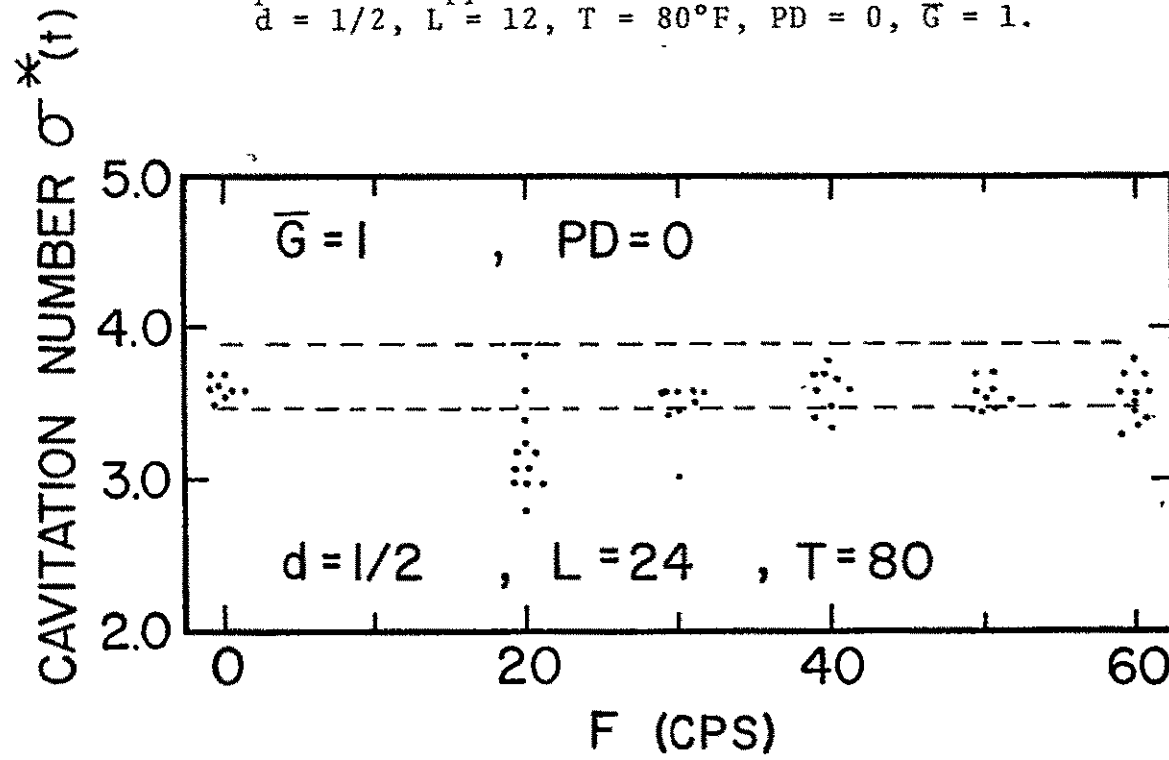

Figure 27. Time Dependent Modified Cavitation Number Compared to Approximated Limits for the Conditions, d = 1/2, L = 24, T = 80°F, PD = 0, $\bar{G}$ = 1.

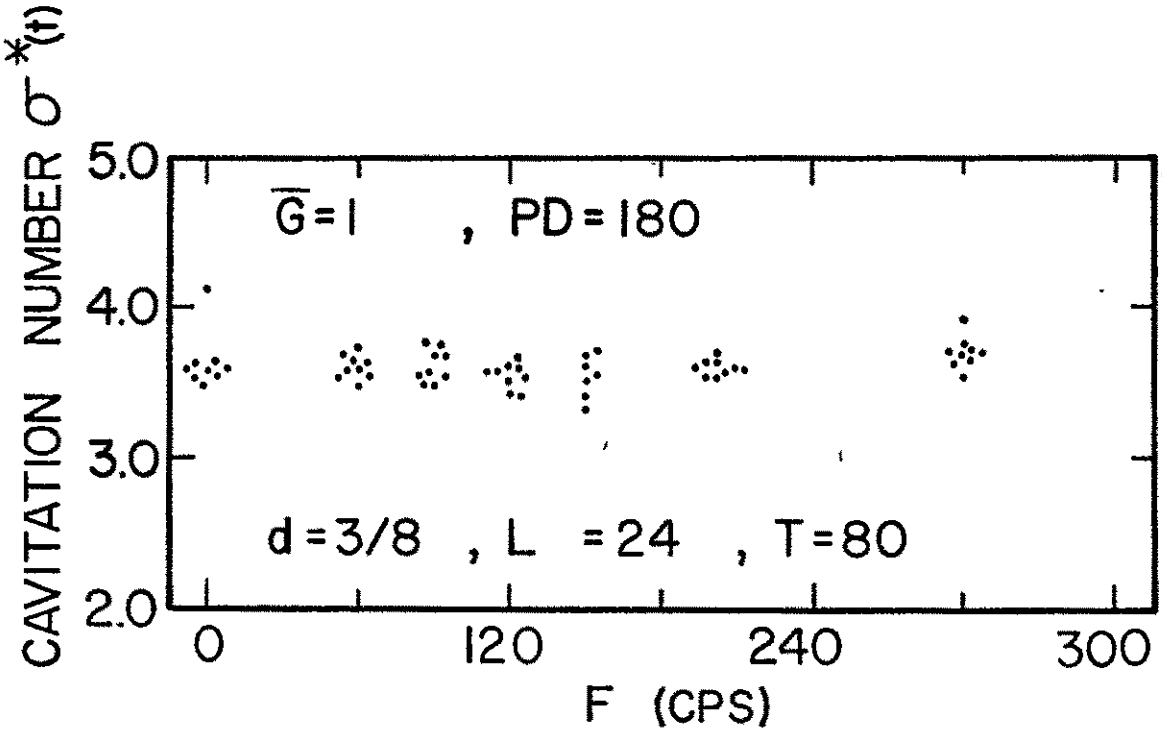

Figure 28. Time Dependent Modified Cavitation Number at Extended Vibrational Frequencies for Conditions, d = 3/8, L = 24, T = 80°F, PD = 180, $\bar{G}$ = 1.

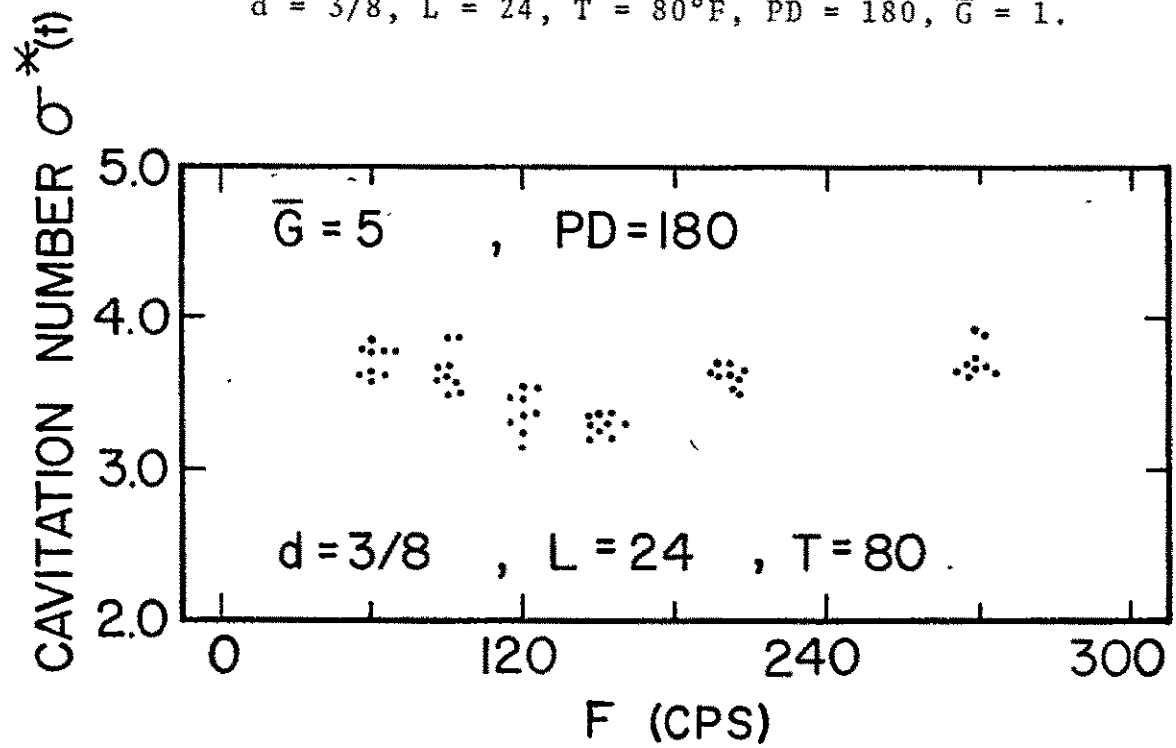

Figure 29. Time Dependent Modified Cavitation Number at Extended Vibrational Frequencies and High $\bar{G}$ Level for Conditions, d = 3/8, L = 24, T = 80°F, PD = 180, $\bar{G}$ = 5.

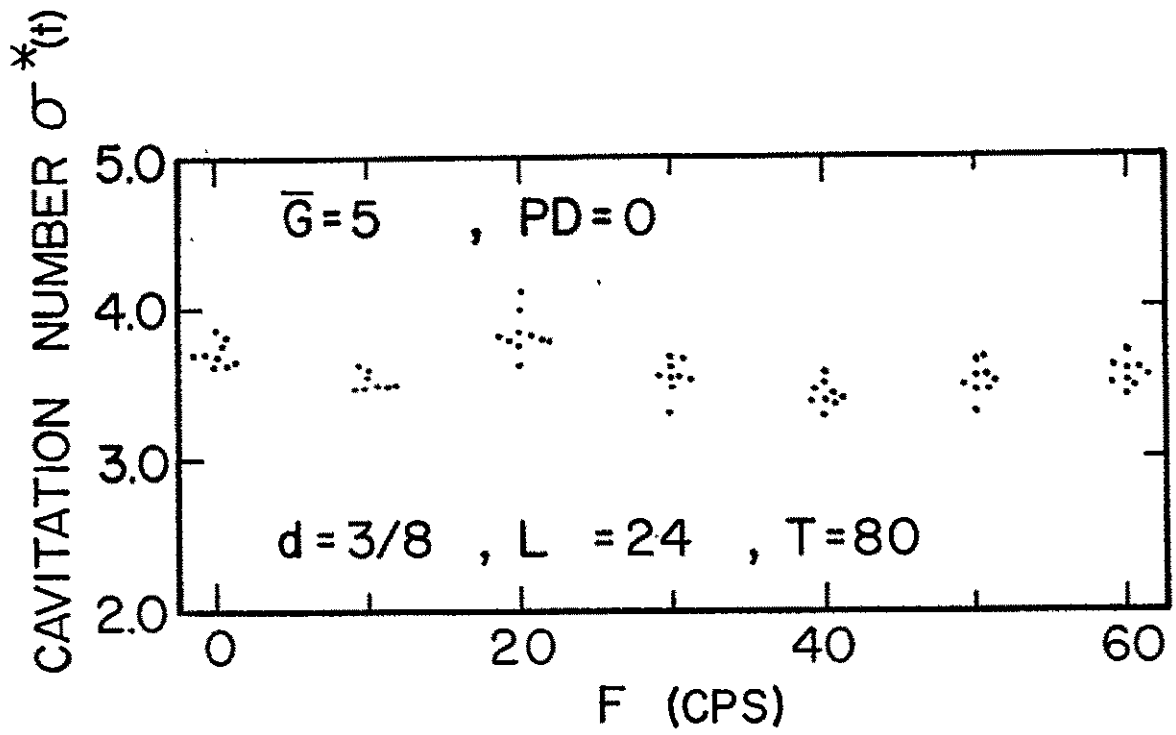

Figure 30. Time Dependent Modified Cavitation Number at Low Vibrational Frequencies and High G Level for Conditions, d = 3/8, L = 24, T = 80°F, PD = 0, $\bar{G}$ = 5.

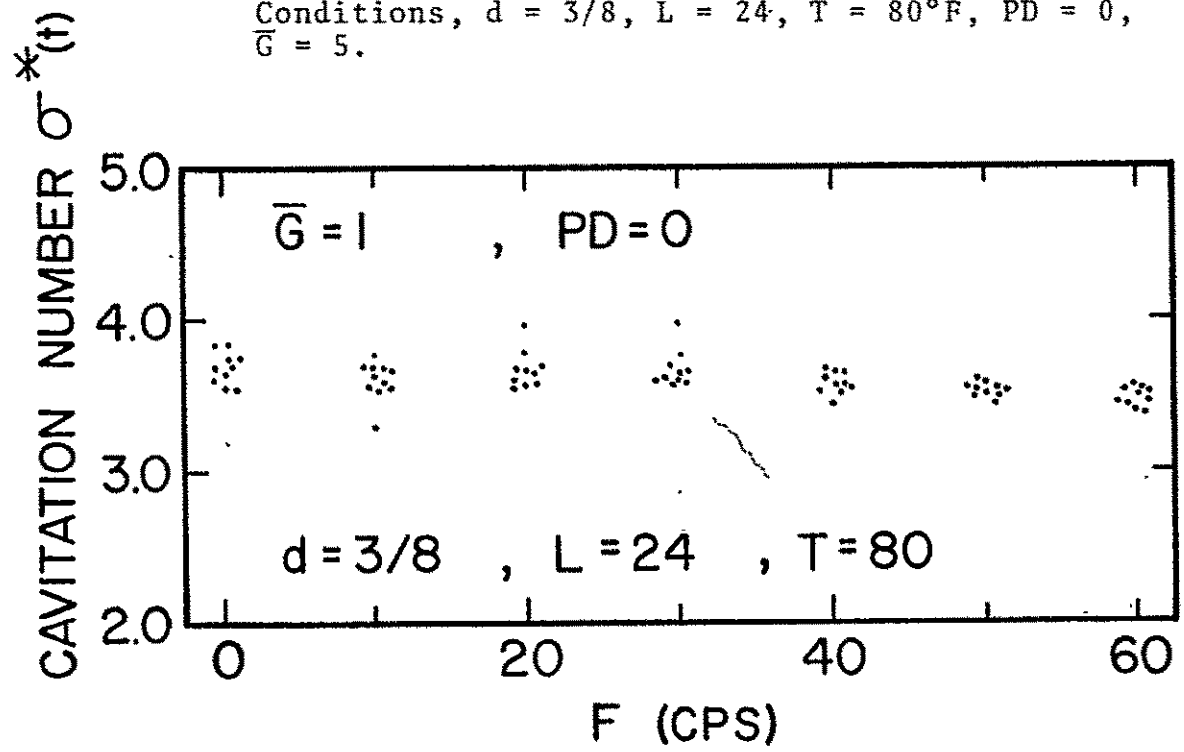

Figure 31. Time Dependent Modified Cavitation Number at Low Vibrational Frequencies for Conditions, d = 3/8, L = 24, T = 80°F, PD = 0, $\bar{G}$ = 1.

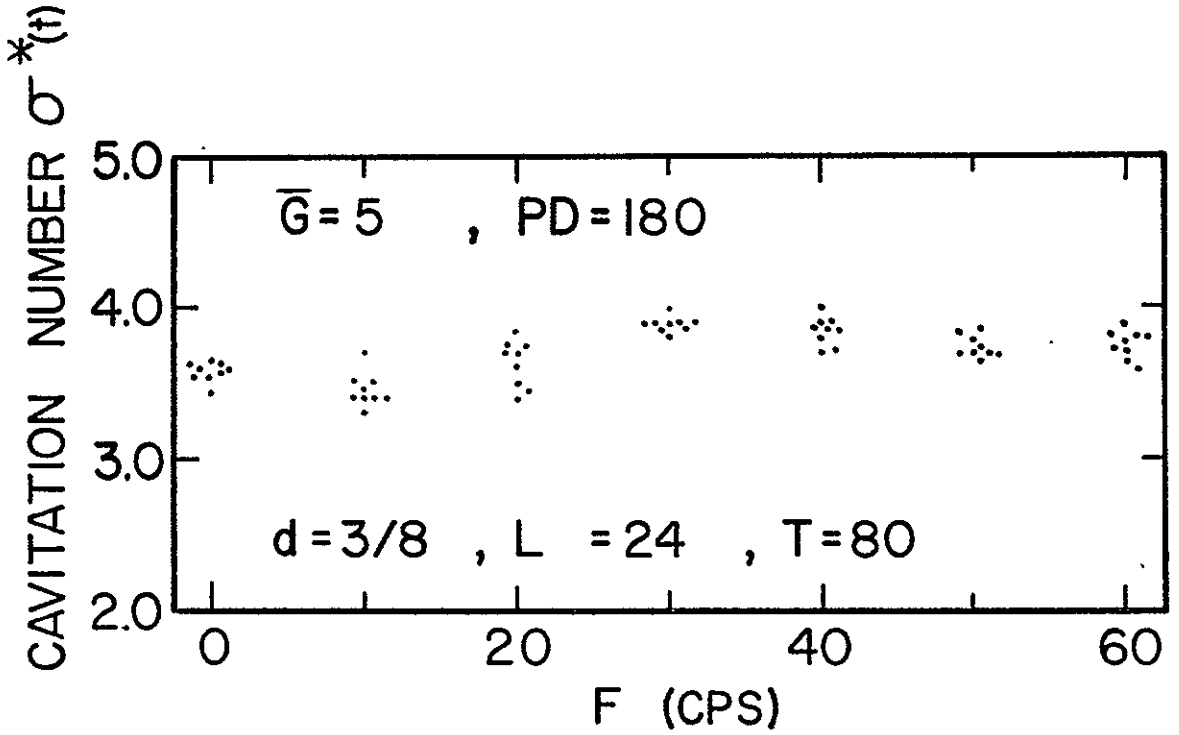

Figure 32. Time Dependent Modified Cavitation Number of Low Vibrational Frequencies and High $\overline{G}$ Level for Conditions, d = 3/8, L = 24, T = 80°F, PD = 180, $\overline{G}$ = 5.

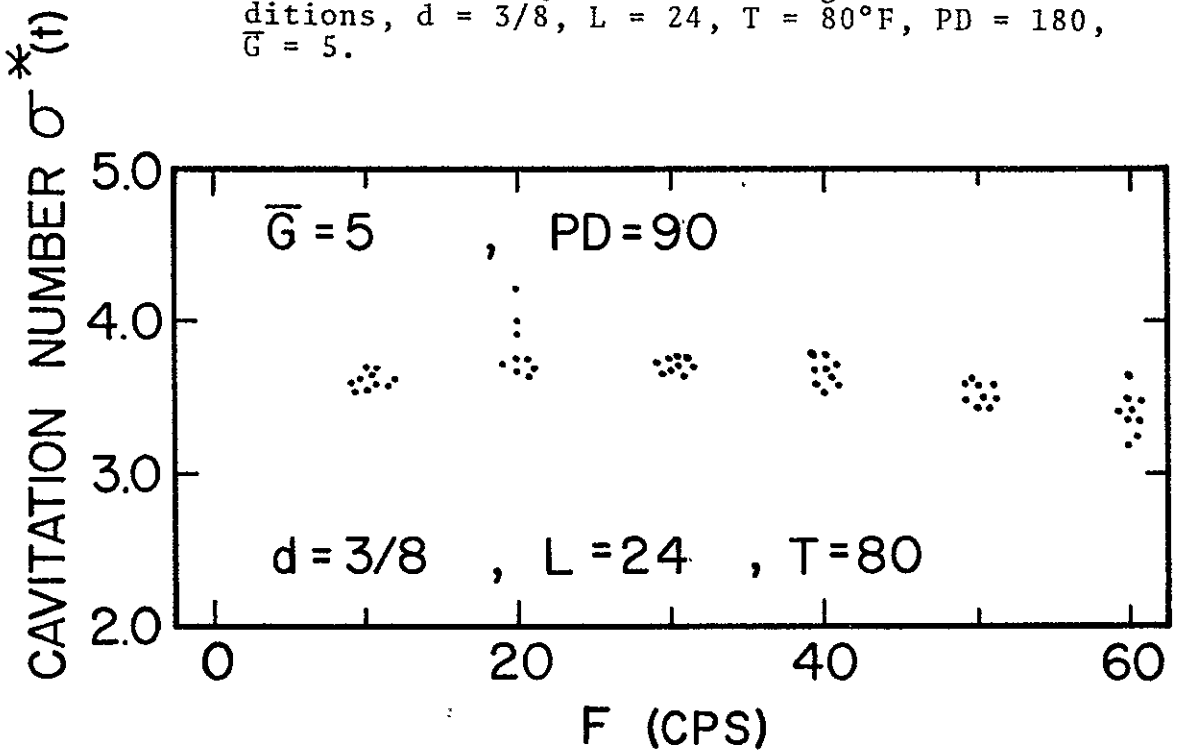

Figure 33. Time Dependent Modified Cavitation Number at Low Vibrational Frequencies and High $\overline{G}$ Level for Conditions, d = 3/8, L = 24, T = 80°F, PD = 90, $\overline{G}$ = 5.

7.3 Results and Conclusions for the Cavitation Analysis of the Discharge Line

The use of the modified cavitation number $\overline{\sigma}^*$ defined in equation (7.13) shows good agreement with measured data. The use of the free streamline analysis in arriving at this relation is a useful extension of this theory to flow in the entrance of a sharp edged discharge line. Extension of equation (7.13) to any similar geometry can evidently be made as long as the correct contraction coefficient is known.

The solution to the cavitation problem in a vibrating system was developed considering the liquid to be a hypothetical fluid, i.e. it can not sustain tensile forces. The theoretical significance of the phase deviation, PD, was discussed in conjunction with Figure 25. Obviously the experimental data presented does not substantiate the importance of the phase deviation.

In order to discuss the apparent lack of sensitivity of the liquid in following the pressure oscillations, a brief discussion of some of the properties of cavitation that may cause this retardation will be made. As mentioned in the Literature Survey, Holl (17) showed that the experimentally observed phenomenon of the existence of incipient and desinent cavitation numbers implies that the process of cavitation is more readily induced when the conditions required by the desinent cavitation number are satisfied. That is, once the

cavitation exists in a liquid, it is easier to maintain the condition than to induce it. This fact is in violation of the hypothetical fluid concept illustrated in Figure 25. The hysterisis effect and a measurable cavitation delay-time discussed in the paper by Holl and Treaster (18) further implies that the hypothetical fluid model is inaccurate in predicting the time dependent response of the fluid. Cavitation investigations have shown that the onset of cavitation in a given liquid requires a lower cavitation number (i.e. incipient cavitation number, σ_i) which is manifested in a higher liquid velocity than is predicted. Once cavitation is induced in a system, then the velocity of the liquid can be reduced to a lower value while cavitation is maintained. The cavitation number for this lower velocity case is called the desinent cavitation number, σ_d. It does not appear that a theory for this cavitation behavior has been extablished.

The work cited in reference (18) yields a possible explanation other than defining the two cavitation numbers. This is the mentioning of a cavitation-delay time for which certain general predictions as to velocity dependency, dissolved gas content, and surface tension are all parameters affecting the onset of cavitation. A significant conclusion stated in this reference is that the phenomenon of delay time was found to be completely random in nature. Until the physical processes are more completely understood the fact

that a real liquid may exhibit a delayed response to a low pressure must be accepted. Thus the lack of experimental phase deviation sensitivity is accounted for by the consideration that a finite response time exists for the liquid to produce sufficient vapor cavities to be visually observable as cavitation. An implication is that the pressure fluctuations associated with high frequency vibrations occur over such small intervals of time that the liquid cannot respond with a phase change when the static pressure drops below the vapor pressure during some part of its oscillation. Of course if the mean value of the static pressure drops to the vapor pressure, then cavitation could be expected to occur continuously. The desinent cavitation number was attributed to the fact that cavitation would prevail upon a slight reduction in flow velocity which can be considered equivalent to a slight increase in the local static pressure. The pressure fluctuations attributed to the vibration of the test section would be minor enough to not affect the cavitation, once started.

Quantitatively, the limits set on the value of the fluctuation of $\Delta\sigma^*$ seem the best method of interpreting the data. Until a more detailed analysis is made available, the use of the analysis by Schoenhals (44) seems to be a reasonably valid approach for a solution to the problem of flow in a vibrating discharge line.

The fact that the cavitation inception begins at the sharp edged entrance to the discharge line has been stated with no proof given. Because of the axisymmetric geometry of the discharge line, photographic attempts to record the phenomenon were unsuccessful. However work performed by the author in a two-dimensional apparatus allowed a successful photographic investigation. Figures 34 are illustrations of the two-dimensional apparatus with a geometry very similar to that of the sharp edged entrance to the discharge line. A cavitation streamer is shown attached to the sharp edge of the test section. The same type of phenomenon was visually observed in the present experimental work.

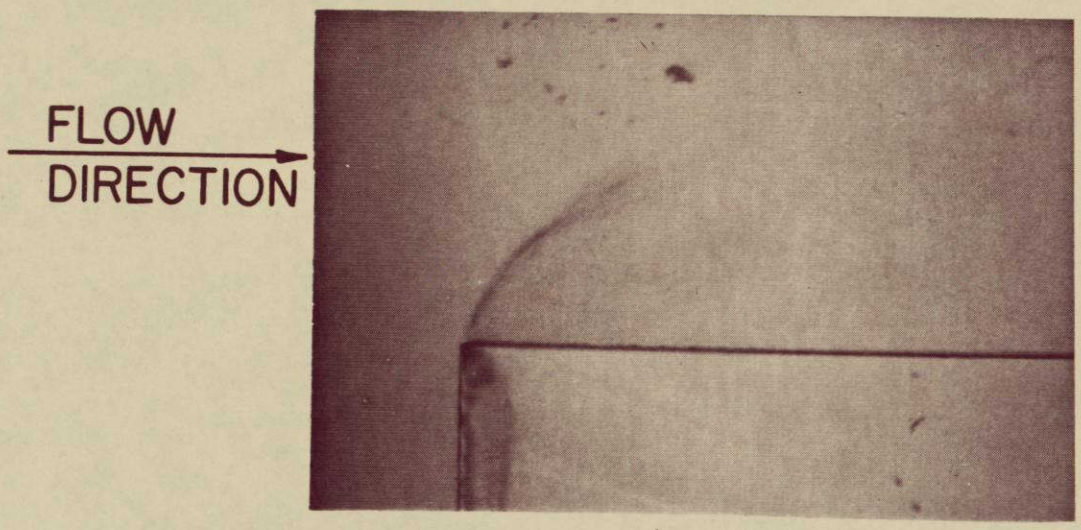

FIGURE 34a. Stroboscopic Picture of Cavitation Along the Free Streamline of a Two-Dimensional Discharge Line (Magnification 8X)

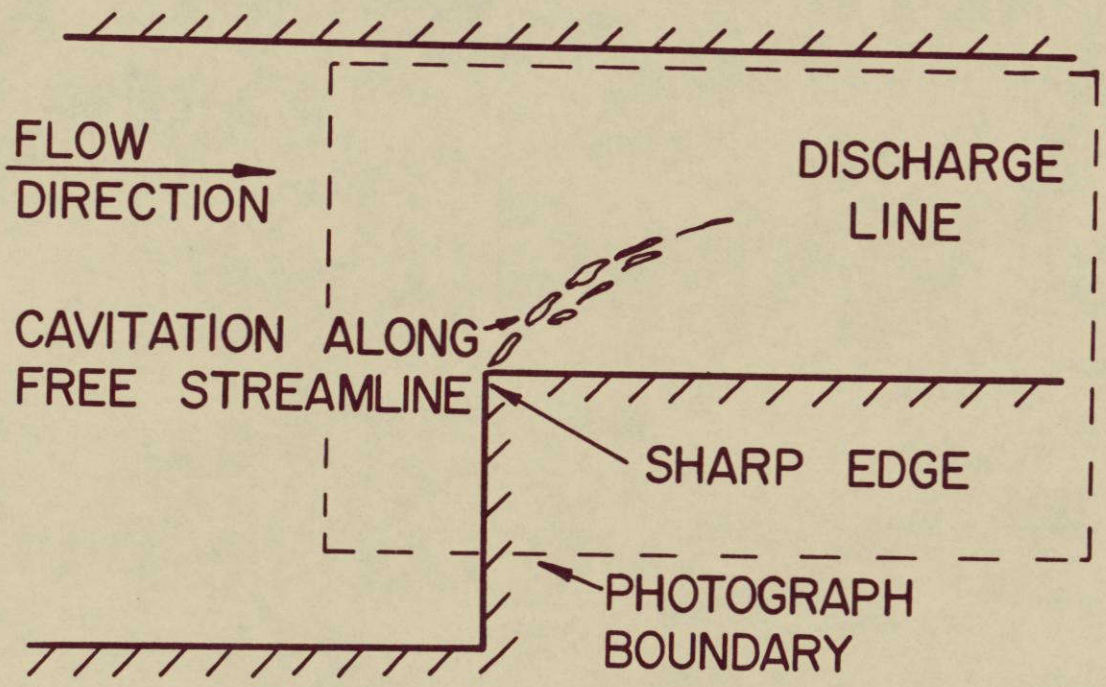

FIGURE 34b. Schematic Diagram Illustrating Two-Dimensional System Used in Obtaining Photograph of Figure

CHAPTER 8

TWO PHASE FLOW IN AN ADIABATIC DISCHARGE LINE AND CHOKING

8.1 Experimental Observations

The cavitation discussed in the preceeding chapter is the first indication that flashing is about to occur. The difference between flashing and cavitation is very subtle unless one has had the opportunity to observe both and come to a qualitative judgement on differentiation between the two. A quote from Collier and Wallis in reference (47) is used as an illustration.

> "If saturated liquid at pressure p_1 flows into a region at a lower pressure, p_2, and is not cooled on the way, some of the liquid will tend to "flash" to vapor."

Cavitation has previously been defined as the formation of vapor in a liquid when the static pressure reaches the vapor pressure because of flow conditions. Cavitation is vapor formation due to a local condition of very limited extent; whereas, flashing is vapor formation throughout the bulk of the fluid. Both phenomena occur due to a pressure reduction within the liquid. With this description in mind, it is now possible to discuss the two-phase flow conditions observed in the discharge line.

Upon the initial occurrence of cavitation, several different regimes of flow existed in the discharge line as illustrated in Figure 35 and are described below.

Regime (1): Cavitation in the form of vapor streamers is observed flowing along the free streamline originating at the sharp edged discharge line. The vapor streamers consisting of large numbers of small bubbles disappear within the liquid flow once the static pressure is high enough (condensation).

Regime (2): A vapor annulus forms at the entrance and extends in the positive z-direction (downward) in response to the pressure drop across the discharge line.

Regime (3): A liquid jet forms from the sharp edged entrance with a vapor layer between the liquid jet and the wall of the discharge line. The jet extends approximately π diameters in the z-direction before becoming unstable with the flow pattern subsequently transforming to a homogeneous one. A normal shock exists at the position where the homogeneous flow abruptly changes to a single-phase liquid flow.

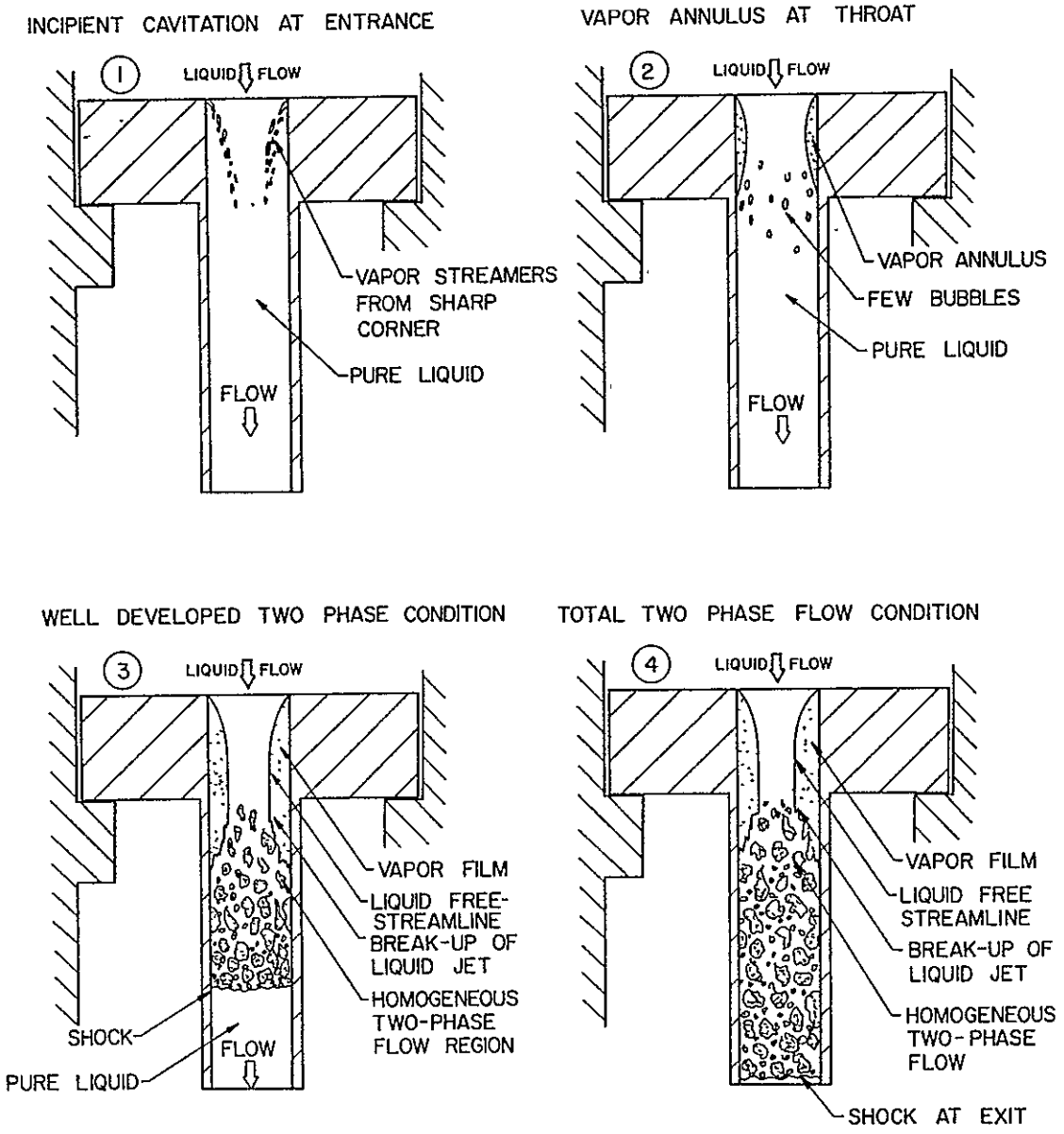

Figure 35. Regimes of Adiabatic Two-Phase Flashing Flow in a Sharp-Edged Discharge Line.

Regime (4): This is an extension of the previous flow pattern with the exception that the shock is now located in the exit plane of the discharge line. It cannot be driven out of the exit plane in a downstream direction.

It should be noted that the location of the shock that first appears in regime 3 is a function of the exit pressure of the test section. Once the shock is established in the line, a reduction of the exit pressure forces the shock front to move toward the exit plane of the line. The difference between flow regimes 3 and 4 described above consists of the fact that in regime 3 a reduction of the exit pressure will dislocate the shock while in regime 4 a further reduction in the exit pressure does not change the location of the shock. The dislocation of the shock front from the exit plane of the discharge line into the downstream plenum of the test section is physically impossible when the flow velocity of the fluid is reduced to such a low value that the corresponding static pressure does not allow the existence of a two-phase flow mixture. The existence of two-phase flow in the discharge line, however, raised the question of maximum flow rates, which are achieved under choked flow conditions, for given stagnation pressures.

An investigation of the pressure difference across the discharge line as a function of the upstream stagnation

pressure, P_s, showed conclusively that the flow under certain conditions could be choked. That is, a maximum flow rate for a given constant stagnation pressure value existed beyond which any further reduction in downstream pressure did not result in an increase of the flow rate. Experimental data illustrating this effect are shown in Figure 36 with "best fit" curves included. The significance of the figure lies in the fact that for a given stagnation pressure, P_s, the flow rate, Q, reaches a maximum value upon which the pressure difference can be increased without a further increase in flow rate. The increase in pressure difference at a constant upstream stagnation pressure value corresponds to a decrease in the exit pressure of the test section.

8.2 Derivation of an Analytical Model

The objectives of the study of the problem of two-phase flow in an adiabatic discharge line are listed below:

1. Determination of the maximum flow rate for given upstream stagnation conditions and line geometry.
2. Definition of the pressure losses which occur in this type of flow.
3. Determination of the parameters that directly affect the normal shock which appears in the line.

The first objective noted above for a two-phase flow situation can best be achieved if a comparison with choking of a perfect gas in a converging-diverging nozzle is made.

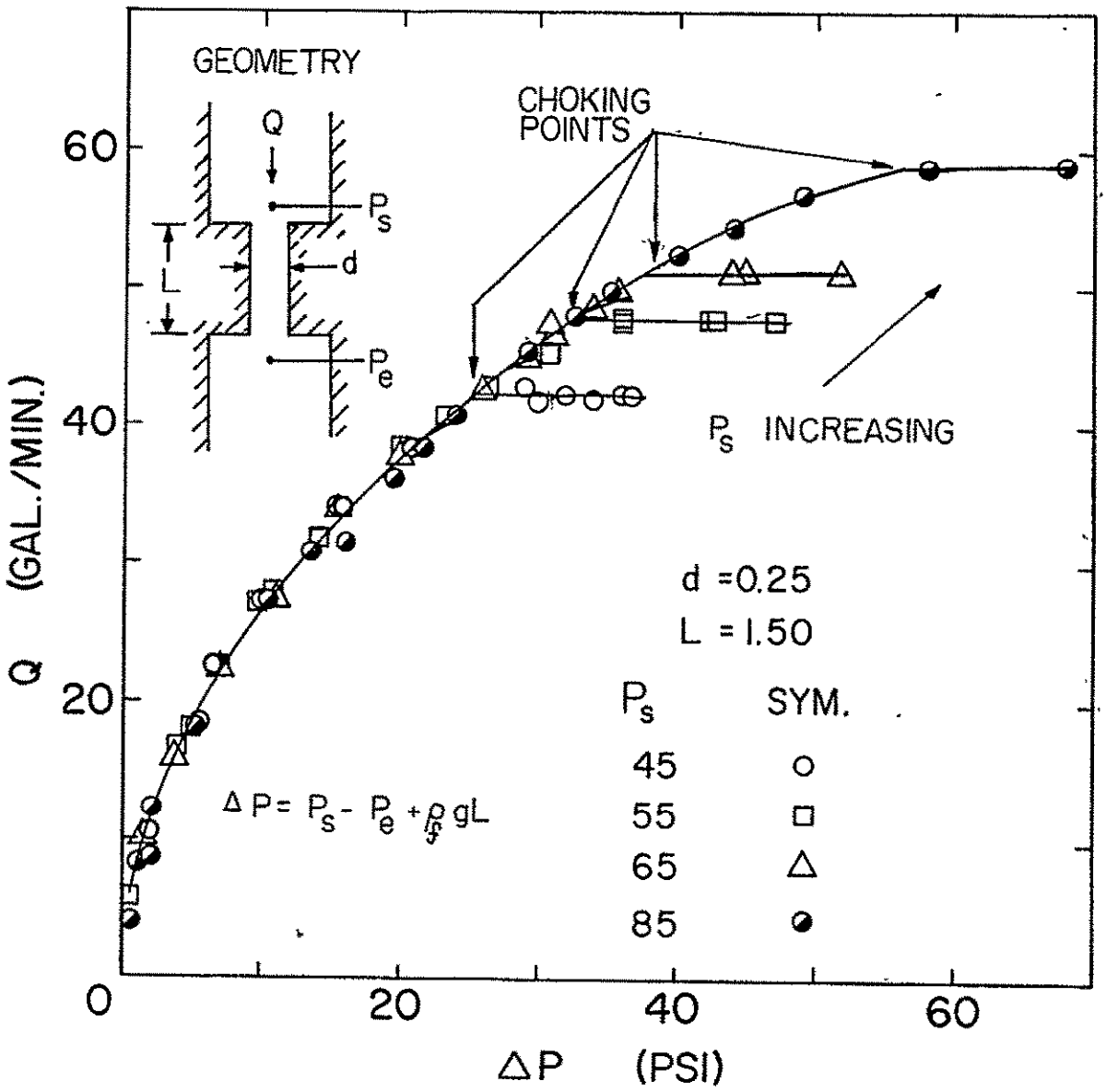

Figure 36. Volumetric Flow Rate for Various Upstream Stagnation Pressure Conditions as a Function of Pressure Drop Across the Discharge Line.

Consider a converging-diverging nozzle with constant upstream stagnation conditions and a variable exit pressure. The working fluid is an ideal gas. When the exit pressure equals the supply pressure, the trivial case of no flow prevails. As the exit pressure is lowered, the nozzle behaves like a typical venturi tube. The flow rate increases and the static pressure in the throat becomes sensitive to the exit pressure. This type of flow behavior continues until an exit pressure is reached where the flow rate at the throat becomes sonic. From this value of the exit pressure on to all lower values the flow rate stays constant. This operating condition is defined as choked flow. A further increase in flow rate would require an increase in upstream stagnation pressure or a change in temperature. The only effect that a change in the exit pressure produces is a change in the location of the shock which forms in the diverging portion of the nozzle.

The flow of a liquid in a discharge line behaves in a manner very similar to that described above for a perfect gas. That is, the liquid flow rate at a given upstream stagnation temperature and pressure depends on the exit pressure in a given system. Once a minimum value of the exit pressure is reached no further increase in flow rate can occur without changing the upstream conditions. This minimum pressure that the liquid can sustain at a given fixed temperature is its vapor pressure. Consideration of a control volume having

its exit plane in the two-phase mixture shows that the maximum flow rate will occur once the exit pressure is identical to the vapor pressure of the liquid. An attempt to further reduce the exit pressure of the liquid would only result in phase change of the liquid and hence an increase in the volumetric flow rate; however, the mass flow rate would remain constant. Experimentally this type of investigation would remain constant. Experimentally this type of investigation would be extremely difficult to perform because it would either require a pump which can handle a two-phase mixture or a very large tank maintained at constant pressure.

Using this criterion for the discharge line problem, the application of the free streamline solution presented by Rouse and Abul-Fetouh (6) provides the limiting flow conditions. Once the pressure along the free streamline reaches the vapor pressure and the pressure drop along the discharge line is sufficient for the jet to develop fully, the static pressure in the cylindrical cross section of the discharge line will be constant with a value equal to the vapor pressure. Since no further reduction in the pressure is possible, the condition for maximum flow now exists. It has to be noted that when the pressure in the liquid jet reaches the vapor pressure, nucleation can occur and the character of the flow changes. The flow in the discharge line has been observed to change from the jet flow to a homogeneous flow pattern with a normal shock present.

The defining relation for choked flow in a discharge line with a sharp edged entrance at a fixed stagnation pressure and temperature is given below. It is a limiting condition for the application of Bernoulli's equation along a streamline.

$$P_s = P_v + \frac{1}{2} \rho_f \left(V_f^*/C_c\right)^2 \tag{8.1}$$

or

$$V_f^* = C_c \sqrt{\frac{2(P_s - P_v)}{\rho_f}} \tag{8.2}$$

Data for several geometric configurations and for different temperatures are illustrated together with the solution to equation (8.2) in Figure 37.

The theoretical curves in Figure 37 represent the maximum possible values of the apparent liquid velocity corresponding to given values of the stagnation pressure, i.e. they are by definition the choking curves. For a fixed value of the upstream stagnation pressure, P_s, all values of the apparent liquid velocity up to and including the value represented by the solution to equation (8.2) are possible. In Figure 37, these possible flow conditions correspond to the areas above the curves. Since these choking curves are plotted as functions of the apparent liquid velocity, a straightforward conversion of V_f^* to the mass flux is possible by simply multiplying values of V_f^* by the density of the liquid. In this manner the mass flow rate is readily

Figure 37. Measured Flow Rates Under Choked Conditions as a Function of Stagnation Pressure for Various Discharge Line Geometries Compared with the Analytically Predicted Maximum Flow Rates.

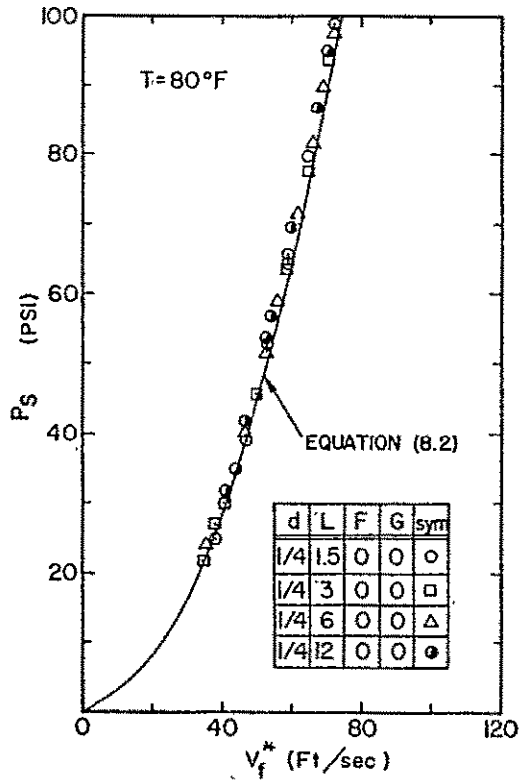
T=80°F
EQUATION (8.2)
d L F G sym
1/4 1.5 0 0 ○
1/4 3 0 0 □
1/4 6 0 0 △
1/4 12 0 0 ◐
P_S (PSI)
V_f^* (Ft/sec)

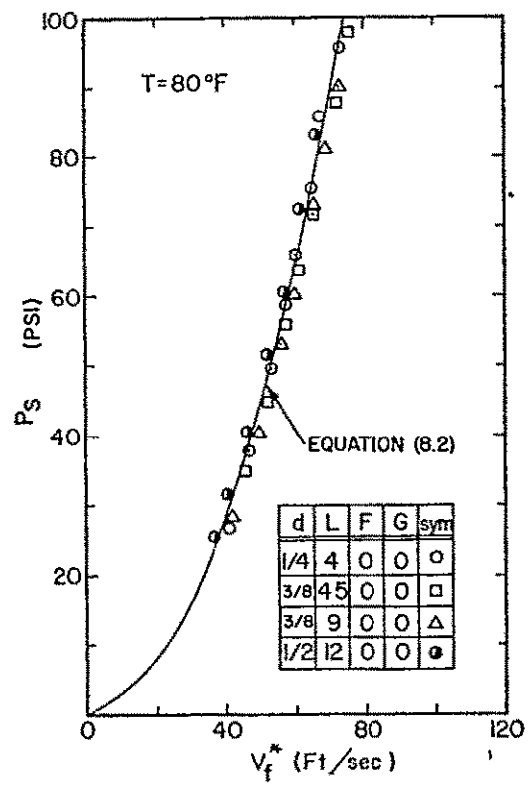
T=80°F
EQUATION (8.2)
d L F G sym
1/4 4 0 0 ○
3/8 45 0 0 □
3/8 9 0 0 △
1/2 12 0 0 ◐
P_S (PSI)
V_f^* (Ft/sec)

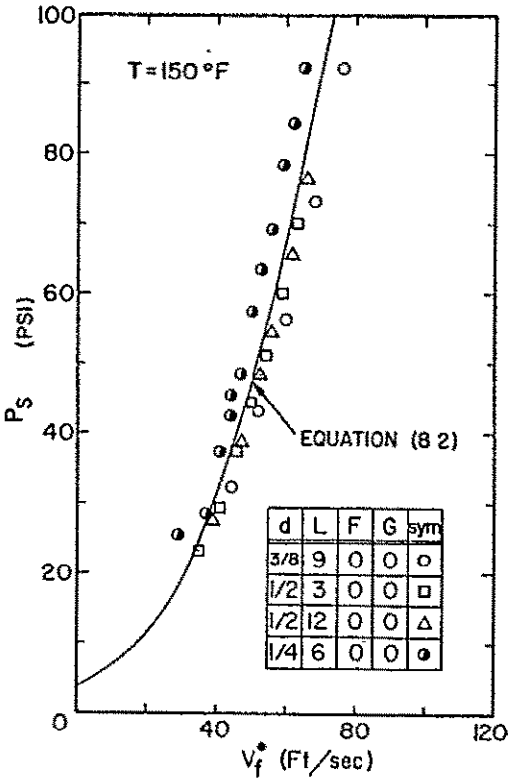
T=150°F
EQUATION (8.2)
d L F G sym
3/8 9 0 0 ○
1/2 3 0 0 □
1/2 12 0 0 △
1/4 6 0 0 ◐
P_S (PSI)
V_f^* (Ft/sec)

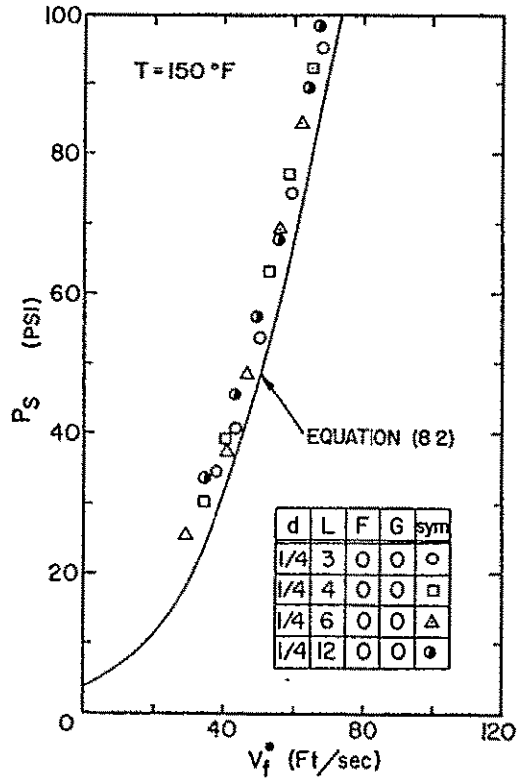
T=150°F
EQUATION (8.2)
d L F G sym
1/4 3 0 0 ○
1/4 4 0 0 □
1/4 6 0 0 △
1/4 12 0 0 ◐
P_S (PSI)
V_f^* (Ft/sec)

Figure 37

determined by knowing the upstream stagnation conditions and the geometry of the discharge line under investigation.

Since the maximum flow rates (choked flow) are determined by equation (8.2), the analysis must proceed in a more specific manner to investigate the flow within the discharge line in view of prevailing static pressures and temperatures. Of primary importance is the prediction of the static pressures and pressure losses incurred by the fluid flowing through the discharge line. An explanation of the notation and geometry used in the subsequent derivation is illustrated in Figure 38.

The static pressure measured along the wall of the discharge line in the region

$$0 < z < \eta$$

equals the vapor pressure of the liquid, and is identical to the static pressure along the free streamline. The liquid jet, however, maintains a pressure field which is a function of the coordinates r, θ, z until its width is close to its asymptotic value. Within the jet the static pressure is not constant until $z = \eta$.

For $0 < z < \eta$

$$p_{static,jet} = p(r, \theta, z) \qquad (8.3)$$

This functional relation is graphically illustrated by Rouse and Abul-Fetouh (6). At the position where the static pressure is constant in a radial direction, the jet changes into a

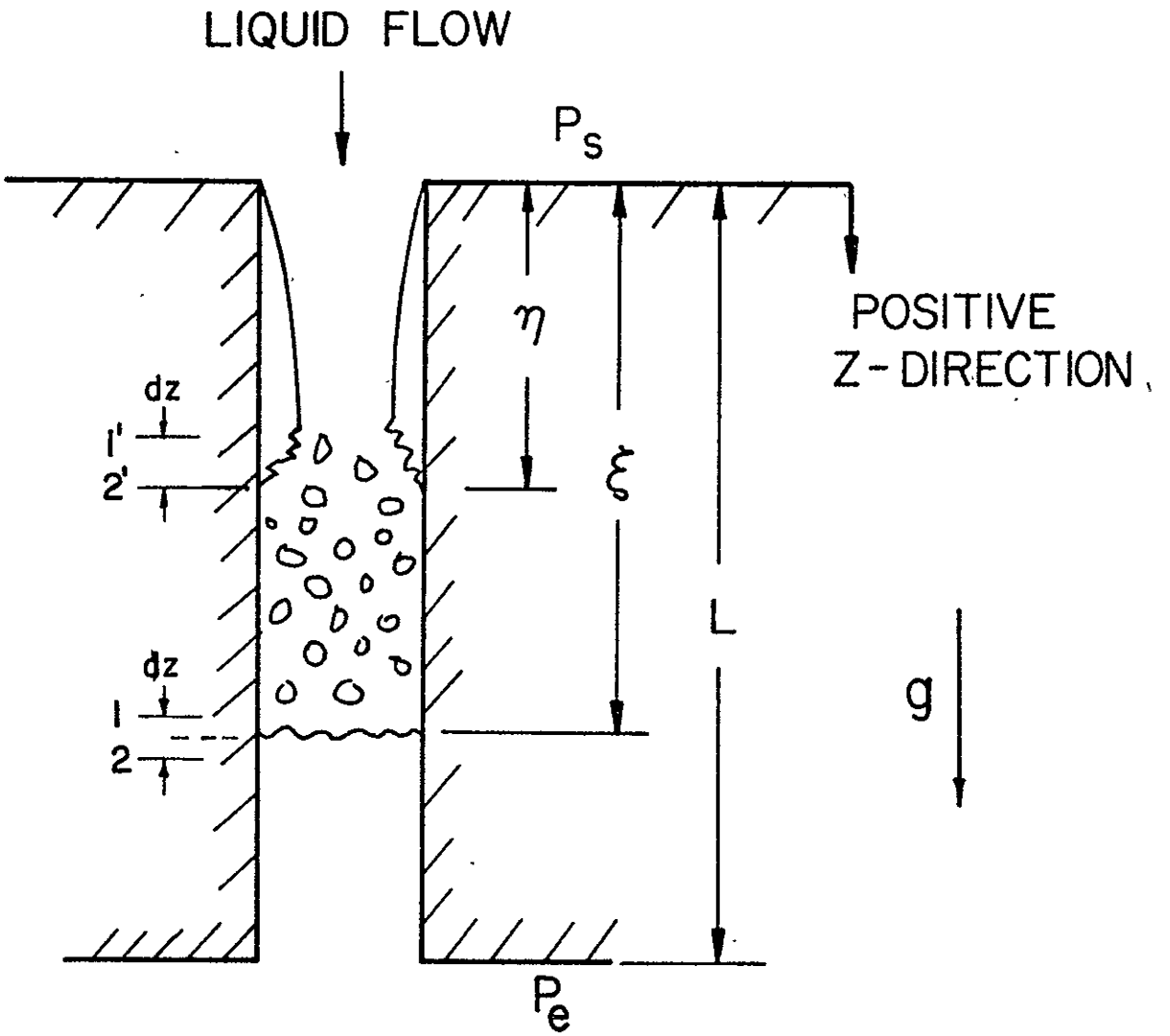

η = LENGTH AT JET TRANSFORMATION (HOMOGENEOUS FLOW STARTING POINT)

ξ = POSITION OF TWO-PHASE : SINGLE PHASE SHOCK

L = LENGTH OF DISCHARGE LINE

Figure 38. Geometry and Coordinate System for Analysis of Adiabatic Two-Phase Flow in Discharge Line.

homogeneous, two-phase flow pattern. In the homogeneous flow regime, the pressure is constant and equal to the vapor pressure. Experimental verification of this fact is presented in Figure 39 where the pressure difference between the upstream stagnation pressure and the static pressure, p_2, is illustrated. The location of the pressure tap through which the static pressures, p_2, were measured is shown in Figure 7. The choked flow curve shown in Figure 39 is derived from the following expression.

$$P_s - p_2 = \frac{1}{2} \rho_f \left(V_f^*/C_c\right)^2 \qquad (8.4)$$

with $p_2 = P_v$

For comparison purposes, a similar set of experiments was performed where the flow conditions were adjusted in such a way that no cavitation or flashing occurred. Again the static pressures in the discharge line were measured and for this situation also displayed in Figure 39. The difference between the given stagnation pressure and the measured static pressure, p_2, is shown as the ordinate while the apparent liquid velocity, V_f^*, which, now in the case of liquid flow only, is the real one-dimensional velocity, appears as the abscissa.

If in a given experiment with constant stagnation pressure, say P_s = 40 psia, the exit pressure is decreased, i.e. the flow velocity, V_f^*, is increased, then the difference between the constant stagnation pressure and the measured

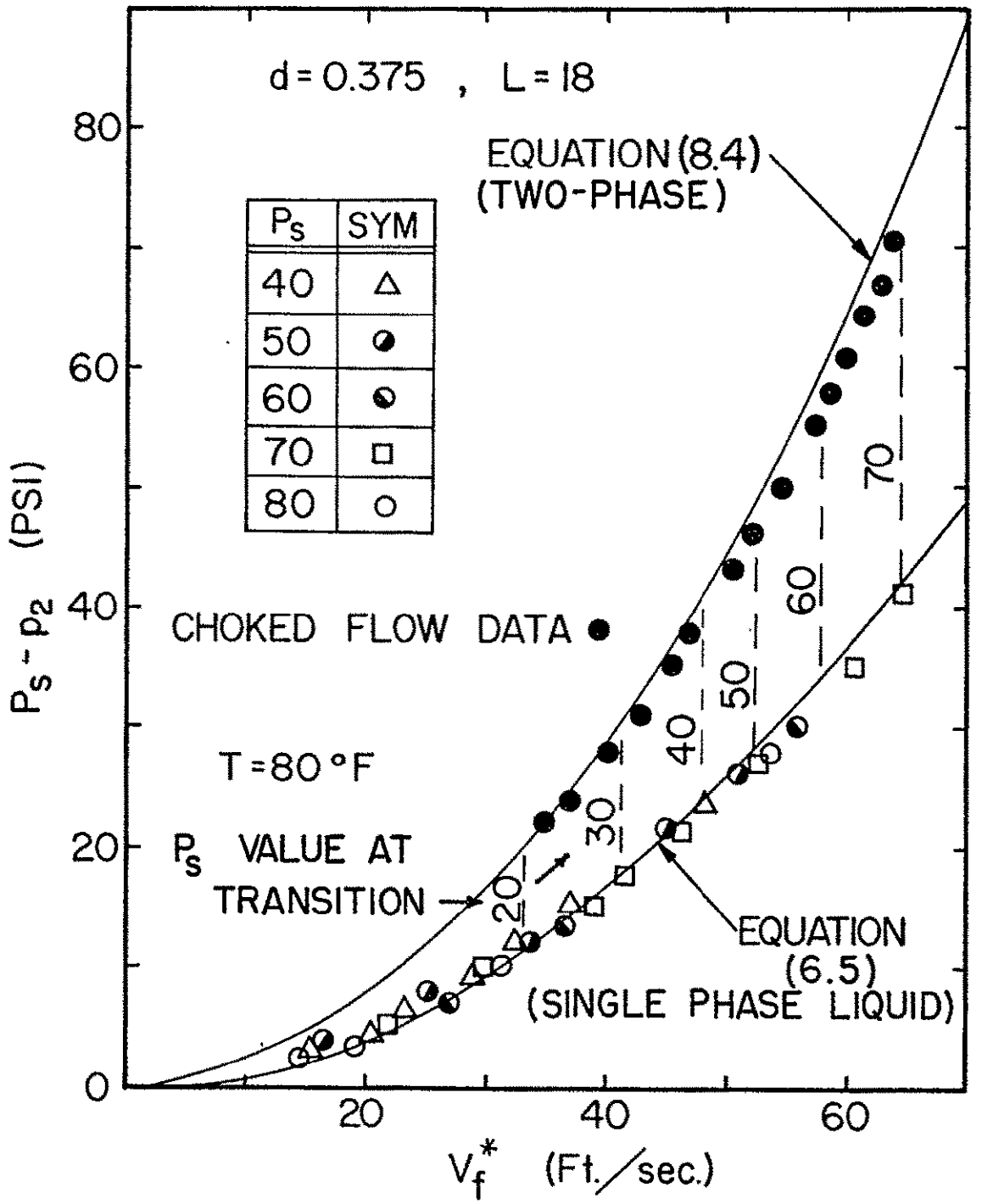

Figure 39. Comparison of the Dynamic Pressure for Single Phase Liquid Flow as a Function of Apparent Liquid Velocity with Difference of Stagnation Pressure and Static Pressure of a Flashing Fluid for Various Stagnation Pressures.

static pressure follows the lower curve as predicted by equation 6.5 shown in Figure 39. Once flashing occurs the static pressure, p_2, reaches the vapor pressure of the liquid and the difference between the stagnation pressure and the new static pressure suddenly increases to a higher value. These observations are shown for various constant stagnation pressures (dashed lines) in Figure 39. Since the pressure tap 2 was located a sufficient distance from the entrance to the discharge line, the flow was always choked when the measured static pressure was equal to the vapor pressure.

The static pressure in the two-phase flow region of the discharge line was found to be equal to the vapor pressure. Now consideration of the stagnation pressure losses must be made. The pressure loss expression for the sudden contraction at the entrance defined for the single-phase liquid in equation (5.2) can be modified and applied to the contraction with flashing. Richardson (49) found a value for the loss coefficient K to be approximately 0.20 for the area ratios used in the present test section configuration. It should be noted that Richardson dealt with two-phase, two-component flow; he did not study flashing. Richardson's value for the loss coefficient was defined on the basis that the fluid density equaled the mixture density rather than that of the single-phase liquid. This implies that the void fraction must be included in the definition of the entrance loss. That is,

for $0 < z < \eta$

$$\Delta P_{entrance,TP} = K(1 - \alpha)\left(\frac{1}{2} \rho_f V_f^{*2}\right) \qquad (8.5)$$

where $K = 0.20$

As demonstrated later, this assumption for the loss at the entrance is justified by the experimental results obtained in this investigation.

The entrance loss defined in equation (8.5) accounts for the stagnation pressure loss due to the contraction and jet formation. This definition explains the pressure loss from the entrance plane of the discharge line to the position η. In this length of the discharge line, the liquid phase of the two-phase mixture does not come into contact with the wall. The vapor annulus separates the liquid jet from contact with the wall, and subsequently the frictional losses over this portion of the flow are negligibly small. This condition is stated below in a more explicit form.

For $0 < z < \eta$

$$\Delta P_{friction,TP} \approx 0 \qquad (8.6)$$

However, when the transition to homogeneous flow takes place in the discharge line, a significant pressure loss due to frictional effects does occur. The friction factors obtained previously for the single-phase flow were applied by taking the two-phase friction factor, f_{TP}, equal to the already known single-phase liquid friction factor. This is illustrated by Collier and Wallis (51) who discuss a suitably defined

two-phase flow friction factor for the homogeneous model, i.e. pseudo-fluid.

$$f_{TP} = f \equiv \psi \left[\frac{(W/A)d}{f}, \ \varepsilon/d\right] \tag{8.7}$$

where $\varepsilon/d \equiv$ relative roughness

The frictional pressure loss can be defined as follows. For $\eta < z < \xi$

$$\left(\frac{\partial p}{\partial z}\right)_{\text{friction,TP}} = \frac{f_{TP}}{d}\left(\frac{1}{2}\rho_m V_m^2\right) \tag{8.8}$$

Obviously the void fraction, α, needs to be known before equation (8.8) can be used because of the functional dependency of the density and velocity of the mixture on α.

Consider now the flow at two locations in the discharge line defined below.

$$z_1' = \eta - dz$$
$$z_2' = \eta \tag{8.9}$$

The continuity and momentum equations are written and simplified between the two control planes.

Continuity: $$G_1' = G_2' \tag{8.10}$$

Momentum:

$$p_1' + \left(G_f V_f + G_g V_g\right)_1' = p_2' + \left(G_f V_f + G_g V_g\right)_2' \tag{8.11}$$

Note that over the interval from z_1' to z_2', the frictional force in the z-direction is still defined as being zero. Here the liquid phase does not come into contact with the wall until $z = \eta$; thus the frictional pressure gradient can

be neglected. The static pressure in the flashing flow regime has been shown previously to be equal to the vapor pressure.

That is,

$$p_{1'} = p_{2'} = P_v \tag{8.12}$$

Since the vapor in the region $0 < z < \eta$ flashes from the surface of the free streamline envelope, the component of velocity of the vapor in the positive z-direction can be assumed to be equal to the free streamline velocity.

$$V_{f_{1'}} = V_{g_{1'}} \tag{8.13}$$

With the assumption of homogeneous flow at $z_{2'}$, another condition can be stated.

$$V_{f_{2'}} = V_{g_{2'}} = V_m \tag{8.14}$$

Substitution of equations (8.12 - 8.14) into (8.11) yields a modified momentum equation.

$$(G_f + G_g)_{1'} V_{f_{1'}} = (G_f + G_g)_{2'} V_m \tag{8.15}$$

From continuity,

$$G_{1'} = (G_f + G_g)_{1'} = G_{2'} = (G_f + G_g)_{2'} \tag{8.16}$$

it is obvious that

$$V_{f_{1'}} = V_m \tag{8.17}$$

The theory of jet flow claims that the area of the jet equals the area of the orifice times the contraction coefficient. The velocity of the liquid at η is defined below.

$$V_{f_1} = \frac{Q_f}{A_{jet}} = \frac{Q_f}{C_c(\pi d^2/4)} = \frac{V_f^*}{C_c} \tag{8.18}$$

With the assumption that the density of the vapor phase is much smaller than that of the liquid phase,

$$\rho_g << \rho_f \tag{8.19}$$

the continuity relation given in equation (8.10) is rewritten as

$$\rho_m V_m = \rho_f V_f^* \tag{8.20}$$

since

$$\rho_m = \alpha\rho_g + (1 - \alpha)\rho_f \simeq (1 - \alpha)\rho_f$$

$$V_m = \frac{V_f^*}{1 - \alpha} \tag{8.21}$$

Upon combining equations (8.17), (8.18), and (8.21), an expression for the value of the void fraction at $z = \eta$ is obtained.

$$\frac{V_f^*}{C_c} = \frac{V_f^*}{1 - \alpha} \tag{8.22}$$

Therefore

$$\alpha = 1 - C_c \text{ at } z = \eta \tag{8.23}$$

With a known value for the void fraction, α, in the plane of transition from jet flow (reversed annular) to homogeneous two-phase flow, it is now possible to analyze the shock phenomena observed in the discharge line under choked flow conditions.

Consider the situation shown in Figure 38 where the normal shock is located at a position ξ in the discharge line. One-dimensional normal shock relations describing the flow dynamics can be used to derive the downstream flow conditions in the single-phase liquid.

According to Figure 38 the coordinates are written below.

$$\text{Let} \qquad z_1 = \xi - dz/2 \qquad z_2 = \xi + dz/2 \tag{8.24}$$

At location z_1, two-phase homogeneous flow exists. At location z_2, single-phase liquid flow prevails. Treating the homogeneous regime as flow of a pseudo-fluid allows the following relations to be formulated.

$$J_2 = V_2 \qquad \rho_2 = \rho_f \qquad V_{f_1} = V_{g_1} \tag{8.25}$$

$$J_1 = V_1 \qquad \rho_1 = \rho_m$$

where J_2 = volumetric flux at position 2, etc.

The continuity equation is applied for the control areas at z_1 and z_2.

$$\rho_1 V_1 = \rho_1 J_1 = \rho_2 V_2 = \rho_2 J_2 = \rho_f V_f^* \tag{8.26}$$

or

$$J_1 = \frac{\rho_2 J_2}{\rho_1} \tag{8.27}$$

The volumetric flux difference (relative flux) is determined to be

$$J_2 - J_1 = J_2(1 - \rho_f/\rho_1) \tag{8.28}$$

$$J_2 - J_1 = \frac{\rho_f V_f^*}{\rho_2} (1 - \rho_f/\rho_1) \tag{8.29}$$

With the assumption that

$$\rho_1 \approx (1 - \alpha) \rho_f$$

it becomes

$$J_2 - J_1 = \frac{\rho_f V_f^*}{\rho_2} \left(1 - \frac{1}{1 - \alpha}\right) \tag{8.30}$$

which simplifies to

$$J_2 - J_1 = \frac{-\alpha V_f^*}{1 - \alpha} \tag{8.31}$$

The momentum equation written for the coordinates z_1 and z_2 can be expressed in the form below.

$$p_1 + GJ_1 = p_2 + GJ_2 \tag{8.32}$$

Once again the fact that the pressure in the flashing flow regime equals the vapor pressure is used to simplify equation (8.32).

$$p_2 = P_v - G (J_2 - J_1) \tag{8.33}$$

Substitution of equation (8.31), the continuity equation, into equation (8.33), the momentum equation, yields the expression for the pressure in the liquid immediately downstream of the normal shock.

$$p_2 = P_v + \frac{1}{2} \rho_f V_f^{*2} \left(\frac{2 \alpha}{1 - \alpha}\right)\Big|_\xi \tag{8.34}$$

From the position z_2 to the exit plane of the discharge line, the one dimensional friction loss relation for a single phase liquid, equation (6.3), is applied. Again the expansion loss defined in equation (6.6) also is applied at the exit plane since the flow is single phase after passing through the shock.

Use of the energy equation between coordinates z_2 and the exit region of the test section determines the downstream stagnation pressure in the test section, P_e.

$$P_e = p_2 + \rho_f g (L - \xi) + \frac{1}{2} \rho_f V_f^{*2} - \Delta P_{friction} \Big|_{\xi}^{L} - \Delta P_{expansion} \tag{8.35}$$

Substituting the relations for the friction and expansion losses in addition to the definition of pressure p_2 into equation (8.35) yields the somewhat complicated expression,

$$P_e = P_v + \frac{1}{2} \rho_f V_f^{*2} \left(\frac{2\alpha}{1 - \alpha} \right) \Big|_{\xi} + \rho_f g (L - \xi)$$

$$+ \frac{1}{2} \rho_f V_f^{*2} - \frac{f(L - \xi)}{d} \frac{1}{2} \rho_f V_f^{*2}$$

$$- (1 - d^2/D^2)^2 \frac{1}{2} \rho_f V_f^{*2} \tag{8.36}$$

After rearranging terms and simplifying, the exit stagnation pressure is given by equation (8.37).

$$P_e = \frac{1}{2} \rho_f V_f^{*2} \left[\frac{1 + \alpha}{1 - \alpha} \Big|_{\xi} - \frac{f(L - \xi)}{d} - (1 - d^2/D^2)^2 \right]$$

$$+ P_v + \rho_f g (L - \xi) \tag{8.37}$$

The total stagnation pressure loss across the discharge line due to fluid flow can now be determined. Note that the losses are zero for the condition of no flow in this definition.

$$\Delta P = P_s - P_e + \rho_f g L \tag{8.38}$$

If flow is occurring within the discharge line, then the pressure losses due to the flow must be subtracted from the exit stagnation pressure, P_e. Thus for flow in the discharge line,

$$\Delta P = P_s + \rho_f g L \left(P_e - \Delta P_{entrance} - \int_n^{\xi} \left(\frac{\partial P}{\partial z}\right)_{f,TP} dz + \int_0^{\xi} g \rho_m(z) dz \right) \tag{8.39}$$

Substitution of equation (8.37) into equation (8.39) yields the expanded relation for the stagnation pressure loss caused by flow in the discharge line.

$$\Delta P = P_s - P_v + \rho_f g L + \Delta P_{entrance} + \frac{1}{2} \rho_f V_f^{*2} \left[\frac{f(L - \xi)}{d} + (1 - d^2/D^2)^2 - \frac{1 + \alpha}{1 - \alpha}\Big|_{\xi} \right] + \int_n^{\xi} \left(\frac{\partial P}{\partial z}\right)_{f,TP} dz - \int_0^{\xi} g \rho_m(z) dz - \rho_f g(L - \xi) \tag{8.40}$$

To simplify equation (8.40), it is possible to combine the hydrostatic pressure terms into one simplified relation.

$$\rho_f g L - \int_0^{\xi} g \rho_m(z) dz - \rho_f g (L - \xi) = \int_0^{\xi} g \left(\rho_f - \rho_m(z)\right) dz \tag{8.41}$$

Substituting equations (8.5) and (8.41) into the pressure loss equation (8.40) with the assumption,

for $0 \leq z \leq \xi$

$$[\rho_f - \rho_m(z)] \approx [\alpha(z)\ \rho_f] \tag{8.42}$$

yields the final form of the pressure loss equation.

$$\Delta P = \frac{1}{2}\rho_f V_f^{*2}\left[0.2(1-\alpha)\Big|_\eta + \frac{f(L-\xi)}{d} + (1-d^2/D^2)^2 - \frac{1+\alpha}{1-\alpha}\Big|_\xi\right]$$

$$+ P_s - P_v + \int_\eta^\xi \left(\frac{\partial p}{\partial z}\right)_{f,TP} dz + \int_0^\xi g\ \rho_f\ \alpha(z)dz \tag{8.43}$$

With equation (8.43), it is now possible to predict the loss in recoverable stagnation pressure across the test section for a given position of the shock. This loss is measured by the differential pressure transducer located between the inlet pipe and exit pipe of the test section. It was adjusted to read zero under the no flow condition, $V_f^* = 0$. It will be demonstrated later that equation (8.43) can be used for the prediction of the location of the normal shock front under given flow conditions.

8.3 Discussion of Choking Conditions

In this section, the definition for choking in two-phase flow is applied to the analytical model described in the previous section. This is done to illustrate that the defining equations satisfy the accepted choking conditions. Use is made of equation (8.43) for the analytical prediction of choking. These predictions are then compared with experimental measurements made on the discharge line.

A one-dimensional steady state analysis of homogeneous two phase flow using the momentum equation yields an expression for the pressure gradient in a system which is the sum of several components, each of which is associated with a particular physical effect. The homogeneous flow model is employed since this flow regime is clearly discernable in the discharge line upstream of the shock, and because it is analytically the most tractable to apply. In analytical form the pressure gradient in the positive z-direction is given by

$$\frac{dp}{dz} = \left(\frac{dp}{dz}\right)_f + \left(\frac{dp}{dz}\right)_a + \left(\frac{dp}{dz}\right)_g \qquad (8.44)$$

where $\left(\frac{dp}{dz}\right)_f \equiv$ frictional component of pressure gradient

$\left(\frac{dp}{dz}\right)_a \equiv$ acceleration component of pressure gradient

$\left(\frac{dp}{dz}\right)_g \equiv$ gravitational component of pressure gradient

Equation (8.44) can be found in the literature in a multitude of forms in terms of various combinations of variables. A pertinant discussion is presented in references (53) and (54). To illustrate the significance of equation (8.44), it can be written in a steady-state analysis as a combination of influence coefficients.

$$\left.\begin{matrix} C_f \\ C_x \\ C_a \\ C_g \end{matrix}\right\} \text{ Influence coefficient of } \left\{\begin{matrix} \text{friction} \\ \text{phase change} \\ \text{area change} \\ \text{gravity} \end{matrix}\right\} \text{ on pressure gradient}$$

Using the concept of an influence coefficient, equation (8.44) can be shown to have the following form.

$$\frac{dp}{dz} = \frac{C_f + C_x \frac{dx}{dz} + C_A \frac{1}{A} \frac{dA}{dz} + C_g \, g \cos \tau}{1 - M^2} \qquad (8.45)$$

The term, M^2, in the denominator represents the Mach number squared of a pseudo fluid, and it has the same significance as in the compressible single component flow equation. If an analogy is made between single phase compressible fluid flow and the homogeneous "pseudo" fluid, a choking criterion can be established. For compressible flow, a condition of Mach number equal to unity at some location along the flow path is always associated with choking. The above derivative, equation (8.45), becomes infinite in value. For homogeneous flow, this derivative is indeterminate not only for Mach equal to one but also for sudden changes in the quality, X.

Consider now the flow at position ξ indicated in Figure 38. At this location a finite change in quality occurs in zero length at the interface between the homogeneous "pseudo" fluid and the single phase liquid. The relation, equation (8.45), becomes infinite at this location; and although the Mach number does not necessarily equal unity the flow is choked.

A special case of the flow in the discharge line can now be discussed. Let the shock be located immediately downstream of the transition from jet flow to homogeneous flow. The following conditions therefore exist.

$$(\xi - \eta) \approx 0 \tag{8.46}$$

$$\int_{\eta}^{\xi} \left(\frac{dp}{dz}\right)_{f,TP} dz = 0 \tag{8.47}$$

Following from the above assumption, the relation for the void fraction can be determined from the contraction coefficient.

$$\frac{1 + \alpha}{1 - \alpha}\Big|_{\xi} = \frac{1 + \alpha}{1 - \alpha}\Big|_{\eta} = \frac{2 - C_c}{C_c} \tag{8.48}$$

Substituting the above conditions into the expression for the pressure loss across the discharge line, equation (8.43), yields a relation which represents the minimum pressure loss for a choked condition. Neglecting the contribution of the hydrostatic pressure change results in

$$\int_{0}^{\xi} g\, \alpha(z)\, \rho_f\, dz \approx 0 \tag{8.49}$$

Therefore

$$\Delta P_{min.} = \frac{1}{2} \rho_f V_f^{*2} \left[0.2(1-\alpha)\Big|_{\eta} + \frac{f(L-\xi)}{d} + (1-d^2/D^2)^2 - \frac{2-C_c}{C_c}\right] + P_s - P_v \tag{8.50}$$

Once again an analogy can be made between the flow in the discharge line and single phase compressible flow. In particular, the pressure profiles for a single phase compressible flow in a converging-diverging nozzle serve as a basis for comparison. There exists a back pressure for the nozzle at which the flow reaches a sonic condition in the throat which can be considered as an infinitely weak shock, and then

exits subsonically with the diverging portion of the nozzle acting as a diffuser. At a value of the back pressure lower than this "critical" pressure a normal shock exists in the nozzle, the location of which is dependent on the value of the back pressure. A similar situation prevails in the discharge line. There exists a back pressure where an infinitely weak shock exists in the liquid. This occurs under the condition of $\eta = \xi$. A further decrease in the back pressure below this "critical" pressure moves the shock in a downstream direction without affecting the flow rate.

Equation (8.50) can be used to determine the maximum value for the pressure loss for non-choked flow. A comparison with experimentally measured values for the pressure loss in two geometric configurations where the shock was located in what is usually the transition region from jet flow to homogeneous flow, $\xi - \eta \approx 0$, is given in Table 4.

Table 4

Comparison of Experimental and Theoretical Values of the Minimum Pressure Loss for Choked Flow

$(\xi - \eta) \approx 0$

L = 24, d = 0.375, f = 0.0155, T = 80°F			
P_s	V_f^*	$\Delta P_{theoretical}$	$\Delta P_{experimental}$
68	61.2	61.2	61
78	65.6	70.0	68
87	69.3	78.5	77
L = 12, d = 0.5, f = 0.0160, T = 80°F			
P_s	V_f^*	$\Delta P_{theoretical}$	$\Delta P_{experimental}$
28	39.0	18.6	18.5
32	41.8	21.0	22
42	48.0	28.0	29
50	52.4	33.5	34

The special case shown in Table 4 has already been described as the minimum pressure loss across the discharge line for choked flow. This means that the exit pressure could continue to decrease for a constant upstream stagnation pressure without increasing the flow rate. The only effect of such a reduction would be to move the shock towards the exit plane of the discharge line. The functional relationship which exists between the motion of the shock and the exit pressure can be determined by a differentiation of equation (8.37) which relates the exit pressure to the shock coordinate, ξ.

$$P_e(\xi) = P_e\Big|_{\xi=\eta} - \frac{\partial \Delta P}{\partial \xi}\,(\xi - \eta) \tag{8.51}$$

The expression for the stagnation pressure loss, equation (8.43), can be differentiated with respect to the coordinate ξ. That is,

$$\frac{\partial(\Delta P)}{\partial \xi} = \frac{1}{2}\rho_f V_f^{*2} \cdot \frac{\partial}{\partial \xi}\left\{0.2(1-\alpha)\Big|_\eta + \frac{f(L-\xi)}{d} + (1-d^2/D^2)^2 - \frac{1+\alpha}{1-\alpha}\Big|_\xi\right\}$$

$$+ \frac{\partial}{\partial \xi}\int_\eta^\xi \left(\frac{\partial p}{\partial z}\right)_{f,TP} dz + \frac{\partial}{\partial \xi}\int_0^\xi g\rho_f \alpha(z)dz \tag{8.52}$$

Simplifying this relation gives,

$$\frac{\partial(\Delta P)}{\partial \xi} = -\frac{f}{d}\frac{1}{2}\rho_f V_f^{*2} + \frac{\partial}{\partial \xi}\int_\eta^\xi \left(\frac{\partial p}{\partial z}\right)_{f,TP} dz$$

$$+ \frac{\partial}{\partial \xi}\int_0^\xi g\,\rho_f\,\alpha(z)dz \tag{8.53}$$

The definition of the frictional pressure gradient was given in equation (8.8) in terms of the mixture density and

mixture velocity. The continuity equation can be used to redefine the frictional pressure gradient in terms of the void fraction and the apparent liquid velocity. This form of the gradient is shown below as equation (8.54).

$$\left(\frac{\partial p}{\partial z}\right)_{f,TP} = \frac{f_{TP}}{d} \frac{\frac{1}{2} \rho_f V_f^{*2}}{(1 - \alpha)} \tag{8.54}$$

The following equation is obtained by substituting equation (8.54) into equation (8.53).

$$\frac{\partial(\Delta P)}{\partial \xi} = - \frac{f}{d} \frac{1}{2} \rho_f V_f^{*2} + \frac{f_{TP}}{d} \frac{1}{2} \rho_f V_f^{*2} \frac{\partial}{\partial \xi} \int_{\eta}^{\xi} \frac{1}{1 - \alpha(z)} dz$$

$$+ \frac{\partial}{\partial \xi} \int_{0}^{\xi} g \rho_f \alpha(z) dz \tag{8.55}$$

Combination of terms in equation (8.55) results in a simplified expression for the change of pressure loss with respect to a change in the coordinate ξ.

$$\frac{\partial(\Delta P)}{\partial \xi} = \frac{f}{d} \frac{1}{2} \rho_f V_f^{*2} \left[\frac{\partial}{\partial \xi} \int_{\eta}^{\xi} \frac{1}{1 - \alpha(z)} dz - 1\right]$$

$$+ \frac{\partial}{\partial \xi} \int_{0}^{\xi} g \rho_f \alpha(z) dz \tag{8.56}$$

To use equation (8.56) the functional relationship of α with respect to z must be specified. Under the assumption that the void fraction undergoes only very minor changes in the flashing mixture as a function of displacement along the discharge line, the following statement can be made.

for $\eta < z < \xi$

$$\alpha(z) = \alpha(\eta) = \text{constant} = 1 - C_c \tag{8.57}$$

Applying (8.57) to the exact relation, equation (8.56), a much simplified expression for the pressure loss dependency is obtained.

$$\frac{\partial(\Delta P)}{\partial \xi} = \frac{1}{2} \rho_f V_f^{*2} \frac{f}{d} \left(\frac{1}{1 - \alpha} - 1 \right) \Big|_\eta + g \rho_f \alpha \tag{8.58}$$

If the equation (8.58) is applied to high speed flows, the apparent dynamic pressure term is very much larger than the hydrostatic pressure term. Thus the additional simplification given as equation (8.59) can be applied to (8.58). That is, with

$$g \rho_f \alpha << \frac{1}{2} \rho_f V_f^{*2} \frac{f}{d} \left(\frac{\alpha}{1 - \alpha} \right) \Big|_\eta \tag{8.59}$$

the final form of the pressure dependency upon the coordinate is obtained.

$$\frac{\partial(\Delta P)}{\partial \xi} \approx \frac{1}{2} \rho_f V_f^{*2} \frac{f}{d} \left(\frac{\alpha}{1 - \alpha} \right) \Big|_\eta \tag{8.60}$$

A comparison of the numerical results obtained from equation (8.60) with experimental data is shown in Figures 40 and 41. Since this equation represents the derivative (i.e. slope) of the pressure loss with respect to ξ, it is illustrated in the Figures 40 and 41 gives lines having slopes equal to the values obtained from the solutions of equation (8.60). The graphical representations of equation (8.60) are inscribed in these figures in positions which most closely

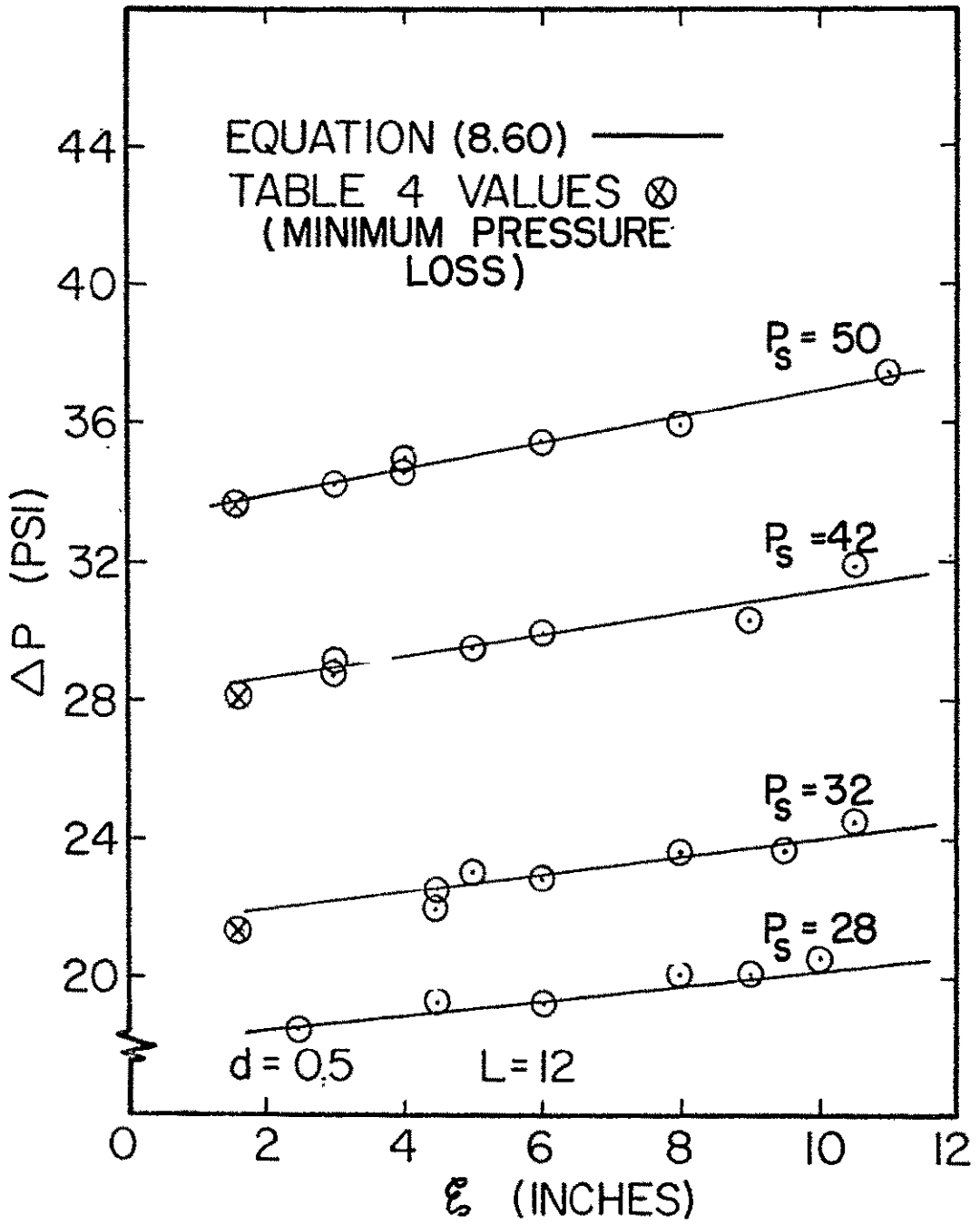

Figure 40. Stagnation Pressure Loss in a Discharge Line of d = 0.5 and L = 12 as a Function of Shock Position with Various Upstream Stagnation Pressures.

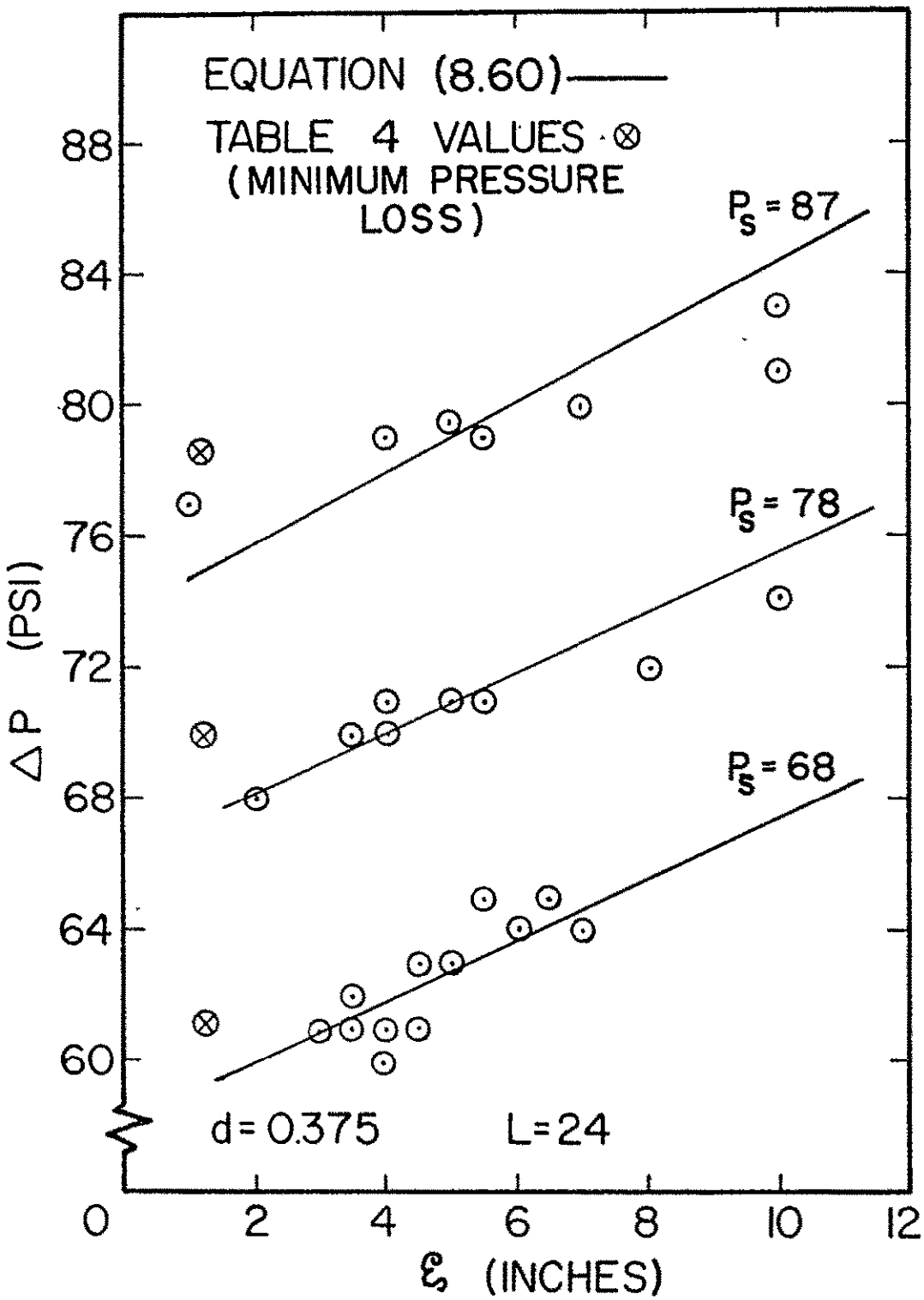

Figure 41. Stagnation Pressure Loss in a Discharge Line of d = 0.375 and L = 24 as a Function of Shock Position with Various Upstream Stagnation Pressures.

Figure 42. Minimum Pressure Losses as Functions of Apparent Liquid Velocities, i.e. Upstream Stagnation Pressures, for Various Geometric Configurations of the Discharge Line.

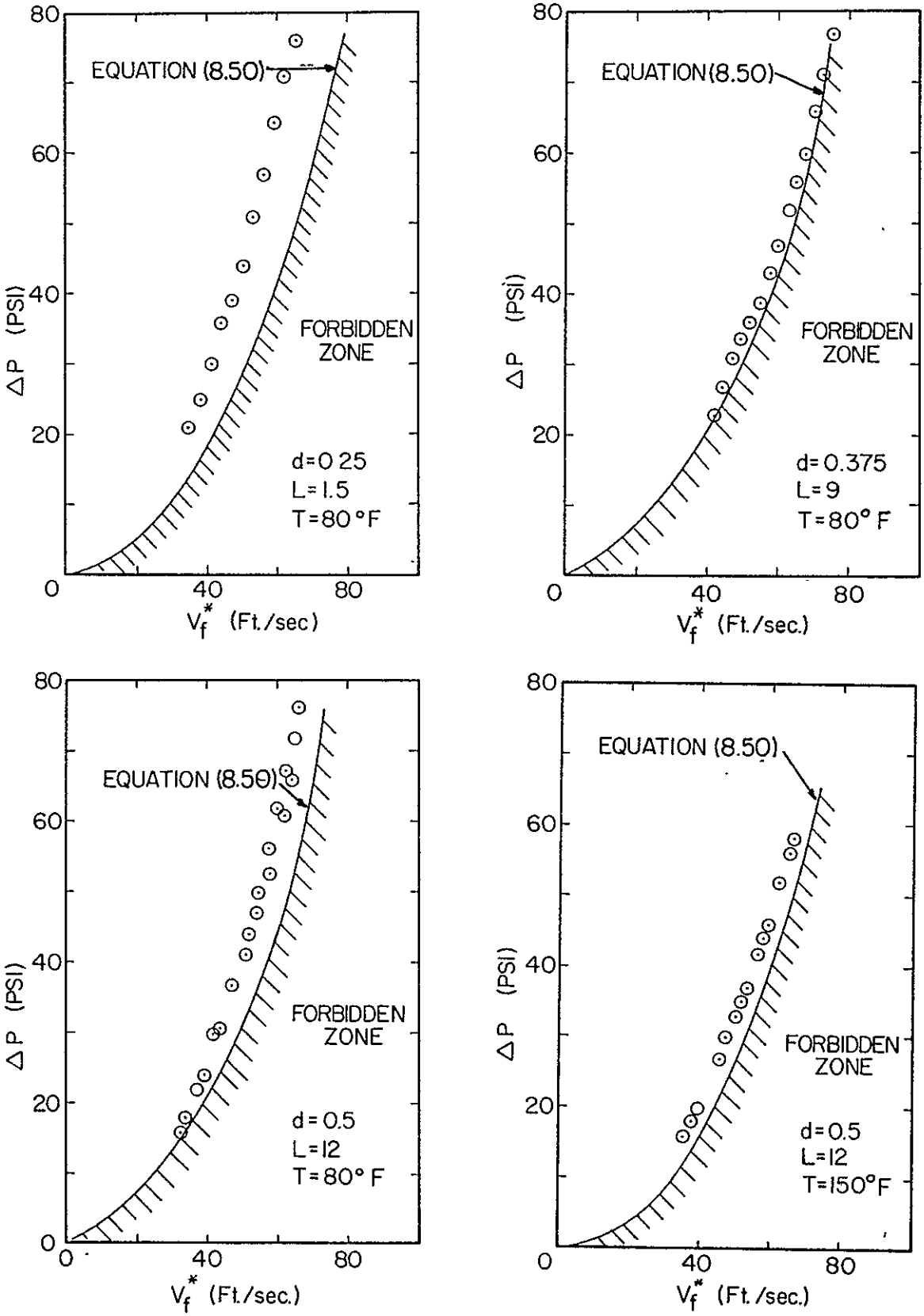
EQUATION (8.50)
FORBIDDEN ZONE
d=0 25
L=1.5
T=80 °F
ΔP (PSI)
V_f^* (Ft./sec)
EQUATION (8.50)
FORBIDDEN ZONE
d=0.375
L=9
T=80° F
ΔP (PSI)
V_f^* (Ft./sec.)
EQUATION (8.50)
FORBIDDEN ZONE
d=0.5
L=12
T=80° F
ΔP (PSI)
V_f^* (Ft./sec.)
EQUATION (8.50)
FORBIDDEN ZONE
d=0.5
L=12
T=150°F
ΔP (PSI)
V_f^* (Ft./sec.)

Figure 42

match the experimental data. Also included in the figures are the theoretical minimum pressure losses noted in Table 4.

A final comparison of the analytical pressure loss relation is made by consideration of the minimum pressure loss for choked flow as expressed by equation (8.50). Since it was defined as a minimum loss relation, all experimental pressure loss data for choked flow necessarily must have values greater than or equal to that predicted by the solutions of this equation. Data for several different geometric configurations of the discharge line are compared with the theoretical minimum loss value in Figure 42. To prove the validity of equation (8.50)', all data must lie on or above the line representing the solution to (8.50), which is indeed observed.

8.4 Investigation of Choking Conditions for a Vibrating Discharge Line

In the preceeding sections, the theory of two-phase single-component non-vibratory adiabatic discharge flow was developed. An extension of this theory to a vibrating discharge system is discussed in this section. Primary consideration is given to the effect which vibration has on two phase flow choking.

The fact that the flow rate attains a maximum value when the jet in the entrance region transforms into a homogeneous two-phase flow with a shock present has been

discussed. For the flow in a vibrating discharge line, the static pressure has an oscillating component super-imposed upon its mean value as shown by Schoenhals (44) and illustrated in this study in equation (7.32). The fact that the sinusoidal variation of the static pressure can only be sustained in the liquid phase becomes obvious when the concept of a hypothetical fluid is used. Once again, the vapor can only exist at one pressure value as long as sufficient liquid is available to undergo a phase transformation to the vapor phase and the vapor maintains an interface with the liquid. If a pressure pulse were to propagate through the single-phase liquid to a liquid-vapor interface, the pressure wave would be absorbed by phase transformation processes. Whether this pressure wave is a compression wave or a rarefaction wave does not matter. The conditions of thermodynamic equilibrium require that the two-phase mixture will be forced to have sufficient amounts of vapor condense to liquid to maintain the mixture pressure at the vapor pressure of the liquid for a compression wave, and the two-phase mixture will be forced to let the liquid phase evaporate in sufficient amounts in order to maintain the mixture pressure at the vapor pressure for a rarefaction wave.

Consider now the case of a real fluid for which transient effects have to be included. This is to say that the fluid cannot respond immediately to a change of pressure. If the same pressure wave were to propagate through the

single-phase liquid to the liquid-vapor interface; the vapor could possibly sustain the wave for a brief period until equilibrium could be reestablished. The real two-phase liquid-vapor fluid would initially damp the pressure wave and finally absorb it if sufficient fluid were available. The amount of two-phase mixture necessary to absorb a wave of known strength would of course depend on the rate processes of the particular fluid involved and such considerations as interfacial area and impurities.

Applying the concepts stated in this brief discussion to the test fluid as it passes into the discharge line, the ratio of interfacial area to liquid volume can be used as a criterion for the rate of maximum phase transformation. The region of greatest interfacial area per unit volume would exist in the homogeneous two-phase flow mixture.

An experimental check on the fluid's behavior when choked was performed. The high frequency pressure transducer measuring pressure p_1 in Figure 6 showed that when the vapor annulus existed between the liquid jet and the wall of the discharge line, no oscillating component of the static pressure was detected. This implies that the test fluid was capable of absorbing pressure oscillations when the two-phase liquid-vapor combination existed.

Because the static pressure in the two-phase region of the discharge line under vibrating conditions did not differ from that which existed in absence of vibration, no change

Figure 43. Measured Flow Rates Under Choked Conditions in Presence of Vibration as a Function of Stagnation Pressure for Various Discharge Line Geometries Compared with the Analytically Predicted Maximum Flow Rates in Absence of Vibration.

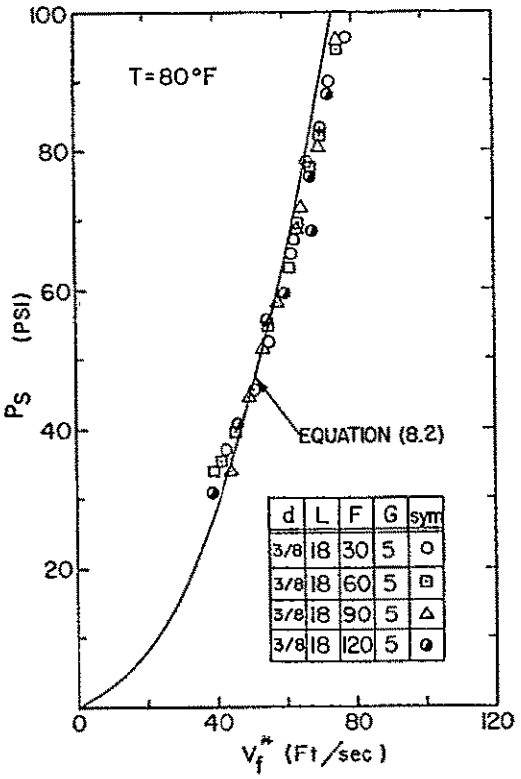
T=80°F
EQUATION (8.2)
d L F G sym
3/8 18 30 5
3/8 18 60 5
3/8 18 90 5
3/8 18 120 5
P_S (PSI)
V_f^* (Ft/sec)

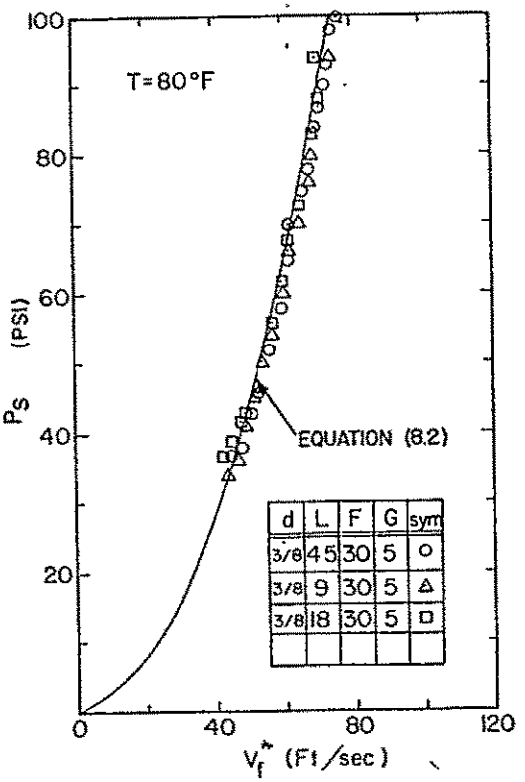
T=80°F
EQUATION (8.2)
d L F G sym
3/8 45 30 5
3/8 9 30 5
3/8 18 30 5
P_S (PSI)
V_f^* (Ft/sec)

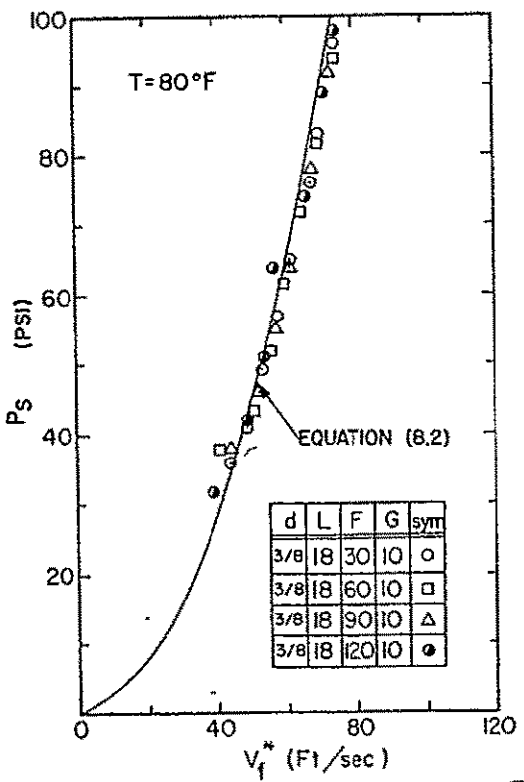
T=80°F
EQUATION (8.2)
d L F G sym
3/8 18 30 10
3/8 18 60 10
3/8 18 90 10
3/8 18 120 10
P_S (PSI)
V_f^* (Ft/sec)

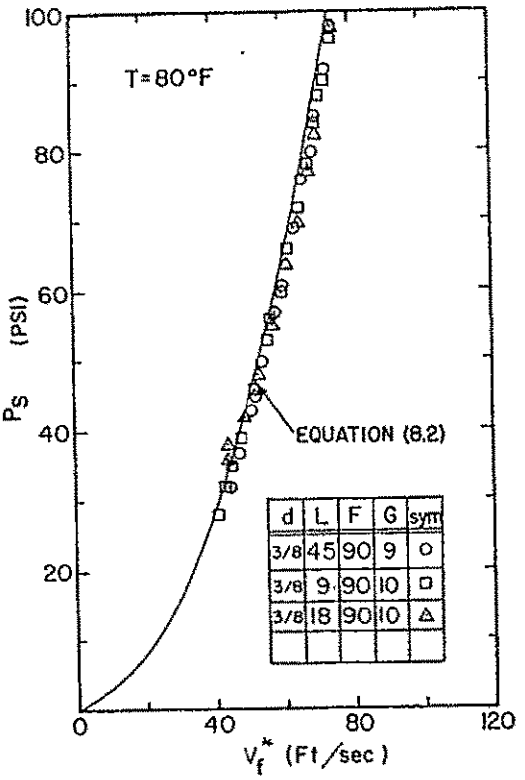
T=80°F
EQUATION (8.2)
d L F G sym
3/8 45 90 9
3/8 9 90 10
3/8 18 90 10
P_S (PSI)
V_f^* (Ft/sec)

Figure 43

in flowrate for given upstream stagnation conditions was expected for the case of longitudinal vibration compared to the case where vibration was absent. Data taken for various geometries, acceleration levels, and frequencies are compared to the prediction for the non-vibrating discharge line, equation (8.2), in Figure 43. No detectable difference from the theoretical prediction was noticed.

8.5 Results and Conclusions for the Two Phase Flow Analysis and Choking in the Discharge Line

Application of the free streamline theory to the flow pattern in the entrance of a sharp edged discharge line yielded a solution which was used to predict the maximum rates under choked flow conditions. Comparison of the theoretical prediction with experimental data in Figure 36 illustrates the accuracy of the prediction. It should be noted that while experimental values of the parameter, d^2/D^2, restricted the correlation between data and theory to the special case of the limiting value of the contraction coefficient, $C_c = 0.611$, the analysis can be applied to any similar geometric arrangement as long as the proper value of the contraction coefficient is available.

The advantage of this type of analysis was realized in transforming the multidimensional flow problem in the entrance region to one which could effectively be treated as a one dimensional problem. This technique consisted of

an extension of the single phase liquid flow analysis presented earlier to a two-phase flow analysis.

The entrance loss coefficient for the single phase liquid flow was found to be very much greater than that of the two-phase flashing flow. The modified correlation from Richardson agreed well with experimental data, although its original application was directed towards a two-component, two phase flow system. As in the case of the single phase liquid flow, the greatest pressure loss occurred in the expansion process rather than in the contraction process. Since the single component flashing flow in the discharge line represented a two phase flow during the transformation from jet flow to homogeneous flow, the similarity between Richardson's flow problem and this flow situation was sufficient to allow the application of a similar relation. In the entrance loss concept frictional losses were disregarded until the jet expansion forced the liquid into contact with the wall.

During the transformation from jet flow to homogeneous flow, the mixture velocity was shown to be equal to the jet velocity. At the coordinate η, this velocity equaled the velocity along the free streamline as formulated in the analytical solution. The existence of continuous liquid velocities in the region of flow transformation allowed a prediction for the void fraction at the point of inception of homogeneous flow. The void fraction at this point is dependent upon the contraction coefficient.

The determination of the void fraction at the position η made it possible to predict the minimum pressure loss for choked flow conditions. Minimum pressure losses occurred when an infinitely weak shock existed in the region of transformation from jet to homogeneous flow. The correspondence between the theoretical prediction and the experimental data shown in Table 4 for this special case is extremely good.

An extension of the pressure loss relation to predict the location of the normal shock (i.e. coordinate ξ), was presented. With the assumption of a constant void fraction, the expression derived in the analysis gave the shock position dependency as a linear function of the pressure loss at a given flow rate.

Two photographs of the normal shock taken with the aid of a stroboscopic flash unit are presented in Figures 44 and 45. The duration of the flash was approximately 9μ seconds. The dark region upstream of the shock interface is the homogeneous mixture. The numerous interfacial regions between liquid and vapor provided many areas of total reflection which effectively reduced the amount of transmitted light energy. The lighter area downstream of the interface is the single phase liquid. Depth of field of the lens and the cylindrical cross section of the discharge line prohibited sharper photographs. However, the contrast of the interface is still apparent.

Data from the experimental investigation into choking of the discharge line under the influence of longitudinal vibration were compared with the analytical prediction formulated for the non-vibrating line. The excellent agreement between the data and predictions proved that the vibration did not affect the maximum flow rates for given upstream conditions of the liquid. No determination of the pressure losses was attempted for the vibrational cases.

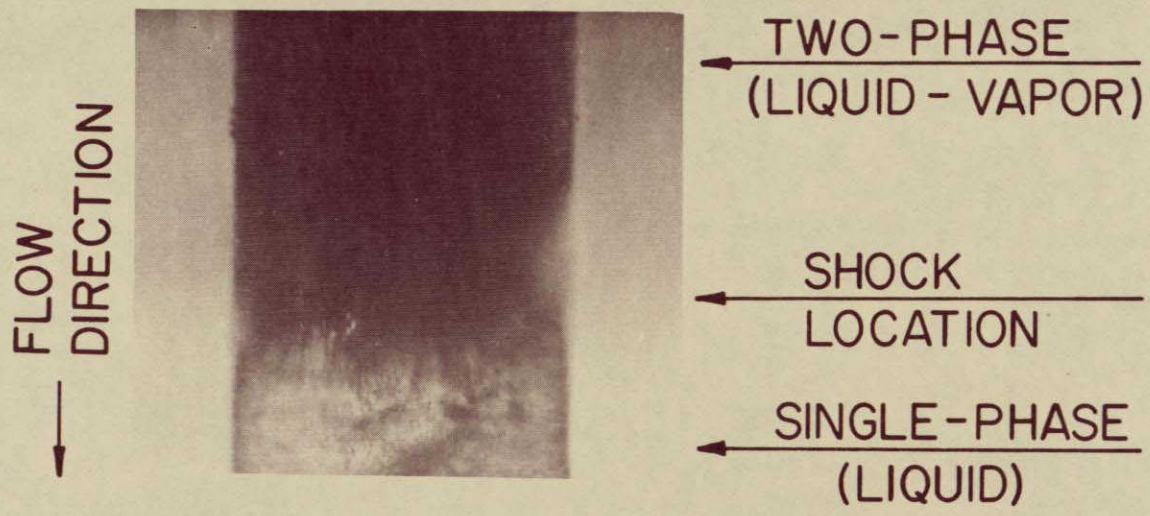

FIGURE 44. Stroboscopic Photograph of Normal Shock in Discharge Line (Magnification 3X)

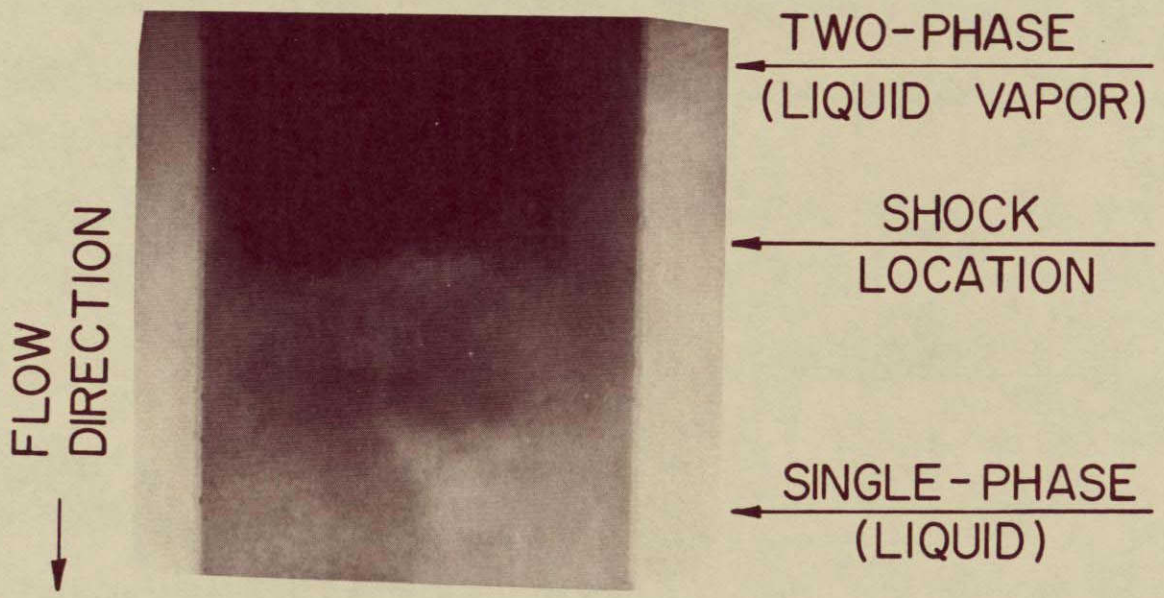

FIGURE 45. Stroboscopic Photograph of Normal Shock in Discharge Line (Magnification 4X)

CHAPTER 9

SUMMARY

This study was concerned with both single phase liquid and two-phase liquid-vapor fluid flow in a discharge line with a sharp edged entrance. Initial efforts were spent determining the applicability of the classical single phase liquid flow relations to this particular type of problem. Following this initial phase of the overall study, a cavitation investigation was performed with emphasis on determining a suitable cavitation parameter which could be used to predict the onset of two-phase conditions within the discharge line. An extension to totally two-phase flow conditions in the discharge line followed the cavitation work. The totally two phase flow condition was attributed to flashing of the liquid to its vapor phase because of the existing flow conditions. All of the flow problems were investigated both in the absence and in the presence of longitudinal vibration of the discharge line.

In order to obtain experimental data for comparison with analytical predictions, a two-phase fluid flow loop facility having a test section mounted on an electrodynamic shaker was designed and constructed. The entire experimental system was a combination of the flow loop and the shaker facility. This

system was quite flexible in terms of operating regimes having a fluid temperature range from 60° F to 180° F, flow rates from 0 to 45 GPM, vibrational frequencies in the range of 10 to 2000 cps and maximum acceleration levels up to 20 g for the test sections used on the shaker.

The check-out of the experimental facility was done with single phase liquid flow through the test section under non-vibratory conditions. The instrumentation of the facility was checked for correct operation by using well known analytical relations of single phase liquid flow as a basis for comparison with experimental data.

More specifically, the one-dimensional analysis presented in Chapter 6 describing the stagnation pressure loss across the sharp edged discharge line for single phase liquid flow yielded an expression the solution of which compared favorably to experimentally obtained data. An analytical solution to the pressure loss across the discharge line under the influence of longitudinal vibration was not attempted; however, an experimental investigation was conducted. The results of this work, presented at the end of Chapter 6, showed in general that the presence of this type of vibration increased the existing pressure losses. A trend of larger losses for lower frequencies at a given acceleration level was noted. Also, at a given fixed frequency, larger acceleration levels usually produced larger pressure losses.

By treating the flow at the sharp edged entrance of the discharge line as a special application of axisymmetric jet flow from an orifice, a satisfactory prediction of local static pressures along the wall of the discharge line entrance was possible. While the jet flow solution was successfully used in this one application, the applicability of typical jet flow solutions to other geometries could be made which would extend the usefulness of the solution presented herein.

The use of the free streamline solution to obtain a modified cavitation number, $\bar{\sigma}^*$, was shown to have good agreement with experimental data. The significance of using this type of analysis for high velocity flows can be profound in application to flows past sharp edged valves of known geometries, or past a rounded protuberance extending into the flow in a pipe. The free streamline solution predicts the values of local velocities which may be very much different from the typical average value, and which therefore require special consideration in any cavitation prediction.

The development of the time dependent cavitation number predicting cavitation in the vibrating discharge line was based on a solution of oscillating pressures in a liquid-filled flexible tank under no flow conditions. The relations for the pressure oscillations were applied to the already derived equations for a non-vibrating test section by considering the pressure to be a combination of steady plus time dependent oscillating components. The velocity was

considered to be constant. This technique of superposition was apparent in the final form of the time dependent cavitation number as it was a combination of the previously obtained constant valued modified cavitation number with the addition of a time dependent oscillating component.

The experimental verification of this analytical model could not be considered as conclusive evidence to either prove or disprove the theory. Since the time dependent cavitation number was shown to have a sinusoidal form, a phase angle relationship between the motion of the test section and the strobe lamp which was used to obtain the experimental data served as the time reference. Extensive experimental work directed towards the time dependency of the cavitation, referred to as phase deviation in the text, showed no definite trends; however, the predictions for the maximum possible variation in the value of the time dependent cavitation number were satisfied by the experimental data.

The lack of phase deviation sensitivity of the experimental data was attributed to two factors. The first consideration was the response time of the liquid-vapor evaporation and condensation processes in the real fluid. The analytical model considered a hypothetical liquid which could not sustain any tension and had no viscosity; a real liquid does not exhibit this type of behavior. The second considera tion was the difficulty of visual detection of the instant at which cavitation occurred in the liquid. A discernable flicker was always noticeable by the observer, and it was particularly distracting at low vibrational frequencies.

The same free streamline solution used for the cavitation analysis was used to establish a choking prediction. This work, described in Chapter 8, resulted in a determination of maximum flow rates which were dependent only on the upstream stagnation conditions and the geometry of the discharge line. Experimental data correlated well with theoretical predictions.

In order to obtain a relation describing the loss in stagnation pressure across the discharge line, it was necessary to model the separate two-phase flow regimes noted in the discharge line. As the liquid entered the sharp edged line, the first flow pattern discernable was identical to jet flow from an orifice except that the jet was separated from contact with the walls of the line by a vapor annulus. At approximately π-diameters downstream of the entrance, the jet flow underwent a transformation to a two-phase mixture most accurately described as being two-phase homogeneous flow. The homogeneous regime terminated with a discontinuity where the vapor bubbles suddenly collapsed and formed a liquid. The analysis treated this phenomenon as a normal shock front. Summing the stagnation pressure losses over the various flow regimes yielded an expression for the stagnation pressure loss across the discharge line. While the relation was very comprehensive, the void fraction dependency in the discharge line did not permit its application to all conditions covered in this investigation. However, the special case of minimum

pressure loss for choked flow was shown to agree very well with experimental data.

An expression was developed for the change in stagnation pressure loss due to a change in the location of the normal shock under the assumption of a constant void fraction in the homogeneous mixture. When compared to experimental data, the solution was shown to be in close agreement. It should be noted that the combination of the minimum pressure loss relation with the change in pressure loss relation yields an analytical prediction for the location of the normal shock in the discharge line as a function of the stagnation pressure loss on the basis of a constant, previously determined, value of the void fraction. While a change in the void fraction was considered to be possible, the magnitude of such change was treated as being small enough to permit the assumption of a constant value.

While the shock and pressure loss analyses were performed only for the situation of flow in the discharge line in the absence of vibration, the choking expression for the non-vibrating situation was applied to the experimental data obtained from the vibrating discharge line with excellent success. Evidentally, the vibration caused no measurable effect on the choking of the discharge line.

The application of the results described in this study can be directed towards several areas of technology dealing with high speed liquid flows. For example, the cavitation

parameter formulated in Chapter 7 represents a prediction of the limit of applicability of a single phase liquid analysis to a high speed liquid flow. The onset of the two-phase condition represents a violation of the single phase liquid model. As another example, the flashing and subsequent choking analyses provided information to predict maximum flow rates and minimum pressure drops required to attain these conditions. While the relations presented herein are complete and well substantiated by an experimental investigation, some specific portions of the overall study represent areas where additional detailed work can contribute significantly to the understanding of the physical processes involved.

It is recommended that a precise determination of the limits of applicability of the jet flow solution used to predict the flow pattern at the sharp edged entrance to the discharge line be made. An experimental study of the pressure profiles in the entrance region could be accomplished by means of a traversing pressure probe. In this manner, an experimentally obtained flow pattern could be compared with the flow pattern analytically obtained from the free streamline analysis.

A recommendation for further work on the problem of cavitation in a vibrating discharge line would be the use of a technique for cavitation sensing not directly dependent on the physical resources of the observer. A possible facility would involve the use of a hydrophone installed very near the entrance plane of the line. The signal output could be very

carefully filtered so that when the characteristic cavitation sound was detected, a marker would be signaled to indicate the instantaneous values of pressure and flow rate on the data recorder. This type of detection system would be considerably more precise than the visual observation technique which was used, especially in determining a phase angle relationship.

Several recommendations can be made to improve the understanding of the flow regimes in flashing two-phase flow in the discharge line. The first would involve the use of a radiation attenuation technique to experimentally measure the void fraction in the discharge line. Photographic techniques for this purpose are burdensome and inaccurate for this type of flow. The void fraction behavior in the immediate neighborhood of the normal shock would be most valuable as an aid in understanding the physical processes involved.

The second recommendation deals with the transformation of the jet flow pattern at the entrance to the homogeneous flow pattern. This could best be accomplished in a two-dimensional test section with high speed photographic equipment. In this manner, perhaps the question of whether nucleation in the core of the liquid or surface instabilities or a combination of both were the principle driving force causing the jet deterioration.

Since the study was concerned only with an adiabatic discharge line, the inclusion of heat transfer would

significantly add to the usefulness of the analysis. Such information as temperature gradients and effects on void fraction, pressure losses and flow regimes in the discharge line could be investigated not only with water as the working fluid but also with some other types of fluids. After a thorough understanding of the effects of heat transfer on the flow in a non-vibrating discharge line was gained, then the extension of the investigation to a vibrating discharge line could be made.

BIBLIOGRAPHY

1. V. L. Streeter, Fluid Mechanics, 2nd Ed., McGraw-Hill Book Co. Inc., 1958.

2. I. H. Shames, Mechanics of Fluids, McGraw-Hill Book Co. Inc., 1962.

3. R. A. Kenyon, Principles of Fluid Mechanics, Ronald Press Co., 1960.

4. R. von Mises, Zeits., Ver. Dtsch. Ing., 61, 21, 1917.

5. M. I. Gurevich, Theory of Jets in Ideal Fluids, Academic Press, 1965.

6. H. Rouse and Abdel-Hadi Abul-Fetouh, "Characteristics of Irrotational Flow Through Axially Symmetric Orifices" ASME Trans., J. of Applied Mech., Vol. 17-4, p. 421, Dec. 1950.

7. S. William Grouse Jr., "An Index to the Two-Phase Gas-Liquid Flow Literature", MIT Report No. 9.

8. J. H. Lienhard and J. H. Stephenson, "Temperature and Scale Effects Upon Cavitation and Flashing in Free and Submerged Jets", ASME Trans., J. of Basic Engr., June 1966, p. 525, ASME Paper No. 65-WA/FE-13.

9. F. Numachi, M. Yamabe, and R. Oba, "Cavitation Effect on the Discharge Coefficient of the Sharp-Edged Orifice Plate", ASME Trans., J. of Basic Engr., March 1960, p. 1, ASME Paper No. 58-A-93.

10. R. Kobayashi, "Effect of Cavitation on the Discharge Coefficient of Standard Flow Nozzles", ASME Paper No. 66-FE-12.

11. N. S. Govinda Rao, K. Seetharamiah, and M. V. Ramamoorthy, "Quadrant-Edge Orifice - Performance Under Cavitating Conditions", ASME Paper No. -6-FE-9.

12. F. Numachi, R. Kobayashi, and S. Kamiyama, "Effect of Cavitation on the Accuracy of Herschel Type Venturi Tubes", ASME Trans., J. of Basic Engr., Vol. 84, Sept. 1962, p. 351

13. J. W. Holl and G. F. Wislicenus, "Scale Effects on Cavitation", ASME Trans., Jour. of Basic Engr., Sept. 1961, p. 385. ASME Paper No. 60-WA-151.

14. R. Oshima, "Theory of Scale Effects on Cavitation Inception on Axially Symmetric Bodies", ASME Trans., Jour. of Basic Engr., Sept. 1961, p. 379. ASME Paper No. 60-WA-136.

15. R. W. Kermeen, J. T. McGraw, and R. B. Parkin, "Mechanism of Cavitation Inception and the Related Scale-Effects Problem", ASME Trans., Vol. 77, 1955, p. 533.

16. R. T. Knapp, "Cavitation Mechanics and Its Relation to the Design of Hydraulic Equipment", Engineering, Vol. 173, 1952, p. 566.

17. J. W. Holl, "An Effect of Air Content on the Occurrence of Cavitation", ASME Paper No. 60-HYD-8, March 1960.

18. J. W. Holl and A. L. Treaster, "Cavitation Hysterisis", ASME Trans., Jour. of Basic Engr., March 1966, p. 199.

19. S. Kamiyama, "Cavitation Tests in Pipe Bends", ASME Trans., March 1966, p. 252.

20. J. G. Collier and G. B. Wallis, Two Phase Flow and Heat Transfer, Vol. 1, 2, 3, and 4. Notes for a summer course July 24-Aug. 4, 1967, Stanford Univ.

21. IBID, pp. 61-76.

22. A. H. Shapiro, The Dynamics and Thermodynamics of Compressible Fluid Flow, Vol. 1, The Ronald Press Co., 1953

23. S. W. Gouse Jr. and G. A. Brown, "A Survey of the Velocity of Sound in Two-Phase Mixtures", ASME Paper No. 64-WA/FE-35.

24. R. V. Smith, "Choking Two-Phase Flow Literature Summary and Idealized Design Solutions for Hydrogen, Nitrogen, Oxygen, and Refrigerants 12 and 11", NBS Tech. Note 179, 1963.

25. S. Levy, "Prediction of Two-Phase Critical Flow Rate", ASME Trans., Jour. of H. T., ASME Paper No. 64-HT-8.

26. H. Fauske, "Critical, Two-Phase, Steam-Water Flows", Proceedings of the 1961 Heat Transfer and Fluid Mechanics Institute, pp. 79-89, Stanford Univ. Press, 1961.

27. F. J. Moody, "Manimum Flow Rate of a Single Component, Two-Phase Mixture", ASME Paper No. 64-HT-35.

28. F. J. Moody, "Maximum Two-Phase Vessel Blowdown from Pipes", ASME Paper 65-WA/HT-1.

29. A. N. Nahavandi and R. F. von Hollen, "Two-Phase Pressure Gradients in the Approach Region to Critical Flow", WCAP-2662, 1964.

30. J. G. Collier and G. B. Wallis, Two-Phase Flow and Heat Transfer, pp. 1299-1300.

31. H. K. Fauske, "The Discharge of Saturated Water Through Tubes", AIChE preprint No. 30, 7th National Heat Transfer Conference, Cleveland, Ohio, 1964.

32. H. K. Fauske, "Two-Phase Critical Flow", Chapter in MIT Summer Course Notes, 1964.

33. F. R. Zaloudek, "The Critical Flow of Hot Water Through Short Tubes", HW-77594, Hanford Labs, May 1963.

34. M. W. Benjamin and J. G. Miller, "The Flow of Saturated Water Through Throttling Orifices", ASME Trans., 63, 1941, p. 413.

35. R. J. Silver, "Temperature and Pressure Phenomenon in the Flow of Saturated Liquids", Proc. Roy. Soc., A, 194, 1948, p. 464.

36. R. B. Eddington, "Investigation of Shock Phenomenon in a Supersonic Two-Phase Tunnel", AIAA Paper No. 66-87, 1966.

37. J. F. Muir and R. Eichorn, "Compressible Flow of an Air-Water Mixture Through a Vertical, Two-Dimensional, Converging-Diverging Nozzle", Proc. of 1963 Heat Transfer and Fluid Mech. Institute.

38. D. Elliott, D. Cerini, Otte and E. Weinberg, "Liquid MHD Power Conversion", SPS-37-23, Vol. IV, JPL, Pasadena, Calif., Oct. 31, 1963, p. 132.

39. H. H. Bleich, "Longitudinal Forced Vibration of Cylindrical Fuel Tanks", Jet Propulsion, Feb. 1956, p. 109.

40. H. H. Bleich, "Effects of Vibrations on the Motion of Small Gas Bubbles in a Liquid", Jet Propulsion, No. 1956, p. 958.

41. M. H. I. Baird, "Resonant Bubbles in a Vertically Vibrating Liquid Column", Canadian Jour. of Chem. Engr., Vol. 41, 1963, p. 52.

42. R. H. Buchanan, G. Jameson, and D. Oedjoe, "Cyclic Migration of Bubbles in a Vertically Vibrating Liquid Column," Industrial and Engr. Chem. Fund., Vol. 1, No. 2, 1962, p. 82.

43. C. A. Pounder, D. H. Blount, and C. G. Fritz, "Bubble Coalescence in a Longitudinally Vibrated Liquid Column," NASA TMX-53180, Huntsville, Ala., Dec. 16, 1964.

44. R. J. Schoenhals and T. J. Overcamp, "Pressure Distributions and Bubble Formation Induced by Longitudinal Vibration of a Flexible Liquid Filled Container," ASME Trans., Series D., Vol. 89, No. 4, Dec. 1967, p. 737.

45. R. J. Schoenhals, E. R. F. Winter, and E. I. Griggs, "Effects of Longitudinal Vibration on Discharge of Liquids from Propellent Tanks," Proc. of the 1967 H.T. and Fluid Mech. Inst., Stanford Univ. Press.

46. J. A. Pesar, "Liquid Discharge from Tanks Subjected to Forced Longitudinal Vibration," M.S. Thesis, Purdue Univ. School of Mech. Engr., June 1968.

47. R. H. Fashbaugh, V. L. Streeter, "Resonance in Liquid Rocket Engine Systems", ASME Paper No. 65-FE-23.

48. B. W. Licht, A. C. Park, "POGO Stability of the Saturn V Second Flight Stage", AAS67-414 (PS-4), Trans. 1967 National Symposium on "Saturn V/Apollo and Beyond", Huntsville, Ala., June 12-14, 1967.

49. J. W. Lehner, "Analog Simulation of Updated Saturn I First Stage Propulsion System Dynamic Characteristics" Paper No. 88, AAS Southeastern Symposium on Missiles and Aerospace Vehicles Sciences, Dec. 5-7, 1966.

50. J. G. Collier and G. B. Wallis, Two-Phase Flow and Heat Transfer, p. 1279.

51. J. G. Collier and G. B. Wallis, Two-Phase Flow and Heat Transfer, Ch. 5.

52. B. L. Richardson, "Some Problems in Horizontal Two-Phase Two-Component Flow," ANL-5949, Dec. 1958.

53. J. G. Collier and G. B. Wallis, Two-Phase Flow and Heat Transfer, p. 62.

54. E. R. F. Winter and M. L'Ecuyer, Notes for Graduate Course, 1968, Purdue Univ. School of Mech. Engr.